Photoresponsive behavior of SPEEK/Cellulose films for oxygen sensing.

by

Samuel Bond

A dissertation submitted to the Graduate Faculty of
Auburn University
in partial fulfillment of the
requirements for the Degree of
Chemistry, Doctor of Philosophy

Auburn, Alabama
December 9, 2023

Keywords: photochemistry, SPEEK, photoreduction, polymer

Approved by

German Mills, Chair, Professor of Chemistry
Joseph V. Ortiz, Professor of Chemistry
Rik Blumenthal, Associate Professor of Chemistry
Paul Ohno, Associate Professor of Chemistry
Rob Jackson, Professor of Mechanical Engineering

Abstract

Illumination of sulfonated poly(ether etherketone) (SPEEK) and cellulose films by 350nm photons resulted in an efficient redox system. The illuminated films resulted in radicals of SPEEK (SPEEKH•) which in the presence of air underwent radical oxidation that lasted minutes to hours depending on the cellulose polymers utilized and relative humidity (R.H.). Different cellulose polymers such as carboxymethylcellulose (NaCMC) and hydroxyethyl cellulose (2-HEC) have similar structures, however, changes in functional groups within the polymer matrix can have a major impact. When illuminated 2-HEC films SPEEKH• oxidation occurred via first-order kinetics with a rate constant of $k = 6 \times 10^{-2}$ min^{-1} at 20% R.H. to 2.5×10^{-1} min^{-1} at 55% R.H., while CMC oxidation occurred at $k = 1.5 \times 10^{-2}$ min^{-1} at 20% relative humidity to 6.7×10^{-2} min^{-1} at 55% R.H. The effect of R.H. on the radical oxidation rate is a result of the polymer matrix expansion in the presence of water. Consecutive illumination produced light-absorbing transients (LAT) which resulted in the failure of 2-HEC films by the 7^{th} illumination. NaCMC films were only slightly affected by LAT after 10 illuminations.

Efficient reduction of methyl viologen (MV^{2+}) took place within SPEEK/cellulose films upon exposure to 350 nm photons. This photoreduction utilized radicals of SPEEKH• which led to the formation of methyl viologen radical (MV^{+}). The resulting redox system yielded higher visible detection by the eye. Illuminated 2-HEC films MV^{+} oxidation occurred via first-order kinetics with a rate constant of $k = 4.6 \times 10^{-2}$ min^{-1} at 20% R.H. to 1.7×10^{-1} min^{-1} at 47% R.H., while CMC oxidation occurred with a rate constant of $k = 2.2 \times 10^{-1}$ min^{-1} at 20% relative humidity to 1×10^{-1} min^{-1} at 55% R.H. The MV^{2+} reduction and reoxidation were successful in both 2-HEC and NaCMC film systems; however, 2-HEC was affected by LAT upon consecutive illuminations.

Reduction of MV^{2+} within argon-sparged SPEEK/cellulose solutions and swollen films with $HCO_2H/HCO2^-$ was attempted with exposure to 350 nm photons. Ar sparged Solutions showed no reduction products while swollen films showed a reduction of MV^{2+}. The reoxidation of MV^+ was observed in the absence of air and showed an increase in the rate of decay upon subsequent illuminations. The half-life of each illumination was 1^{st} $t_{1/2}$ ≈16 min, 2^{nd} $t_{1/2}$ ≈ 11.2 min, and 3^{rd} $t_{1/2}$ ≈ 4.6 min which followed second-order kinetic and then progressed to zero-order kinetics. This was the result of a LAT product being produced in excess during each illumination.

Acknowledgment

I would like to express my sincere gratitude to my supervisor, Dr. Mills, for all the support and help throughout my time at Auburn University. I would also like to thank Dr. Christopher Greco, Dr. Paul Ohno, and Dr. J.V. Ortiz for agreeing to be part of my committee and for helping me see alternatives. A special thanks to Dr. Rob Jackson for being my outside reader and for the opportunity to work with him on lubricant research. Dr. Michael Miller, thank you for helping me with SEM/TEM measurements. Dr. Rob Jackson, thank you for the chance to work with you and explore lubricants and arcing effects. Dr. E. Duin, thank you for helping me with EPR measurements. A special thanks go to my lab mate Radini Dissanyaka for the help and discussions on research topics. I would also like to thank Dr. Cheryl Colquhoun for helping with atomic absorption. Finally, I would like to thank my family members, all my friends and well-wishers.

Table of Contents

List of Abbreviations

BP	benzophenone
BPK	benzophenylketyl
PEEK	poly(ether ether ketone)
SPEEK	sulphonated poly(ether ether ketone)
PVA	poly(vinyl alcohol)
NaCMC	sodium carboxymethyl cellulose
2-HEC	2-hydroxyethyl cellulose
Glu	Glutraldehyde
Tar	Tartaric Acid
MV^{2+}	Methyl Viologen
Th	Thionine
CV	Cresol violet
LAT	Light absorbing transient
C	degree Celsius
EPR	electron paramagnetic resonance
ε	extinction coefficient
λ	wavelength
hr	hour
hν	photon
M	molar concentration
mM	millimolar
μM	micromolar

min	minute
nm	nano meter
UV	ultraviolet
Vis	visible
I_0	light intensity

List of Figures

List of Tables

Chapter 1

Photoresponsive behavior of SPEEK/Cellulose films for oxygen sensing.

1.1 Introduction:

Over the years photoactive materials have become an increasingly attractive prospect as they are able to experience reversible alterations upon exposure to light.[1-7] Photoactive materials can be used in a variety of systems because of the control over what activation energy is needed and the ability to focus and control the stimuli such as electromagnetic radiation. The responsiveness of such materials to various forms of electromagnetic radiation enables manipulation of some of their properties by means of variables such as light intensity, wavelength, and exposure time. In addition, photoactive materials can respond to other stimuli induced by the presence of certain gases or applied voltage changes. Photoactivated systems can be designed to be altered either reversible or irreversible depending on the desired application. They frequently function as key components of controlled drug delivery systems, oxygen sensors and other applications. [2,5,8] Many photoactive systems are fairly complex as they require organic molecules or inorganic compounds as photosensitive chromophores, together with redox indicators, reducing agents and macromolecular binders. [9] However, less complicated systems are feasible if light-sensitive polymers act as sensitizers while other macromolecules function as transparent matrix as well as reducing agents. Such a strategy would lead, in principle, to simpler systems useful in a variety of practical applications such as food packaging, pharmaceuticals, oxygen sensing, holography, and others.[10-14]

1.2 Benzophenone and PEEK

Photosensitizers or photoinitiators utilize light for the formation of intermediates such as radicals, cations, or anions which can induce further reactions; in fact, many redox processes use

free radicals as key intermediates. For the generation of radical intermediates, the process starts with excitation of the molecule to an excited singlet state that can lead to dissociation of a chemical bond or transformation into a reactive intermediate. [15] In the case of carbonyl chromophores the reactive intermediate is an (n, π*) triplet excited state generated via fast and efficient intersystem crossing. The triplet excited state can relax through phosphorescence or create radicals via hydrogen abstraction from a suitable donor. H-atom abstraction results in the formation of two radicals, one from the photoinitiator and another from the hydrogen donor.

Benzophenone (BP) is a well-known chromophore that can generate triplet (n, π*) excited states upon exposure to UV light (230 nm – 380 nm).[15] These excited states can produce reducing radicals via hydrogen abstraction from several hydrogen atom donors.[15-22] Depicted in Scheme 1.1 are the elementary processes to produce α-hydroxy (or ketyl) radical of BP using 2-propanol as H-atom donor. The H-atom abstraction of 2-propanol by BP* generates two α-hydroxy radicals: one from BP and the alcohol derived 1-hydro-1-methylethyl radical. Following the generation of the two α-hydroxy radicals, the 2-propanol radical may reduce a second BP molecule forming an additional benzophenone ketyl radical. Thus, under optimal reaction conditions a single photon could generate two α-hydroxy radicals of benzophenone.

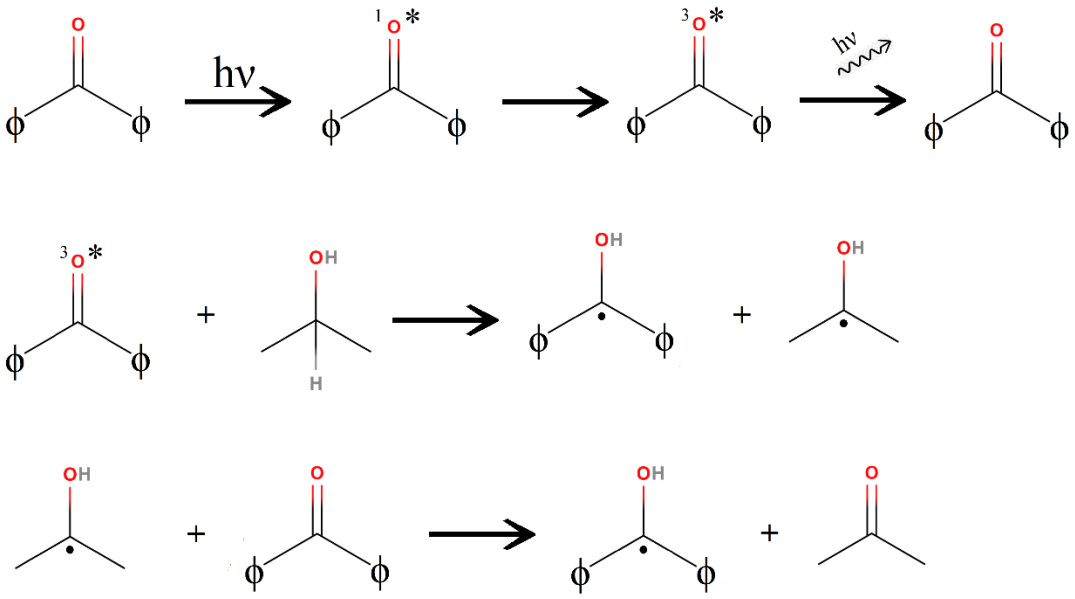

Scheme 1.1: Schematic representation of the reactions leading to benzophenone ketyl radicals of benzophenone.[15]

As is typical of α-hydroxy radicals, the BP ketyl radical experiences dimerization forming several products.[15,16] Scheme 1.2 illustrates the possible dimerization processes experienced by the α-hydroxy radical of BP; the most important products are pinacols produced via steps 2 and 4. In addition, insertion of a second ketyl radical into the ortho, meta and para positions of a benzene ring from a BP radical can yield species called light absorbing transient, LAT.[16] The three different LAT products exhibit different reactivities, while some appear inert others react with O_2. [21,22] Included in scheme 1.2 are possible products of the LAT generation process. Steps 5 and 6 illustrate the formation of the two most probable LAT structures generated by addition of a radical R• (generated via H-atom abstraction from the donor RH) to the ortho and para positions of a benzene ring from the ketone function.

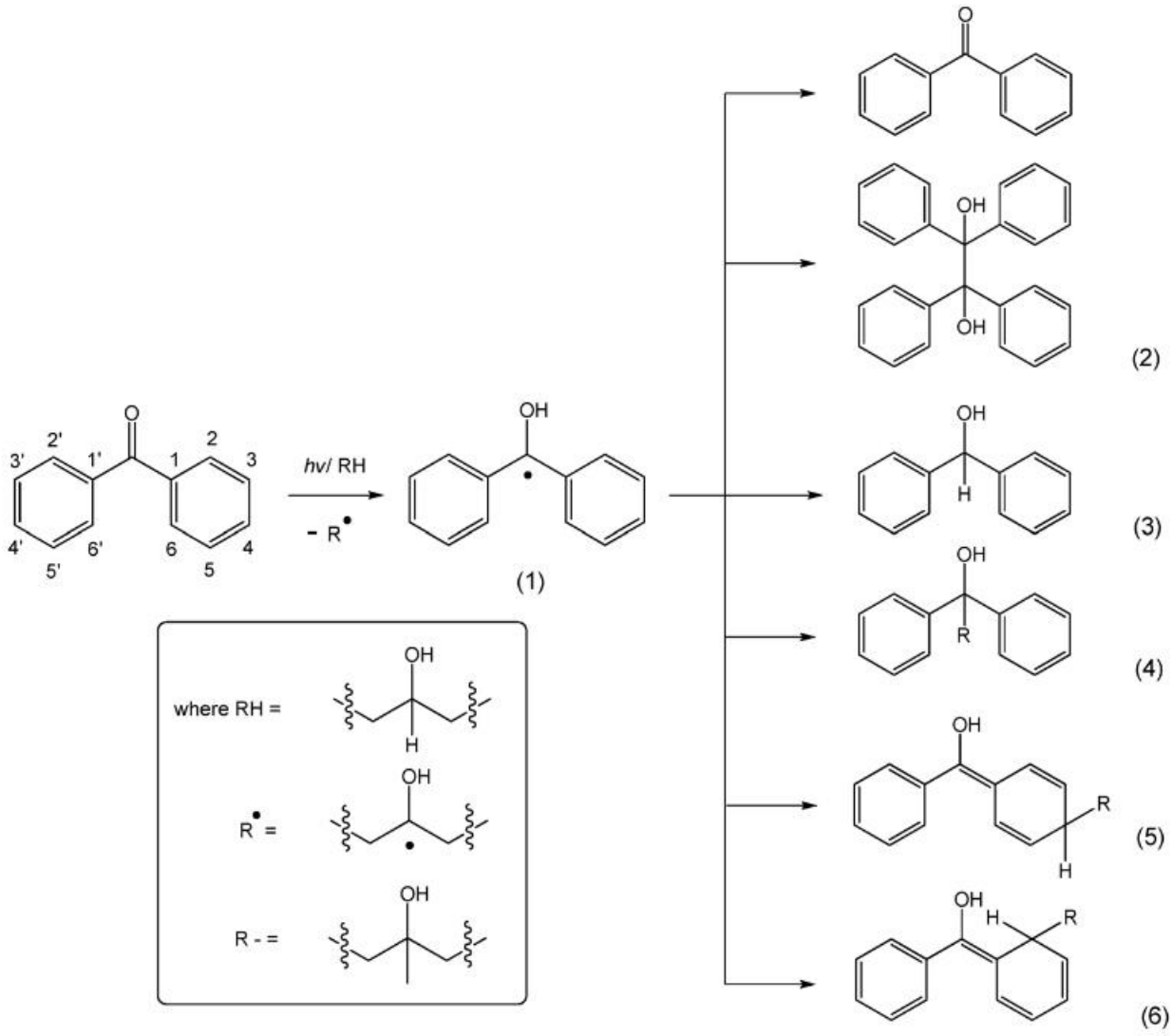

Scheme 1.2: Proposed reactions of the α-hydroxy BP radical inside poly(ethylene-vinyl alcohol) films free of oxygen.[20]

While the BP/2-propanol is an efficient system to form reducing radicals in solution, no simple system is known that produces BP radicals with high efficiency in solid-state matrices. In principle, photochemical systems comprising a polymeric photosensitizer containing BP functions together with a macromolecular H-atom donor could constitute a solid matrix capable of photogenerating BP radicals. Poly(ether ether ketone) (PEEK) is a highly ordered polymer containing a BP group in each monomer unit; however, this macromolecule possesses high

crystallinity and low solubility in most solvents. [23] Thus, sulfonation of PEEK was required to yield a derivative containing sulfonic groups that are soluble in water and useful as a solution photoinitiator.

1.3 Sulfonation and SPEEK/PVA system

Sulfonation of PEEK attaches a sulfonic acid group to the benzene ring linked, but not part of the ketone function, as shown in Scheme 1.3.

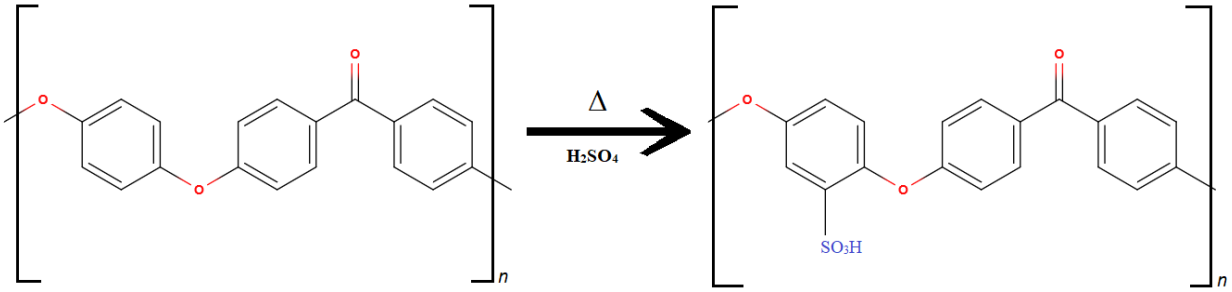

Scheme 1.3: Reaction scheme for the Sulfonation of PEEK

The sulfonation of PEEK has been confirmed with NMR, IR and elementary analysis, which showed that the degree of sulfonation, DS, determines the solubility of sulphonated poly(ether ether ketone), SPEEK. [24-27]. A high degree of sulfonation in SPEEK results in complete dissolution into water, allowing SPEEK to be used in liquid systems analogous to those containing BP. Similar to the BP/2-propanol solution system, combinations (or blends) of SPEEK and poly(vinyl alcohol), PVA, are assumed to form triplet (n, π*) excited states from the SPEEK carbonyl BP chromophore. Such excited states are anticipated to react with PVA through hydrogen abstraction with the generation of two α-hydroxy radicals: one of SPEEK (SPEEKH•) and another derived from PVA. The latter radical can then reduce another BP group of SPEEK forming a second BP α-hydroxy radical.[28] Previous studies on SPEEK/PVA mixtures (blends) in aqueous solutions have determined that photochemical reactions can be induced using

such polymer combinations.[28-31] Photolysis of SPEEK/PVA mixtures in solution yields SPEEKH• displaying an optical signal with a wavelength of maximum absorption (λ_{max}) of 565 nm; a representation of the formation process is presented in Scheme 1.4.[28]

Scheme 1.4

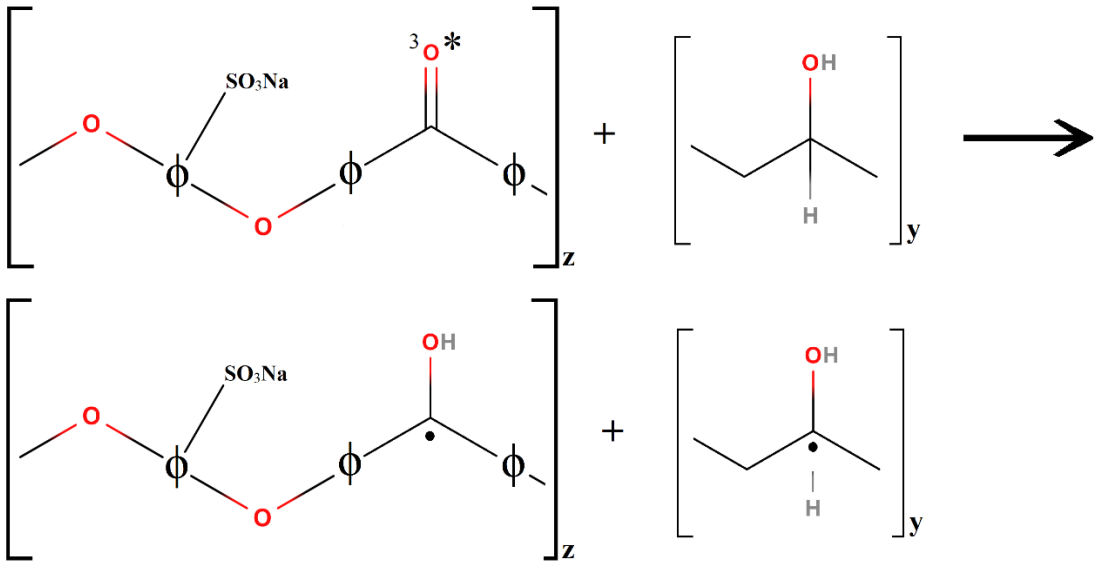

Scheme 1.4: Schematic representation of the reaction leading to SPEEK and PVA radicals. [28]

In the absence of air, the absorption of SPEEKH• centered at 565 nm decayed slowly via a second-order reaction between polyketone radicals. No such optical signal was detected in the presence of oxidizers such as Ag^+, O_2 and others, because SPEEKH• reduces them to metallic particles and H_2O_2, respectively. [28-31] Analogous reactions were detected upon exposure of films of SPEEK/PVA blends to light. [33-38] This was feasible since simple casting procedures enabled the preparation of transparent and flexible films of the blends with adjustable thicknesses in the micron range. H_2O_2 was formed efficiently in aqueous solutions of the blends as well as in water-swollen SPEEK/PVA films, the proposed reaction mechanism is shown in Scheme 1.5. However, reduction of O_2 in dry films is inefficient because oxygen diffusion is very slow in

such matrices.[34,35] The absence of oxygen reduction would facilitate radical-radical termination reactions, step 8 of Scheme 1.5.

Scheme 1.5

(1) $\{R'RC=O\}_z + h\nu \rightarrow {}^3\{R'RC=O\}_z^*$

(2) ${}^3\{R'RC=O\}_z^* + \{R'RCHOH\}_y \rightarrow \{R'RC\cdot OH\}_z + \{R'RC\cdot OH\}_y$

(3) $\{R'RC=O\}_z + \{R'RC\cdot OH\}_y \rightarrow \{R'RC\cdot OH\}_z + \{R'RC=O\}_y$

(4) $\{R'RC\cdot OH\}_z/\{R'RC\cdot OH\}_y + O_2 \rightarrow \{R'RC(OH)OO\cdot\}_z/\{R'RC(OH)OO\cdot\}_y$

(5) $\{R'RC(OH)OO\cdot\}_z/\{R'RC(OH)OO\cdot\}_y \rightarrow \{R'RC=O\}_z/\{R'RC=O\}_y + HO_2\cdot$

(6) $HO_2\cdot \rightarrow H^+ + \cdot O_2^-$

(7) $HO_2\cdot + H^+ + \cdot O_2^- \rightarrow H_2O_2 + O_2$

(8) $2\{R'RC\cdot OH\}_z/\{R'RC\cdot OH\}_y \rightarrow$ Combination/disproportionation products and light absorbing transients (LAT)

Scheme 1.5: Elementary steps for the photogeneration of radicals via photolysis of SPEEK/PVA systems and oxidation by O_2.[29,34] SPEEK is denoted as $\{R'RC=O\}_z$ and $\{R'RCHOH\}_y$ corresponds to PVA; $\{R'RC\bullet OH\}_z$ denotes SPEEKH• while the PVA radical is represented by $\{R'RC\bullet OH\}_y$. ${}^3\{R'RC=O\}_z^*$ corresponds to the triplet excited state of SPEEK.

LAT formation in SPEEK/PVA systems is anticipated to take place via radical-radical reactions similar to those occurring in the case of BP, except the para position of the benzene ring is blocked by the structure of the SPEEK polymer.[20] While several forms of LAT are unstable products that ultimately result in the irreversible transformation of BP that cannot be detected, addition of a radical at the ortho position of the ketone phenyl rings results in species that can be detected with UV/Vis spectroscopy. This LAT species is probably responsible for the signal exhibiting a maximum at ~ 410 nm that was noticed in air-free SPEEK/PVA solutions

illuminated for extended times. [33] A representation of a LAT species is presented in Figure 1.1. An undesirable consequence is that the LAT species can compete with the BP carbonyl group for the 350 nm photons, decreasing the ability of SPEEK to initiate photochemical reactions.

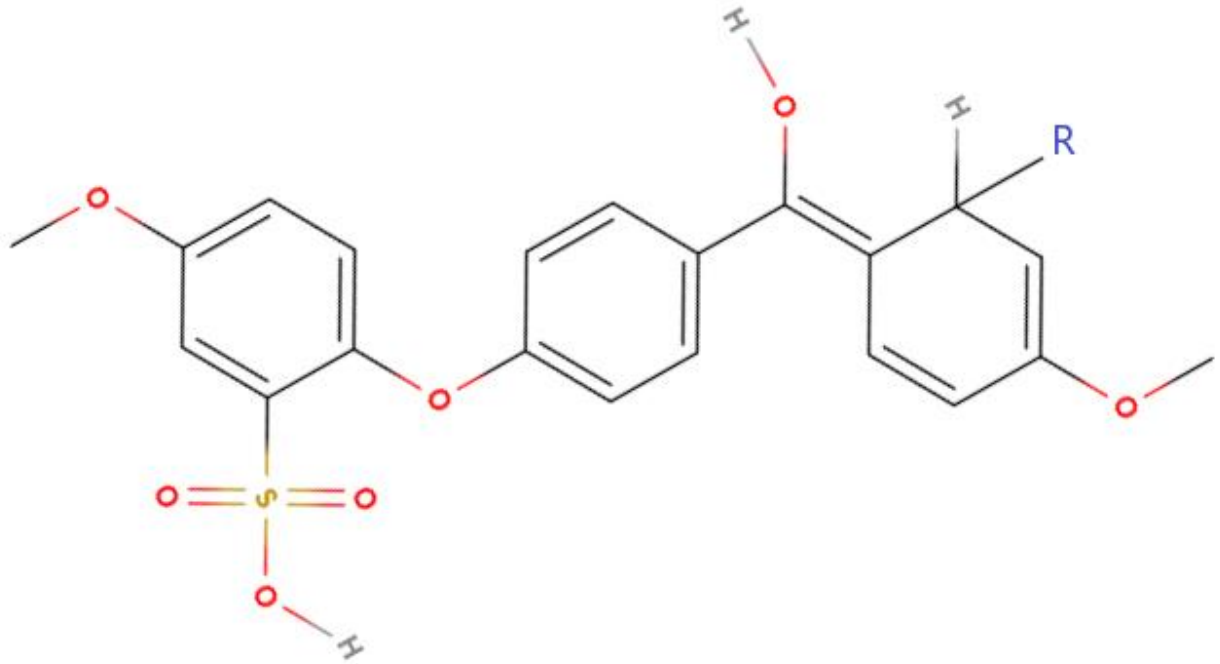

Figure 1.1: Structure of a possible LAT from the reaction between SPEEKH• and radical R•, with the latter representing either $\{R'RC\bullet OH\}_z$ or $\{R'RC\bullet OH\}_y$.

1.4 SPEEK/PVA redox dyes

There is a growing interest in thin film sensors that can warn of the presence of O_2 in food packages.[10] This is a key component of "intelligent" packaging that aims to limit O_2 exposure of edible materials thereby improving their preservation. Most studied are multicomponent systems loaded with redox indicating dyes.[9] They function as O_2 indicators exhibiting different colors depending on the redox state of the dye, which, in turn, can be altered by the presence of oxygen. A brief illumination of the sensitizer present in the films with UV light induces dye reduction to a stable state but exposure to O_2 reverts the redox indicator to the initial oxidized state exhibiting

an identifiable change. While such sensors work, they are complex and leakage of the toxic dyes from the systems into the food is a recurrent and serious issue. Previous work on SPEEK/PVA films involved incorporating such redox dyes and utilized thionine (Th) and cresyl violet (CV) which were reduced by SPEEKH• to their leuco forms. [39] Reduction of Th proceeded via a zero-order rate law with a rate constant of $k = 1 \times 10^{-5}$ Ms^{-1}. Complete oxidation of leuco Th and reduced CV took 30 - 45 days in dry SPEEK/PVA films; however, in wet films the oxidation occurred via first-order kinetics with $k = 2.37$ s^{-1}. [39] The oxidant that attacks the reduced dyes is O_2, and their slow oxidation processes result from the low oxygen permeability in PVA. [40,41] This is consistent with the increased oxidation rate noticed for swollen films that expand during water incorporation allowing for increased [O_2] and faster diffusion.

1.5 Purpose and goals

Extensive past investigations have shown that oxygen indicators using multicomponent films can be developed.[3,4] However, in most cases the re-oxidation of the reduced dye by reaction with O_2 (the reaction that indicates the presence of oxygen) is exceedingly slow, limiting the usefulness of the indicator system.[42] A similar problem plagued the previously studied SPEEK/PVA system containing Th and CV.[39] Additional issues of leaching of toxic components out of the films were also noticed. The overall goal of the project is in the reduction of complexity and toxicity which is desired for oxygen-permeable polymeric matrices used in dry film applications such as food packaging, biomedical applications, and personal protective equipment (PPE). The current investigation goal is the preparation of SPEEK-based films able to perform colorimetric sensing of oxygen under dry conditions relatively fast. To achieve this cellulose will be used in place of PVA which will serve as a transparent, flexible matrix and will also be the source of H-atoms that induce SPEEK photoreduction. These SPEEK/cellulose films

will also be cross-linked to hinder the migration of SPEEK into any aqueous solutions. As with the SPEEK/PVA system, SPEEK will not only be the sensitizer but also the color-changing element since photoreduction of this polymer yields a pink coloration due to the SPEEKH• signal centered at 565 nm.[33] As is typical of reducing α-hydroxy radicals, SPEEKH• decays quickly via reaction with O_2 and also through radical-radical processes.[28] The long lifetime of SPEEKH• in SPEEK/PVA films results from the exceedingly slow permeation of O_2 into dry PVA-based solid polymer matrices.[40,41] In contrast, some cellulose polymers exhibit a higher O_2 permeability;[3] for this reason cellulose-derived polymers were used in the present study.

The first objective, discussed in Chapter 2, was to develop a photoactive oxygen indicating system consisting of SPEEK and a cellulose polymer, followed by gaining an understanding about the operating reaction mechanism. Two different polymers, 2-hydroxyethyl cellulose (2-HEC) and carboxymethyl cellulose (NaCMC), were used as replacements for PVA. Cellulose-based polymers have been used previously as components of oxygen indicators,[3] but their potential ability to function as film matrices compatible with SPEEK and to serve as efficient H-atom donors for the triplet excited state of SPEEK were unknown. An increase in performance compared to previously studied SPEEK/PVA films was anticipated based on the higher O_2 permeability exhibited by 2-HEC and NaCMC. However, potential effects due to the different functional groups present in the cellulosic macromolecules were not easily predictable. The cross-linker was also changed from glutaraldehyde (Glu) to tartaric acid (Tar) to determine if a less toxic material could be used. Environmental conditions such as temperature and humidity were also studied in terms of how they affected the properties and performances of the films.

The second objective, which will be discussed in Chapter 3, was to incorporate the redox dye methyl viologen (MV^{2+}) into the SPEEK/cellulose systems. Previous work with SPEEK/PVA and SPEEK/cellulose systems with Th and CV indicated that their reduced leuco forms were oxidized very sluggishly by oxygen presumably because of electrostatic binding of the dyes to SPEEK due to the charge localization on the unhindered terminal amines.[39] MV^{2+} was chosen because charge localization was on the nitrogen atoms located in the aromatic ring hindering the ability to electrostatically bind to SPEEK and hinder O_2 diffusion. MV^{2+} present in SPEEK/cellulose is anticipated to be reduced by photogenerated SPEEKH• into the MV^{+} radical cation that exhibits a strong blue color. MV^{+} is oxidized by O_2, and the decay of the blue color will serve as an indication of the presence of oxygen. Studies of SPEEK/cellulose films containing methyl viologen will be centered on the oxidation kinetics of MV^{+} and the effect of environmental conditions.

The last objective, discussed in Chapter 4, involved an investigation of the photochemical behavior of SPEEK/NaCMC solutions and swollen films. Past experiences have shown that determination of reaction mechanisms is simpler when SPEEK photoreactions are studied in aqueous solutions as compared with films.[29,35] The reason is that diffusional restrictions of reactive intermediates typical of solid matrices are not significant in the fluid medium. In fact, knowledge gained in solution investigations served to explain mechanistically the photoreactions operating in films. Surprisingly, attempts to reproduce the photoreactions taking place in SPEEK/NaCMC films using air-free aqueous solutions were unsuccessful as no reduction of MV^{2+} was observed. On the other hand, illumination of SPEEK/NaCMC films swollen in Ar-bubbled solutions containing formate ions yielded MV^{+}, but the radical cation remained bound to the solid matrices. Furthermore, MV^{+} decayed subsequently (in the absence

of air) via an oxidation process and numerous cycles of photoreduction and dark oxidations were induced in a reproducible fashion. Results from efforts to understand the unusual reactions are presented.

References

1. Malone, K.; Weaver, S.; Taylor, D.; Cheng, H.; Sarathy, K. P; Mills, G. Formation kinetics of small gold crystallites in photoresponsive polymer gels. *J. Phys. Chem. B* **2002**, *106*, 7422-7431.
2. Lee, S.; Sheridan, M.; Mills, A. Novel UV-activated colorimetric oxygen indicator. *Chem. Mater.* **2005**, *17*, 2744-2751.
3. Wang, X.; Wolfveis, O. S. Optical methods for sensing and imaging oxygen: materials, spectroscopies and applications. *Chem. Soc. Rev.* **2014**, *43*, 3666-3761.
4. Mills, A.; Hazafy, D.; Lawrie, K. Novel photocatalyst-based colourimetric indicators for oxygen. *Catal. Today* **2011**, *161*, 59-63.
5. Vu, C. H.; Won, K. Novel water-resistant UV-activated oxygen indicator for intelligent food packaging. *Food Chem.* **2013**, *140*, 52-56.
6. Marek, P.; Velasco-Velez, J. J.; Haas, T.; Doll, T.; Sadowski, G. Time-monitoring sensor based on oxygen diffusion in an indicator/polymer matrix. *Sens. Actuators, B* **2013**, *178*, 254–262.
7. Khankaew, S.; Mills, A.; Yusufu, D.; Wells, N.; Hodgen, S.; Boonsupthip, W.; Suppakul, P. Multifunctional anthraquinone-based sensors: UV, O_2 and time. *Sens. Actuators, B* **2017**, *238*, 76–82.
8. Yan, Q.; Han, D.; Zhao, Y. Main-chain photoresponsive polymers with controlled location of light-cleavable units: from synthetic strategies to structural engineering. *Polym. Chem.* **2013**, *4*, 5026–5037.
9. Mills, A. Oxygen indicators and intelligent inks for packaging food. *Chem. Soc. Rev.* **2005**, *34*, 1003-1011.

10. Yousefi, H.; Su, H.-M.; Imani, S. M.; Alkhaldi, K.; Filipe, C. D. M.; Didar, T. F. Intelligent food packaging: a review of smart sensing technologies for monitoring food quality. *ACS Sens.* **2019**, *4*, 808-821.

11. Gibis, D.; Rieblinger, K. Oxygen scavenging films for food application. *Procedia Food Sci.* **2011**, *1*, 229–234.

12. Ghaani, M.; Cozzolino, C. A.; Castelli, G.; Farris, S. An overview of the intelligent packaging technologies in the food sector. *Trends Food Sci. Technol.* **2016**, *51*, 1-11.

13. Ollis, D.; Mills, A.; Lawrie, K.; Kinetics of methylene blue (MB) photocatalyzed reduction and dark regeneration in a colorimetric oxygen sensor, *Appl. Catal. B,* **2016**, *184*, 201-207.

14. Wells, L. A.; Lasowski, F; Fitzpatrick, S. D.; Sheardow, H. CRC *Crit. Rev. Bioeng.* **2010**, *38*, 487–50.

15. Gilbert, A.; Baggott, J. Essentials of molecular photochemistry, CRC *Press: Boca Raton*, **1991**; 287-353.

16. Rubin, M. B. New observations on the photopinacolization of benzophenone in aliphatic alcohol. *Tetrahedron Lett.* **1982**, *23*, 4615-4618.

17. Chilton, J.; Giering, L.; Steel, C. The effect of transient photoproducts in benzophenone-hydrogen donor systems. *J. Am. Chem. Soc.* **1975**, *98*, 1865.

18. Du, Y.; Ma, C.; Kwok, W. M.; Xue, J.; Phillips, D. Time-resolved resonance raman identification and structural characterization of a light absorbing transient intermediate in the photoinduced reaction of benzophenone in 2-propanol. *J. Org. Chem.* **2007**, *72*, 7149-7156.

19. Brauchie, C.; Burland, D. M.; Bjorklund, G. C. Hydrogen abstraction by benzophenone studied by holographic photochemistry. *J. Phys. Chem.* **1981**, *85*, 127-129.

20. Scully, A. D.; Horsham, M. A.; Aguas, P.; Murphy, J. Transient products in the photoreduction of benzophenone derivatives in poly(ethylene-vinyl alcohol) film. *J. Photochem. Photobiol. A,* **2008**, *197*, 132–140.

21. Demeter, A.; Berces, T. Study of the long-lived intermediate formed in the photoreduction of benzophenone by isopropyl alcohol. *J. Photochem. Photobiol. A,* **1989**, *46*, 27 - 40.

22. Costa, C. V.; Grela, M.A.; Churio, M.S. On the yield of intermediates formed in the photoreduction of benzophenone. *J. Photochem. Photobiol. A,* **1996**, *99*, 51-56.

23. Devaux, J.; Delimoy, D.; Daoust, D.; Legras, R.; Mercier, J.P. On the molecular weight determination of a poly(aryl-ether-ether-ketone) (PEEK). *Polymer,* **1985**, *26*, 1994-2000.

24. Jin, X.; Bishop, M. T.; Ellis, T. S.; Karasz, F. E. A sulphonated poly(aryl ether ketone). *Brit. Poly. J.* **1985**, *17*, 4-10.

25. Xing, P.; Robertson, G. P.; Guiver, M. D.; Mikhailenko, S. D.; Wang, K.; Kaliaguine, S. Synthesis and characterization of sulfonated poly(ether ether ketone) for proton exchange membranes. *J. Membr. Sci.* **2004**, *229*, 95–106.

26. Lakshmi, M.; Choudhary, V.; Varma, I. K. Sulphonated poly(ether ether ketone): synthesis and characterisation. *J. Mater. Sci.* **2005**, *40*, 629-636.

27. Bishop, M.T.; Karasz, F.E.; Russo, P.S. Solubility and properties of a poly(ary1 ether ketone) in strong acids. *Macromolecules* **1985**, *18*, 93-98.

28. Korchev, A. S.; Shulyak, T. S.; Slaten, B. L.; Gale, W. F.; Mills, G. Sulfonated poly(ether ether ketone)/poly(vinyl alcohol) sensitizing system for solution

photogeneration of small Ag, Au, and Cu crystallites. *J. Phys. Chem. B,* **2005**, *109*, 7733-7745.

29. Little, B. K.; Lockhart, P.; Slaten, B. L.; Mills, G. Photogeneration of H_2O_2 in SPEEK/PVA aqueous polymer solutions. *J. Phys. Chem. A* **2013**, *117*, 4148-4157.
30. Black, J. R.; Islam, M.S.; Carmichael, H.L.; Slaten, B.L.; Little, B. K.; Mills, G. Radical chain reduction of CCl_4 initiated by illumination of SPEEK solutions. *J. Phys. Chem. A* **2017**, *121*, 3918-3928.
31. Islam, M.S.; Duin, E.C.; Slaten, B.L.; Mills, G. Photoreduction of $CHCl_3$ in aqueous SPEEK/HCO_2^- solutions involving free radicals. *J. Phys. Chem. A* **2018**, *122*, 7118−7130
32. Korchev, A. S. ; Bozak, M. J.; Slaten, B. L.; Mills, G. Radical-induced generation of small silver particles in SPEEK/PVA polymer films: direct metal photopatterning. *J. Am. Chem. Soc.* **2004**, *126*, 10-11.
33. Korchev, A. S.; Konovalova, T.; Cammarata, V.; Kispert, L.; Slaten, B. L.; Mills, G. Radical-induced generation of small silver particles in SPEEK/PVA polymer films and solutions: UV-Vis, EPR, and FT-IR Studies. *Langmuir* **2006**, *22*, 375-384.
34. Lockhart, P.; Little, B. K.; Slaten, B. L.; Mills, G. Photogeneration of H_2O_2 in Water-Swollen SPEEK/PVA Polymer Films. *J. Phys. Chem. A* **2016**, *120*, 3867–3877.
35. Korchev, A.S.; Sartin, M.; Mills, G.; Slaten, B.L.; Gale, W.F. Light induced metal nanoparticle formation (M=Ag,Au,Cu,Pd,Pt) in aqueous solutions and polymer films composed of SPEEK-PVA. *Int. Symp. Clusters Nano-Assem.* **2003**, *10*, 371-377.
36. Jena, P.; Khanna, S. N.; Rao, B. K.; Korchev, A. S.; Sartin, M.; Mills, G.; Slaten, B. L.; Gale, W. F. Light induced metal nanoparticle formation (M=Ag,Au,Cu,Pd,Pt) in aqueous solutions and polymer films composed of SPEEK-PVA. *In Clusters and nano-*

assemblies: Physical and biological systems: International symposium on clusters and Nano-Assemblies: Physical and biological systems, held in Richmond, Virginia from November 10-13, 2003; World Scientific, **2005**; pp 371–377.

37. Korchev, A.S.; Bozack, M.J.; Slaten, B. L.; Mills, G. Polymer-initiated photogeneration of silver nanoparticles in SPEEK/PVA films: direct metal photopatterning. *J. Am. Chem. Soc.* **2004**, *126*, 10-11.

38. Korchev, A. S.; Foti, K.; Sartin, M.; Slaten, B. L.; Gale, W.; Mills, G. Photogeneration kinetics of Ag nanoparticles in light sensitive polymer films. *NSTI Nanotech* **2007**, *2*, 140-142.

39. Dissanayaka, R. H. Reversible and irreversible light-induced reactions initiated by SPEEK/PVA polymer systems. Ph.D. Thesis, Auburn University, May 2021.

40. Lien, L.; Fellows, C. M.; Copeland, L.; Hawkett, B. S.; Gilbert, R, G. Water-binding and oxygen permeability in poly(vinyl alcohol) films. *Aust. J. Chem.* **2002**, *55*, 507-512.

41. Chuang, W.Y.; Young, T.H.; Chiu, W.Y.; Lin, C.Y. The effect of polymeric additives on the structure and permeability of poly(vinyl alcohol) asymmetric membranes. *Polymer* **2000**, *41*, 5633–5641.

42. Ollis, D.; Mills, A.; Lawrie, K. Kinetics of methylene blue (MB) photocatalyzed reduction and dark regeneration in a colorimetric oxygen sensor. *Appl. Catal. B Environ.* **2016**, *184*, 201-207.

Chapter 2

2.1 Introduction

Photoactive mixtures of the polymers SPEEK and PVA have been shown to initiate numerous photoreactions in aqueous solutions. Previous work with the SPEEK/PVA system determined that in the absence of air, the absorption of SPEEKH• centered at 565 nm decayed slowly via second-order reactions between the radicals.[1] In the presence of oxidizers such as metal ions (Ag^{+}, Cu^{2+}, Au^{3+}) and halomethanes, SPEEKH• induced efficient formation of metal particles or reductive dehalogenations.[1] Photolysis of air-containing solutions or of water-swollen SPEEK/PVA films resulted in O_2 reduction to H_2O_2.[2,3] In contrast, the reduction of oxygen via illumination of dry SPEEK/PVA films is not efficient due to the low O_2 permeability in PVA, the main macromolecular component of the solid matrices.[3,4] The slow oxygen diffusion in PVA limits the usefulness of SPEEK/PVA blends free of H_2O for processes that require the participation of O_2 as a reactant. Such limitation may be circumvented through identification of polymers possessing a higher O_2 permeability which could act as substitutes for PVA. This would allow SPEEK systems not to be limited to wet applications, opening possibilities for utilization in sensing applications of specialized packaging that prevent food spoilage due to oxygen intrusion. [5-8]

The first goal of the present study is to assess the suitability of oxygen permeable polymer blends of cellulose-based systems using a procedure like the previously developed for SPEEK/PVA films.[9] SPEEKH• reacts swiftly with oxygen in films,[4] and spectrophotometric detection of the radical signal was used to determine if O_2 diffusion occurred in dry SPEEK/cellulose films. A second objective was to determine if high enough [SPEEKH•] was attainable using SPEEK/cellulose films, in which case the radical could serve directly as the

sensor for O_2 without the need of redox dyes., Ideal oxygen sensors are expected to indicate the presence of O_2 via a color change large enough to be detected visually. Large [SPEEKH•] can be photogenerated in SPEEK/PVA films under air due to the small oxygen concentrations present in such systems. However, the faster diffusion of oxygen anticipated for SPEEK/cellulose films could limit the [SPEEKH•] attainable in such systems. This, in turn, may limit the usefulness of SPEEK/cellulose films as oxygen indicators. Detection of the SPEEKH• signal will enable the assessment of the reaction kinetics for the SPEEK/cellulose systems in comparison with that of SPEEK/PVA films, providing information about any mechanistic differences. This will also be used to determine kinetic differences between the two cellulose systems, 2-HEC and NaCMC, and to assess possible effects induced by the different functional groups present in the two polymers. In addition, the influence of an alternative cross-linker as well as environmental conditions (temperature and ambient humidity) on the reaction kinetics will be investigated.

2.2 Methods and Procedures

Preparation of SPEEK used PEEK provided by Solvay with an average molar mass of M_n = 4.0 x 10^4 g/mol. Both 2-HEC and NaCMC (with an average molecular weight M_n = 9.0 x 10^4 g/mol) were from Sigma-Aldrich. NaOH, HCl, and H_2SO_4 were purchased from Fisher Scientific while other materials were provided by VWR. All solutions were prepared with purified water obtained from a Milli-Q Biocel system. Sulfonation of PEEK involved heating under stirring a suspension of the polymer in 40 mL of concentrated H_2SO_4 with an oil bath utilizing a VWR 7x7 hot/stir plate, the temperature was controlled at 55°C using a HH11B Omega digital thermometer equipped with a type K thermocouple. Once the desired temperature was achieved, 9 g of powered PEEK were added and the reaction was carried out for 7 days. At this point, the solution contained sulfonated poly(ether ether ketone), SPEEK, with a degree of sulfonation of about

99%.[3] The hot solution was slowly poured into a 3 L of a 1:5 HCl:H_2O mixture at T < 5 °C under constant stirring. Slow addition of the hot solution averted formation of large SPEEK aggregates and prevents the temperature from rising above 5 °C, which would increase the SPEEK dissolution in the aqueous mixture. The solution was then filtered using a Buchner funnel with Whatman 41 filter paper and rinsed with 250 mL of water at T < 5 °C. Then the solid SPEEK was repeatedly rinsed with 250 mL of a 0.2 M NaOH solution (also at T < 5 °C); this was followed by another rinse with 250 mL of cold water until the pH was between 5-7. The resulting SPEEK was then dried at 90 °C in an oven and ground utilizing a motorized grinder. If the powder retained a reddish color, the polymer was rinsed again using the funnel/filter paper combination together with cold H_2O until either a brownish/yellow product or white crystals resulted.

Cellulose/SPEEK films were made via preparation of an 8.4 x 10^{-6} M SPEEK solution (in terms of polymer chains mass) in a 50 mL beaker heated at ~45-50 °C under continuous stirring. A separate solution with 8.1 x 10^{-4} M (in terms of polymer chains) cellulose was prepared in another 50 mL beaker under the same conditions; in the case of NaCMC an equivalent molar amount of HCl was added (using a 1.5 M acid solution) to protonate the carboxylate groups of the cellulose. These solutions were then mixed under constant heating and stirring for a minimum of 30 min. After slowly cooling the resulting solution to room temperature, 0.375 mL - 2.25 mL of a 0.1 M glutaraldehyde (Glu) or tartaric acid (Tar) solution was added while maintaining stirring to achieve a homogeneous mixture. Then 0.75 mL – 3 mL of 0.5 M HCl (based on the amount of crosslinker used) were added; the resulting mixture was stirred for 30 s to facilitate polymer cross-linking. Finally, the solution was poured onto a 12.7 cm by 12.7 cm glass mold shown in Figure 2.1 and dried at room temperature overnight (~22°C). The dried

films were then removed and stored at 4°C until additional testing could be conducted. Initial attempts to fabricate water-insoluble films using hydroxypropyl cellulose were unsuccessful; presumably because the low molar mass of the polymer prevented efficient crosslinking. 2-HEC or NaCMC with M_n similar to that of PVA (M_n = 8.9-9.8 x 10^4 g/mol) served to prepare polymer films containing 30:70 wt% SPEEK/polymer.[3] Tar or Glu served as cross-linkers and β-cyclodextrin was added to possibly increase oxygen diffusion. The structures of these compounds are shown in Scheme 2.1.

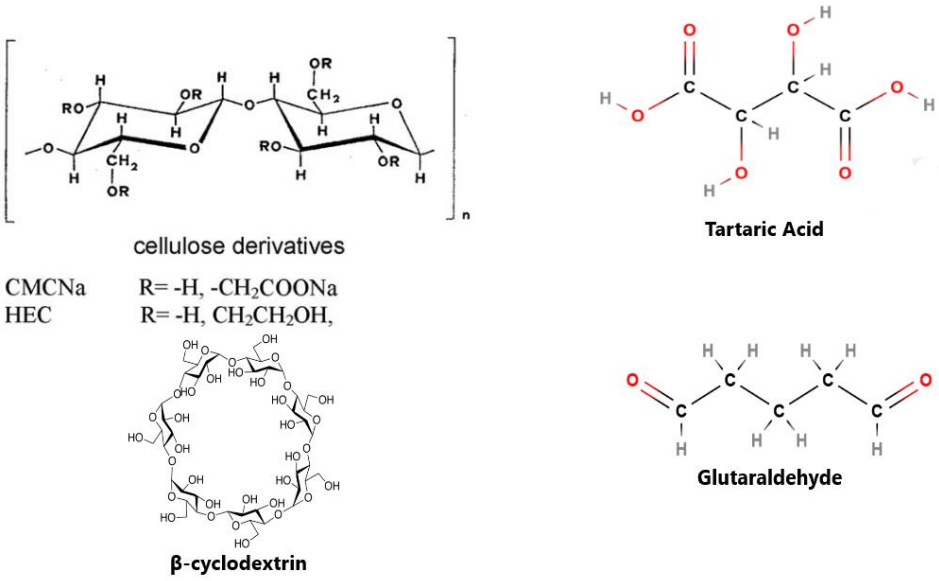

Scheme 2.1: Structures of the compounds involved in the preparation of cellulose-SPEEK photosensitive films including those of the crosslinkers Tar and Glu.[10]

Miniwax fast drying polyurethane (PU) was used as a coating to prevent SPEEK loss from the films. Determination of film thickness used digital micrometers Mitutoyo model 1″ SFB and iGaging model 1″. SPEEK/2-HEC films were brittle as compared to their PVA counterparts and exhibited a typical thickness of 50 (±10) μm. The speed of solution stirring impacted the properties of the resulting cellulose-based films, velocities below 500 rpm yielded uniform and bubble-free materials. Above 500 rpm, the solutions contained numerous microbubbles that

remained in the films after drying. Illumination of cellulose polymer films was conducted inside a Rayonet RPR-100 circular illuminator equipped with 16 RPR-3500A lamps. The Rayonet generates 350 ± 15nm photons with a light intensity (I_0) of 10 μM/s as determined using the Aberchrome 540 actinometer.[11] Under photolysis the temperature inside the illuminator amounted to 29 °C; unless otherwise specified all other experiments occurred at room temperature (~22 °C). Reproducible exposure of the films was achieved by inserting them in a Shimadzu film holder shown in Fig. 1.

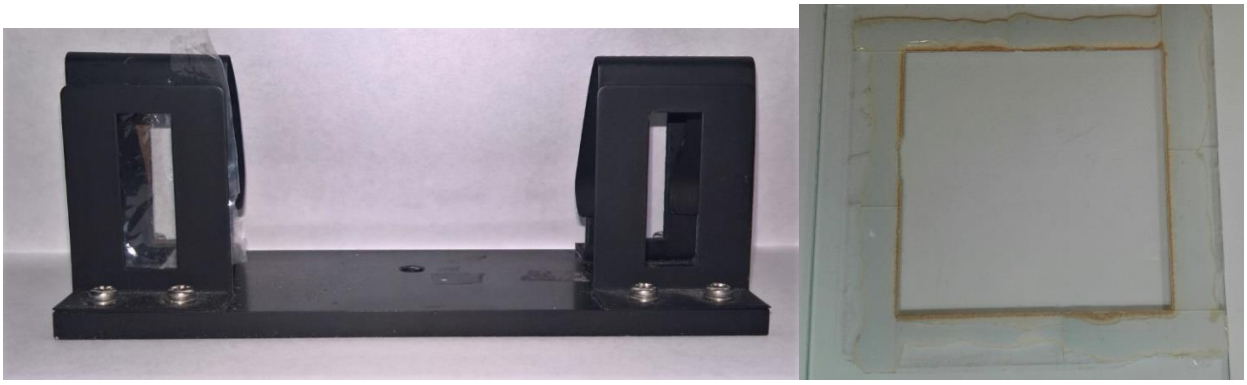

Figure 2.1: The left image shows the Shimadzu holder with a polymer film positioned on the left clip; a 12.7 cm x 12.7 cm film mold with a depth of 1.2 mm is presented in the right image.

Films were rinsed in 40 mL of water for a minimum of 5 min to remove excess acid, elimination of HCl was needed since protons quench the excited state of SPEEK. Illuminations occurred under air and lasted 3 min since preliminary experiments identified this period as the optimum to generate a maximum absorbance of SPEEKH• in films. Optical spectra were collected by means of a Shimadzu UV-2501 PC UV-VIS spectrophotometer. Efforts to detect H_2O_2 as a product of the reduction of O_2 by SPEEKH• employed the I^-/I_3^- method used previously to quantify [H_2O_2] in experiments with SPEEK/PVA films swollen in water.[3] While this method can detect μM concentrations of H_2O_2 (or of organic peroxides),[2] no such compounds were found upon immersing photolyzed films into a solution of the iodide reagent. All experiments were run at

least in triplicate; the resulting kinetic results exhibited deviations of about 20%, which is typical of heterogeneous film systems.[3] Environmental conditions of relative humidity (R.H.) and temperature were measured using JEDEW hygrometer/thermometers model ROUND which have a relative humidity range of 20% - 90%.

2.3 Results and Discussion

Preparation of structurally stable and optically transparent polymer films containing 30:70 SPEEK/polymer wt% was successful employing 2-HEC and NaCMC as the main polymeric

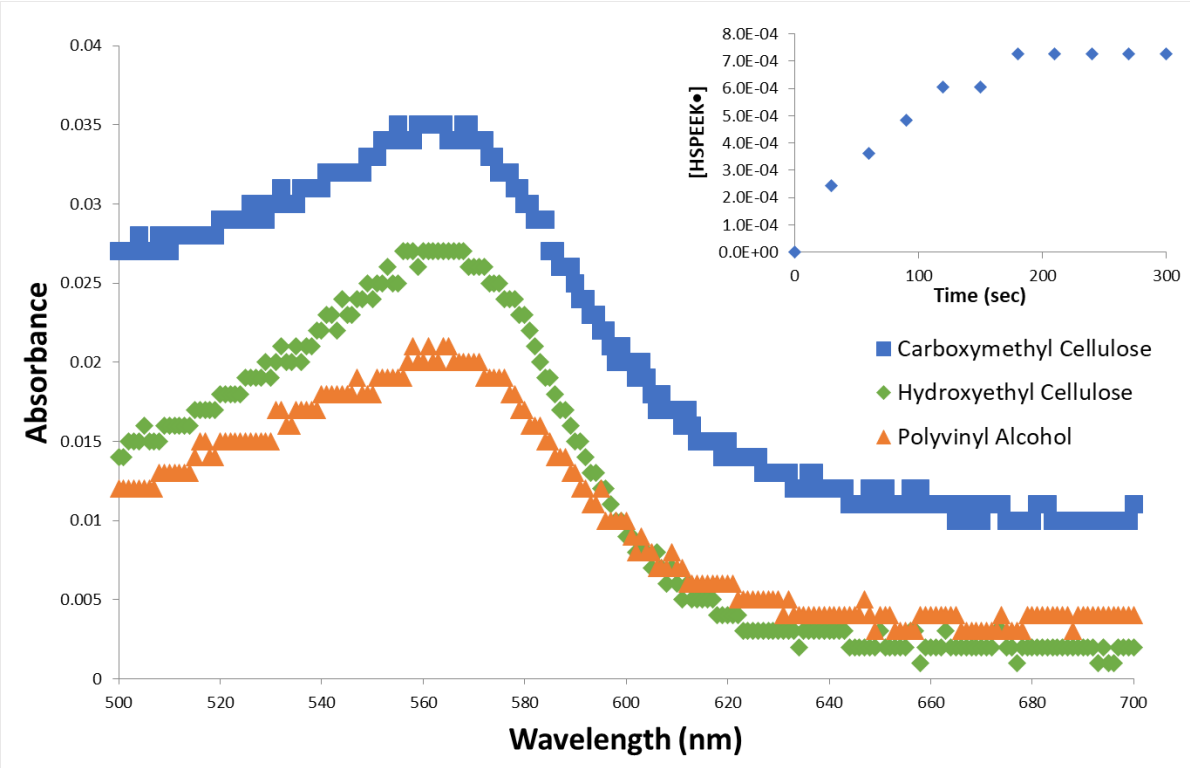

Figure 2.2: Comparison of spectra obtained from SPEEK-based films illuminated with 350 nm photons for 3 min featuring the radical signal with λ_{max} = 565 nm; (▲) PVA film, (■) NaCMC film, and (♦) 2-HEC film. The inset depicts the evolution of [SPEEKH•] in a SPEEK/2-HEC film over 5 min using 30 s illumination intervals.

component. Exposure of SPEEK/cellulose films to 350 nm photons resulted in a pink coloration due to generation of the polyketone radicals.[4] Depicted in Figure 2.2 are optical spectra collected

after 3 min of illumination of SPEEK/cellulose films and of a SPEEK/PVA film. In all cases a signal with λ_{max} = 565 nm was noticed and the spectrum of the SPEEK/PVA film matched the one reported earlier for such system.[12] These observations demonstrate that SPEEKH• was indeed generated in SPEEK/cellulose films. Considering that SPEEKH• is sensitive to the presence of O_2,[4] the results of Figure 2.2 indicate that the SPEEK photoreduction was faster at short illumination times than competing dark reactions such as the O_2-induced SPEEKH• oxidation and the radical-radical decay process. A constant intensity of the signal at 565 nm resulted at illumination times ≥ than 3 min, implying that a steady-state radical concentration was reached shown in the inset of Figure 2.2.

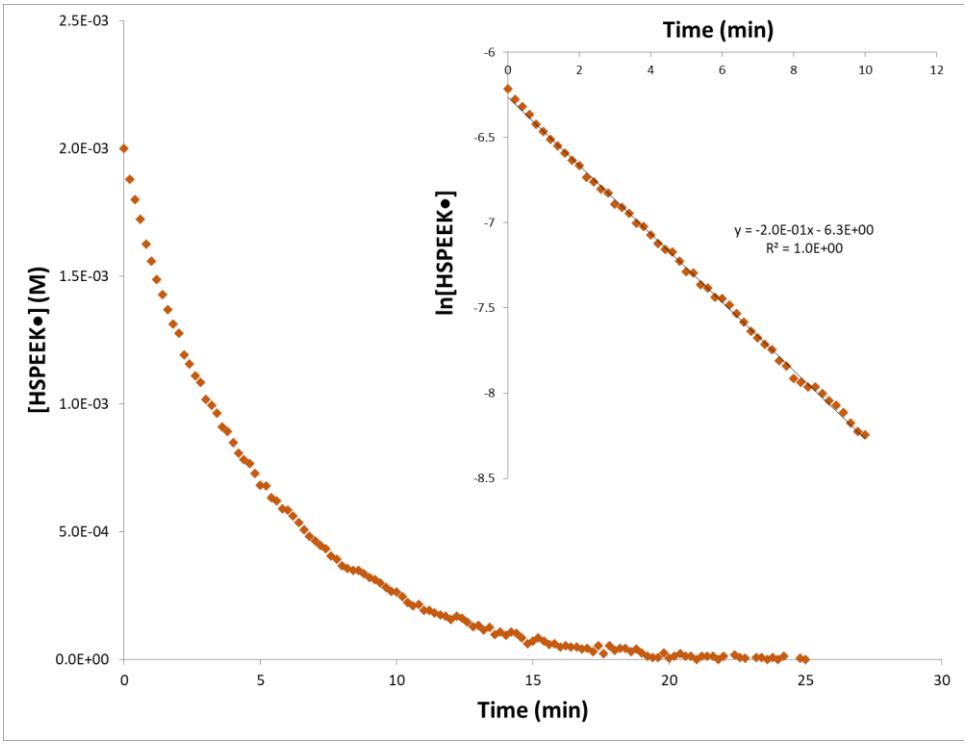

Figure 2.3: Kinetics of the radical oxidation under air in a SPEEK/2-HEC film cross-linked with 7.5 x 10^{-5} mol Glu with 0.051 mm thickness; the inset shows a first-order plot of the data.

The rate at which SPEEKH• is consumed (both via oxidation and radical-radical decay) increases as [SPEEKH•] rises. Conditions will eventually be reached during illumination where

the rate of radical decay is equal to the speed of the SPEEK photoreduction. Obviously, such conditions were achieved at illumination times of 3 min or longer. The kinetics of SPEEKH• oxidation in the presence of air in SPEEK/2-HEC films was monitored spectrophotometrically by following the decay of the signal at 565 nm over time, typical results are shown in Figure 2.3. Fits to the data were attempted using first and second-order rate laws after evaluation of [SPEEKH•] from the absorbance values. The calculation employed the Lambert-Beer law and an extinction coefficient (ε) for the radical signal at 565 nm of 3.5×10^3 M^{-1} cm^{-1},[1] together with a pathlength equal to the thickness of the particular film. As shown in the inset of Figure 2.3, a straight line resulted upon plotting the data according to a first-order rate law with $k = 0.2$ min^{-1}, or 3.3×10^{-3} s^{-1}. Efforts to fit the results in terms of a second-order decay were unsuccessful. For films consisting of 30:70 wt% SPEEK/PVA a pseudofirst-order rate constant of 1×10^{-3} s^{-1} was reported for the SPEEKH• decay in the presence of air.[4] In contrast, the polyketone radical persisted for several hours when photolysis of such films was conducted in the absence of air and the SPEEKH• decay obeyed no simple rate law. This is not surprising as the α-hydroxy radical of PVA decayed via complex kinetics in air-free solutions due to entanglement and hindered diffusion of the macromolecules.[13] The rate constant for the SPEEKH• decay under air is 3 times higher for films containing 2-HEC instead of PVA presumably due to the 100 times higher oxygen permeability in cellulosic materials as compared with that of PVA.[14]

The radical formation and oxidation in SPEEK/cellulose films can be understood in terms of the mechanism shown in Scheme 2.2, which is a modified version of the elementary steps proposed for SPEEK/PVA films.[3] Since peroxide products were not detected, a logical conclusion is that O_2 was fully reduced to H_2O. While the steady state $[O_2]$ within SPEEK/cellulose films remains unknown, reduction of oxygen to H_2O is a four-electron process

consuming 4 polymer radicals. This means that SPEEKH• is consumed faster than oxygen, which preserves the condition of an O_2 excess and enables step 5 to proceed via pseudofirst-order kinetics. Under such conditions,

Scheme 2.2

(1) $\{R'RC=O\}_z + h\nu \rightarrow {}^1\{R'RC=O\}_z^*$

(2) ${}^1\{R'RC=O\}_z^* \rightarrow {}^3\{R'RC=O\}_z^*$

(3) ${}^3\{R'RC=O\}_z^* + \{R'RCHOH\}_y \rightarrow \{R'RC\cdot OH\}_z + \{R'RC\cdot OH\}_y$

(4) $\{R'RC=O\}_z + \{R'RC\cdot OH\}_y \rightarrow \{R'RC\cdot OH\}_z + \{R'RC=O\}_y$

(5) $\{R'RC\cdot OH\}_z/\{R'RC\cdot OH\}_y + O_2 \rightarrow \{R'RC(OH)OO\cdot\}_z/\{R'RC(OH)OO\cdot\}_y$

(6) $4\{R'RC(OH)OO\cdot\}_z/\{R'RC(OH)OO\cdot\}_y \rightarrow 4\{R'RC=O\}_z/\{R'RC=O\}_y + 2H_2O + 3O_2$

(7) $2\{R'RC\cdot OH\}_z/\{R'RC\cdot OH\}_y \rightarrow$ Combination/disproportionation products and light absorbing transients (LAT)

Scheme 2.2: Mechanism for the formation and oxidation of SPEEKH• in SPEEK/cellulose films, adapted from Scheme 1.5 from Chapter 1. SPEEK is denoted as $\{R'RC=O\}_z$ and $\{R'RCHOH\}_y$ corresponds to cellulose; $\{R'RC\bullet OH\}_z$ denotes SPEEKH• while the cellulose radical is represented by $\{R'RC\bullet OH\}_y$. ${}^1\{R'RC=O\}_z^*$ corresponds to the singlet excited state of SPEEK. ${}^3\{R'RC=O\}_z^*$ corresponds to the triplet excited state of SPEEK.

that is $[O_2] >> [SPEEKH\bullet]$, the pseudofirst-order radical decay is anticipated to follow the expression: $\ln[SPEEKH\bullet] = -kt + \ln[SPEEKH\bullet]_0$. According to the mechanism shown in Scheme 2.2, the data of Figure 2.3 corresponds to step 5 with $k_5 = 3.3 \times 10^{-3}$ s^{-1}. When oxygen diffusion in the film is less efficient $[O_2]$ may approach that of SPEEKH•, in which case step 5 would proceed according to the second-order equation: $1/[SPEEKH\bullet] = 1/[SPEEKH\bullet]_0 + kt$. However, decay of SPEEKH• via step 7 may also follow second-order kinetics as noticed in air-

free SPEEK/PVA solutions.[1] (Included in step 7 is the formation of LAT due to insertion of the radical from the H-atom donor, cogenerated in step 4, into one of the aromatic rings of a benzophenone group from SPEEKH• discussed in the previous chapter.) This means that, in principle, two different reaction channels for the decay of SPEEKH• may follow a second-order rate law.

To test if step 7 was the predominant SPEEKH• decay process in the absence of O_2, photolytic experiments were performed in the absence of air using a sealed quartz cell.

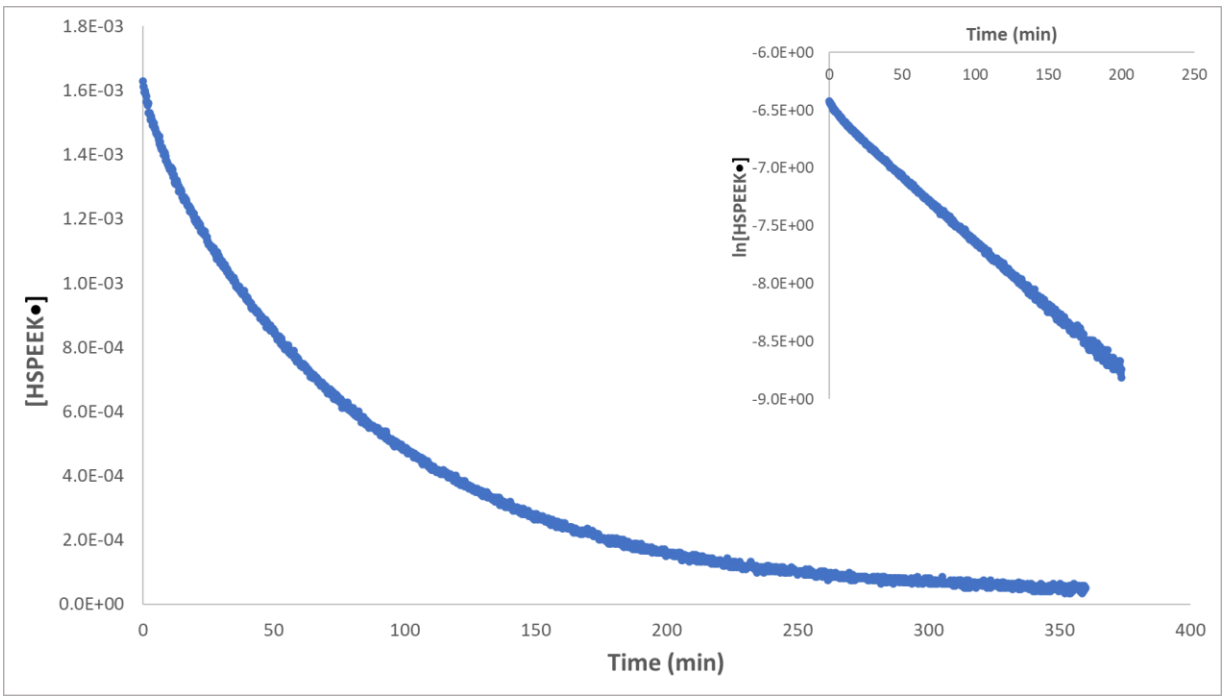

Figure 2.4: Kinetics of the radical oxidation of a SPEEK/2-HEC film under N_2; the inset shows the corresponding first-order plot of the data.

Presented in Figure 2.4 is [SPEEKH•] displayed as a function of time for a SPEEK/2-HEC film first degassed with nitrogen for several hours and then photolyzed. While the radical signal decayed initially via a complex process, at longer times the decay was slow following a pseudofirst-order function of time with k_{decay} = 1.13 x 10^{-2} min^{-1} or 1.88 x 10^{-4} s^{-1} shown in the

inset of figure 2.4. This finding was surprising because the usual decay of α-hydroxy radicals is via step 7, as was found for SPEEKH• in air-free solutions.[1] However, the SPEEKH• decay in the absence of air was much slower than that observed when air was present; the rate constant of the former process being about 18 times lower than k_5. The fact that the oxygen attack on SPEEKH• via step 5 was always faster than the radical decay in the dark is unsurprising due to restrictions on radical diffusion imposed by the solid matrix. Indeed, findings about LAT formation to be presented later indicate that step 7 occurred mainly under illumination, where the steady state [SPEEKH•] is high. According to the data of Figure 2.4, a second-order SPEEKH• decay via step 7 was not predominant after stopping photolysis. The slow first-order decay of SPEEKH• in the absence of O_2 implied that another oxidizer was photogenerated, which will be discussed in Chapter 4.

An important difference between film experiments with and without air is that degassing with dry N_2 induces drying of the films. Such an effect was made evident by the fact that the flexibility of dry films is lower than that those exposed to ambient air humidity. Since the amount of O_2 present in the films is dependent on the water content, degassing with nitrogen contributes to extracting oxygen out of the solid polymer matrices. This means that $[O_2]$ in the films is influenced by the H_2O content of the solid polymer matrices, which correlates with the humidity of ambient air. This line of reasoning predicts that the kinetics of step 5 will be influenced by the humidity of air, and the experimental results presented below are consistent with such prediction.

Experiments employing different cross-linker concentrations showed that [Glu] < 3.75×10^{-5} mol yielded SPEEK/2-HEC films that dissolved during washing steps aiming to eliminate the HCl from the solid matrices. Thus, [Glu] > 3.75×10^{-5} mol were utilized and yielded more compact

and rigid films in which the SPEEKH• decay followed a pseudofirst-order rate law, see Figure 2.5A. Obviously, the radical oxidation rate was not affected (within experimental error) by changes in cross-linker concentration. However, entanglement of SPEEK with the cellulose polymer chains was inefficient when [Glu] < 1.5 x 10^{-4} mol, resulting in an unacceptable

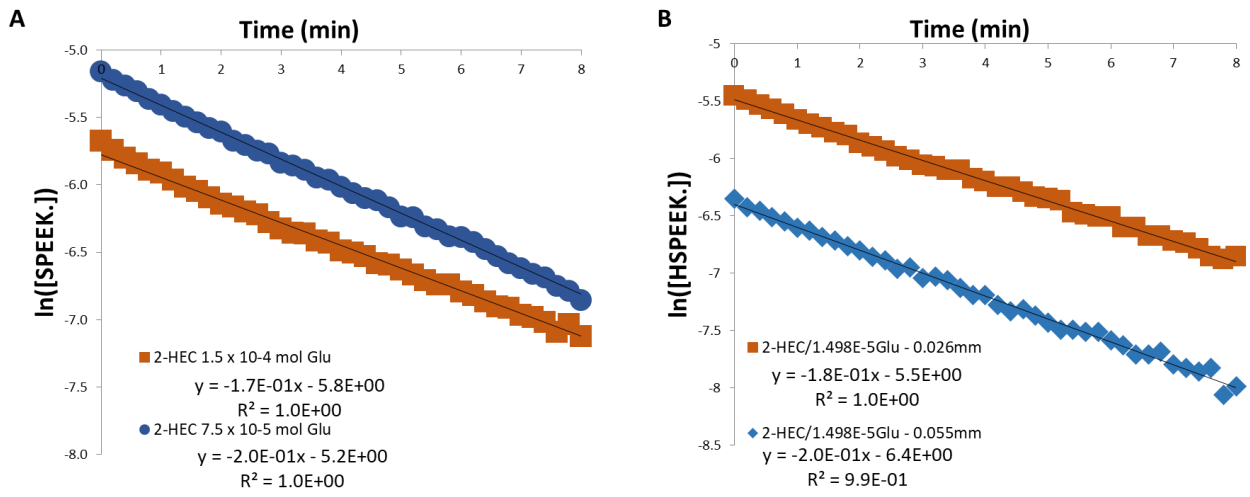

Figure 2.5: A) First-order plot of radical oxidation data for SPEEK/2-HEC films cross-linked with: 7.5 x 10^{-5} mol Glu (♦), film thickness = 0.050 mm; and 1.5 x 10^{-4} mol Glu (■), film thickness = 0.053 mm. B) First-order plots of radical oxidation for SPEEK/2-HEC films with 1.5 x 10^{-4} mol Glu, film thickness of 0.026 mm (■) and 0.055 mm (♦).

polyketone loss (larger than 5 %) during the film rinsing with H_2O. Presented in Figure 2.5B are pseudofirst-order plots of the SPEEKH• decay when the film thickness ranged between 0.026 and 0.055 mm, no statistical difference in radical oxidation rate was found. Variations in film thickness were achieved by using different solution volumes in the mold. The fact that the rate of radical oxidation was unaffected by the film thickness supports the idea that this process was fast, and that surface radicals played no significant contribution. The absence of contributions from surface SPEEKH• is not surprising given that no radical signal was detected in air saturated SPEEK/PVA solutions due to the efficient oxidation of this species in the presence of oxygen.[2]

The results shown in Figure 2.6 indicate that the SPEEKH• oxidation rate in SPEEK/cellulose was dependent on relative humidity (R.H.). Under high humidity (~50 % R.H.) the SPEEKH• oxidation in SPEEK/2-HEC films followed pseudofirst-order kinetics while second-order kinetics predominated at low humidity (~20 % R.H.). This resulted from structural changes caused by H_2O which altered the O_2 diffusion and $[O_2]$ within the film. Exposure of films to a high relative humidity induces H_2O uptake and film expansion, increasing $[O_2]$ and enhancing diffusion of the gas in the solid matrix. A low humidity induces film shrinkage resulting in a lower oxygen concentration and slower gas diffusion.

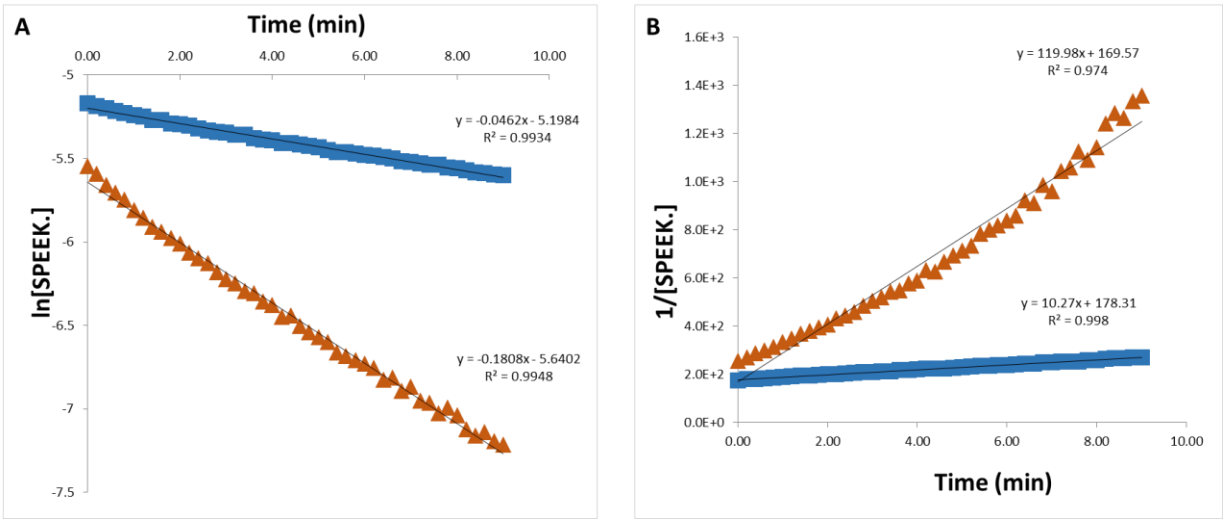

Figure 2.6: A) First-order plots of data from the radical decay in a SPEEK/2-HEC film prepared with 1.5 x 10^{-4} mol Glu; results obtained under (▲) high and (■) low humidity. B) Second-order plots of the data obtained under (▲) high and (■) low humidity.

The water uptake of films exposed to different R.H. values was monitored via gravimetric determination of mass changes over multiple days; the results are shown in Figure 2.7. For both 2-HEC and NaCMC films the mass increased linearly with rising R.H., clearly demonstrating that adsorption of H_2O from air takes place. The inset of Figure 2.7 indicates that SPEEK/cellulose films experienced fluctuations in mass over time as the ambient humidity of

the laboratory varied daily. A possible explanation for such changes assumes that H_2O adsorption is a faster process than the readjustment of the film to the forces induced by the water uptake.

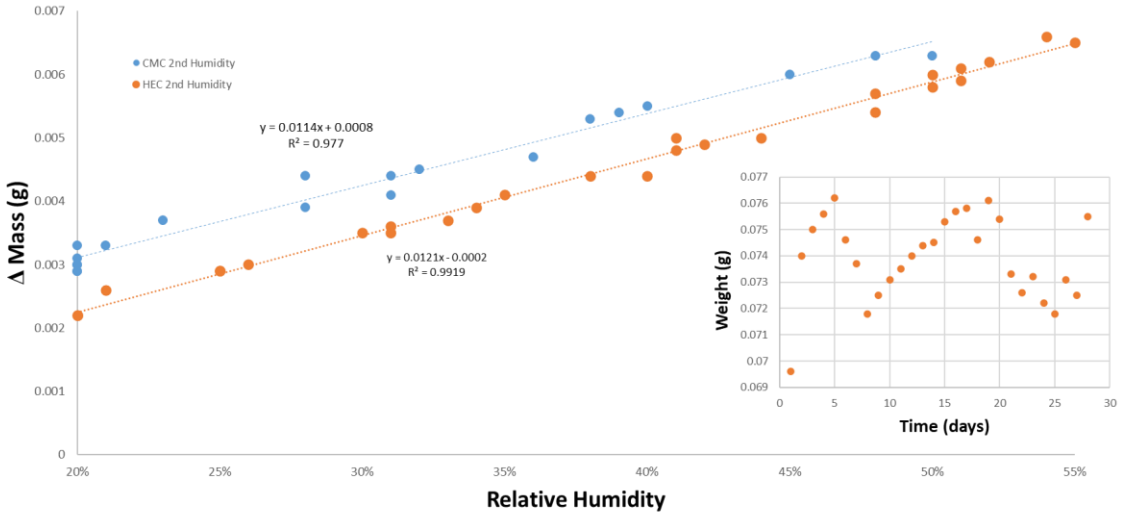

Figure 2.7: Change in mass of 5 cm x 2.5 cm SPEEK/NaCMC (●) film prepared with 2.25 x 10^{-4} mol Glu and SPEEK/2-HEC (●) film prepared with 1.5 x 10^{-4} mol Glu at different relative humidity. The inset shows the daily mass variation for an SPEEK/NaCMC film.

To determine if structural changes are occurring in parallel with the water uptake a film was dried in a desiccator. Then, the film was exposed to air with 56% R.H. and both mass and dimensions were simultaneously monitored, the results are presented in Figure 2.8. The water uptake was nearly instantaneous resulting in a continuous mass increase until an equilibrium position was established. The equilibrium position corresponded to an 11% increase in the mass of the film. In contrast, as illustrated in the inset of Figure 2.8, the film dimensions changed slowly and full expansion of the solid polymer blend was reached only after a time delay. The early negative dimensional changes originated from film curling that took place when laying on the plate of the analytical balance, probably yielding an uneven distribution of mass. Large increases in film dimensions were noticed after 30 minutes, at which point [H_2O] in the solid

polymer blend was high enough to induce a large expansion of the film structure to a maximum change of 5 % in the length of the film.

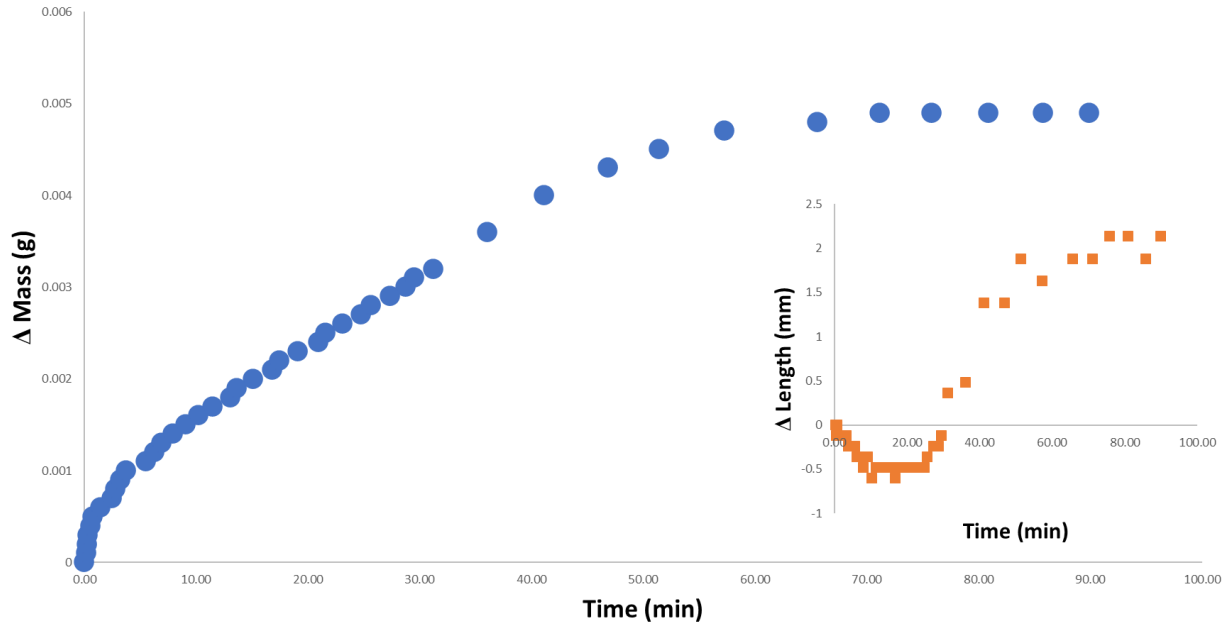

Figure 2.8: Mass changes of a dried SPEEK/NaCMC film (initially 5 cm x 1.25 cm) made with 2.25 x 10^{-5} mol Glu exposed to 56% R.H. (Initial mass 45.2 mg) Inset: changes in film length with time. (Initial length 46.5 mm)

Figure 2.9 exemplifies the effect of relative humidity on the transformations induced by photolysis of SPEEK/2-HEC film. Depicted in Figure 2.9A are three kinetic runs showing the SPEEKH• photogeneration at 20% R.H. whereas the inset depicts the corresponding decay curves obtained during radical oxidation. Highly reproducible results were obtained during both SPEEKH• generation and decay. The effect that relative humidity exerts on the SPEEKH• formation and decay is illustrated in Figure 2.9B. Raising R.H. from 20% to 69% markedly decreased the steady state [SPEEKH•] obtained during photolysis. Exposure of films to 20% R.H. resulted in a low H_2O content and shrinkage of the solid polymer blend. This, in turn, resulted in a decrease in oxygen diffusion and [O_2], thereby slowing down step 5 and allowing a

higher steady state [SPEEKH•] to be achieved. Under those conditions the radical-radical decay step 7 contributed to limiting the steady state SPEEKH• concentration. As the water content in the films increased

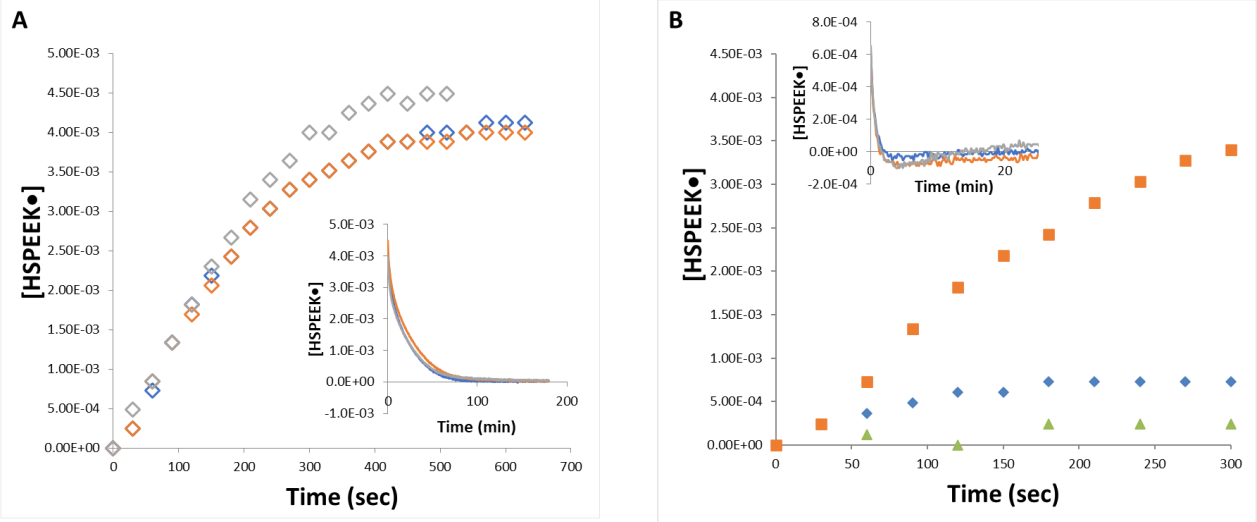

Figure 2.9: A) Triplicate runs of a SPEEK/2-HEC photoreduction during 30 s illumination at 20% R.H. The inset shows the SPEEKH• oxidation runs at 20% R.H. after illumination. B) Radical photogeneration in a SPEEK/2-HEC film during 30 s illuminations at (▲) 69%, (♦) 50%, and (■)20% R.H. Inset shows the radical oxidation at 50% R.H for three repeat experiments.

with raising R.H., expansion of the solid polymer blends ensued. Such change increased the amount of O_2 present in the solid polymer blends, which increased the rate of SPEEKH• oxidation via step 5. This, in turn, induced a systematic decrease in the radical steady state concentration achievable during photolysis. Support for this interpretation is provided by the results shown in the insets of Figures 2.9A and 2.9B. Indeed, at 20% R.H. the SPEEKH• oxidation required over 60 minutes (Figure 2.9A) which is in stark contrast with the decay at 69% R.H. occurring in less than 5 min (Figure 2.9B).

To determine the potential effects induced by repeated reduction and oxidation cycles, 10 consecutive illuminations were performed on a SPEEK/2-HEC film prepared utilizing 1.5 x 10^{-4} mol of either Glu or Tar as cross-linkers. The results presented in Figure 2.10 show the decay profile of the radical absorption versus time. Clearly, a continuous decrease in initial [SPEEKH•] took place with each subsequent illumination. This repetitive photolysis also rendered SPEEK/2-HEC films increasingly yellow due to a rise in absorbance at $\lambda \leq 450$ nm. An analogous coloration took place in SPEEK/PVA films yielding a signal with $\lambda_{max} = 420$ nm

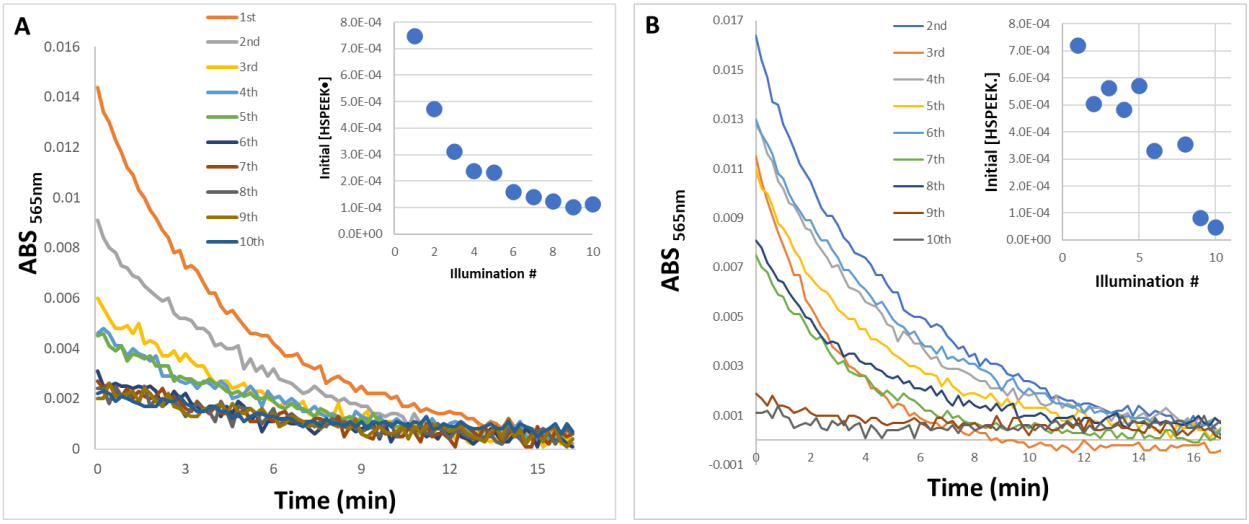

Figure 2.10: Comparison of the radical decay profiles for A) SPEEK/2-HEC film (0.058 mm thick) made with 1.5 x 10^{-4} mol Glu, and B) SPEEK/2-HEC film (0.064 mm thick) prepared with 1.5 x 10^{-4} mol Tar, exposed to 10 consecutive illuminations. The insets show the maximum [SPEEKH•] attained during each illumination.

due to LAT formation.[4] In the case of SPEEK/2-HEC films the LAT signal exhibited no maximum but continuously increased in intensity with decreasing wavelength. The results of Figure 2.10 indicate that absorption of light with wavelengths at around 350 nm by the LAT was significant, which impeded SPEEK from absorbing the photons generated by the illuminator and stopped photogeneration of SPEEKH•. Obviously, LAT formation in SPEEK/2-HEC films was

significantly faster than in SPEEK/PVA solid matrices given that the latter turned yellow only after several hours of photolysis.[4] These findings suggest that SPEEK interacts with 2-HEC more strongly than with PVA, thereby enhancing LAT formation via step 7. Comparison of the results from Figures 2.10A and 2.10B indicates that SPEEK• decayed within 15 mins irrespective of the cross-linker nature. However, the data of both insets indicate that the steady state [SPEEKH•] produced during each illumination was generally higher when Tar served as a cross-linker. This means that non-toxic Tar can be used as a cross-linker without a negative impact on the rate of radical generation and oxidation during consecutive illuminations.

Formulation of SPEEK/NaCMC polymeric system was a result of efforts to suppress LAT photogeneration, which negatively affected the performance of films containing 2-HEC. Preparation of SPEEK/NaCMC films with methods used in 2-HEC experiments resulted in film dissolution during rinsing to extract HCl. Part of the H^+ needed to catalyze cross-linking of the cellulose was consumed due to protonation of the carboxylate groups from NaCMC. This led to a decrease of the cross-linking effectiveness and resulted in polymer matrices that dissolved upon rinsing with H_2O. Thus, preparation of SPEEK/NaCMC films required an excess of HCl to ensure complete protonation of the carboxylate groups from NaCMC. In addition, the cross-linker concentration was also increased to 2.25×10^{-4} mol, which decreased the amount of SPEEK being washed out to < 5%.

A comparison of SPEEKH• decay profiles for SPEEK/2-HEC and SPEEK/NaCMC films is presented in Figure 2.11. While SPEEK/NaCMC films exhibited a radical oxidation 4 times slower than for SPEEK/2-HEC solid matrices, the kinetics of SPEEKH• oxidation remained unchanged during 9 consecutive illuminations and yellow coloration of the films was not observed. This means that photogeneration of LAT was not significant in SPEEK/NaCMC films.

A possible reason is that both SPEEK and the cellulose macromolecules are negatively charged, which hinders insertion of the cellulose radical into the BP rings of SPEEKH•. The absorption of LAT generated in SPEEK/cellulose films was detected at 400 nm; simultaneous measurements were conducted at 700 nm to ensure that the signal at the shorter wavelength was not a result of

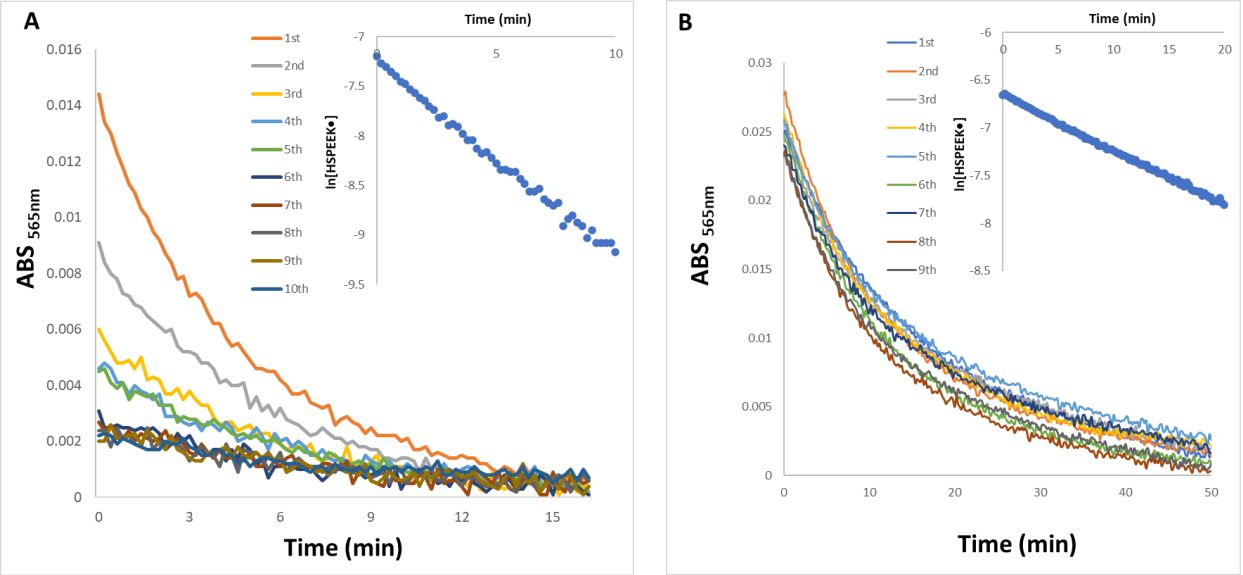

Figure 2.11: Comparison of radical decay profiles for films exposed to consecutive illuminations. A) SPEEK/2-HEC film (0.058 mm thick) with 1.5 x 10^{-4} mol Glu and B) SPEEK/NaCMC film (0.054 mm thick) prepared with 2.25 x 10^{-4} mol Glu. Both insets show the first-order plot of [SPEEKH•].

light scattering effects. Figure 2.12A illustrates the negative effect exerted by photogenerated LAT on the initial [SPEEKH•] obtained during consecutive illuminations. The first illumination resulted in a 30% lower [SPEEKH•] for SPEEK/2-HEC films as compared with those containing NaCMC. Such finding is consistent with both a higher O_2 permeability and faster radical-radical reactions occurring in SPEEK/2-HEC films. The initial [SPEEKH•] decreased by 86% after consecutive irradiations of a SPEEK/2-HEC film, but only 9% for films containing NaCMC. According to the data depicted in the insets of Figure 2.12, films prepared with 2-HEC exhibited

a 7 times more intense LAT absorption than those made with NaCMC. These findings support the notion that absorption of photons at 350 nm by LAT interfered with the formation of the SPEEK* thereby hindering SPEEKH• generation.

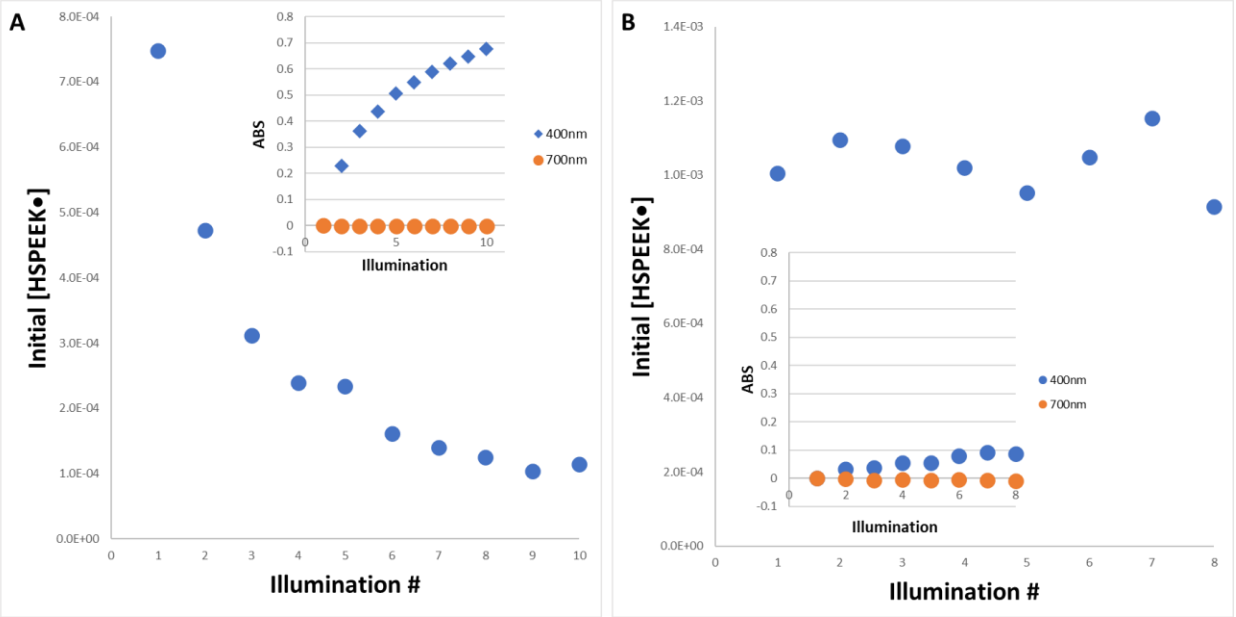

Figure 2.12: A) Initial [SPEEKH•] of a SPEEK/2-HEC film with 1.5 x 10^{-4} mol Glu exposed to consecutive illuminations. Compared in the inset are the LAT absorbance at 400 nm (●) and at 700 nm (●). B) Initial [SPEEKH•] for a SPEEK/NaCMC film with 2.25 x 10^{-4} mol Glu after consecutive irradiations. Inset shows absorbance at 400 nm of LAT (●) and at 700 nm (●).

An important observation was that the absorption at 400 nm remained unchanged after photolysis was terminated, meaning that LAT formation was fast and occurred only at high [SPEEKH•]. While films containing NaCMC exhibited a lower rate of radical oxidation as compared to those made with 2-HEC, in both cases the rate constant was dependent on the ambient R.H. as shown in figure 2.13. For SPEEK/2-HEC films the rate constant varied from 0.072 min^{-1} at 22% R.H. to 0.25 min^{-1} at 50% R.H. On the other hand, for SPEEK/NaCMC films the values ranged from k = 0.015 min^{-1} at 22% R.H. to k = 0.084 min^{-1} at 50% R.H. A

comparison of films containing 2-HEC with those using NaCMC indicated that the rate of radical oxidation was between 70-80% lower for the latter system. In addition, for both film systems the rate of radical oxidation increased drastically above ~45% R.H. This change in the rate of oxidation is caused by increases in the amount of H_2O present in the films. As demonstrated in Figure 2.8, large increases of [H_2O] also cause alterations in the film dimensions due to expansion. In contrast, the

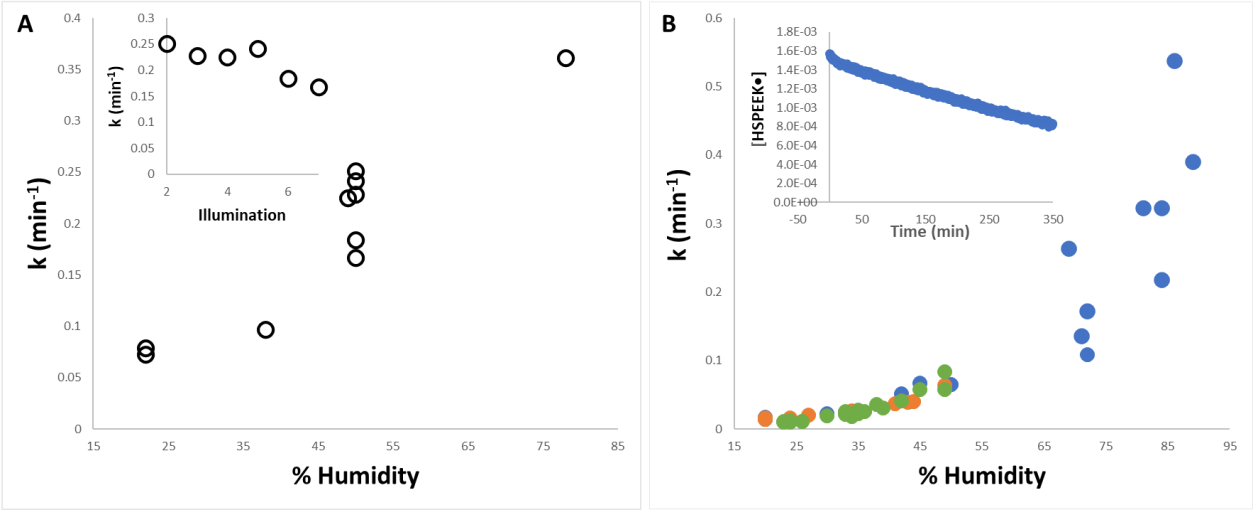

Figure 2.13: A) Plot of pseudofirst-order rate constant as a function of R.H. for a SPEEK/2-HEC film with 1.5 x 10^{-4} mol Glu. Inset: drop in oxidation rate constant at 50% R.H. after consecutive irradiations. B) Pseudofirst-order rate constant plotted versus R.H. for SPEEK/NaCMC films made with 2.25 x 10^{-4} mol Glu (●), 2.25 x 10^{-4} mol Tar (●) and 3.0 x 10^{-4} mol Glu (●). Inset: decay of SPEEKH• in a SPEEK/NaCMC film with 2.25 x 10^{-4} mol Glu degassed with N_2.

photogenerated LAT slowed down the oxidation process, for example the data of the inset in Figure 2.13A indicates that at 50% R.H. the rate constant for the SPEEKH• decay diminished with each subsequent illumination. This effect originated from chain crosslinking that took place during LAT formation, which decreased the internal film volume and hindered oxygen diffusion thereby decreasing the [O_2] in the polymer matrices.

An interesting finding shown in figure 2.13B is that for SPEEK/NaCMC films the SPEEKH• oxidation rates were not affected by addition of higher Glu amounts. Pseudofirst-order rate constants for SPEEK/NaCMC films with 3 x 10^{-4} mol Glu ranged from k = 0.0141 min^{-1} at 20% R.H. to k = 0.0642 min^{-1} at 49% R.H.; no significant differences were noticed at the lower Glu concentration. As illustrated in Figure 2.13B, the values of k scatter significantly at humidity values > 65% due to fluctuations in ambient humidity (±10% R.H.). Another contributing factor was the higher temperature existing inside the Rayonet illuminator, which decreased R.H. around the films during photolysis. The lower SPEEKH• oxidation rates in SPEEK/NaCMC films were not induced by increases in Glu but due to crosslinking of carboxylic acid functions. In fact, crosslinking of films containing NaCMC was possible without the addition of a crosslinker. However, washing of such films resulted in unacceptable SPEEK losses that always exceeded 5 %. A possible explanation for such a finding is that crosslinking of NaCMC chains with Glu or Tar generated structures in which the cellulose macromolecules were separated from each other by the crosslinker. This created space between the cellulose chains allowing entanglement of SPEEK and NaCMC macromolecules. No such space existed during direct crosslinking of NaCMC chains, yielding more compact crosslinks and less entanglement between the polyketone and cellulose macromolecules. This enabled more SPEEK to diffuse out of the films upon immersion in water.

Figure 2.13B includes values of the rate constant for the SPEEKH• oxidation in films made with 2.25 x 10^{-4} mol of Tar films as crosslinker. The rate constants ranged from k = 0.011 min^{-1} at 23% R.H. to k = 0.0578 min^{-1} at 49% R.H. which are 10 to ~40% lower than the values measured for films prepared with Glu. A possible reason for such a difference is that more compact films resulted using Tar because this molecule is smaller than Glu. The difference in

oxidation rate constant was most pronounced at the lowest humidity values. Under such conditions the influence of H_2O on film expansion was not significant, implying that the effect induced by the crosslinker size played an important role in decreasing the oxidation rate. At R.H. $\geq$ 45% the difference in rate constants became less pronounced as the influence exerted on the radical decay by the increasing amount of H_2O in the films became predominant. In analogy to the data shown in Figure 2.12B, the initial [SPEEKH•] photogenerated in NaCMC films containing Tar decreased slightly during 10 consecutive illuminations.

SPEEK/NaCMC films were also tested to assess the significance of the SPEEKH• decay in the absence of air. Presented in the inset of Figure 2.13B is the evolution of [SPEEKH•] as a function of time for a NaCMC film first degassed with nitrogen for several hours and then photolyzed under N_2. During the first 10 min a small consumption of SPEEKH• took place that followed no simple rate law. At longer times the decay was slow following a linear function of time with $k_{decay} = 1.96 \times 10^{-6}$ M/min^{-1}. Comparison of the results depicted in Figure 2.11B with those shown in the inset of Figure 2.13B indicates that the oxygen attack on SPEEKH• via step 5 was much faster than the radical decay in the absence of air. Interestingly, for films containing NaCMC the SPEEKH• decay in the absence of O_2 obeyed a zero-order rate law with a half-life of about 350 min. A faster radical consumption under N_2 ($t_{1/2} \approx 60$ min) took place in films made with 2-HEC, which followed a first-order rate law, see Figure 2.4. These curious kinetic differences seem to suggest that the SPEEKH• decay in the absence of O_2 originated from a reaction between some photogenerated LAT species and the negatively charged polyketone radical. For SPEEK/NaCMC films LAT formation involves insertion of a negatively charged cellulose radical into a BP aromatic ring of SPEEKH•, yielding a species carrying a charge of -2. For films containing 2-HEC the resulting LAT species will exhibit a single negative charge.

Obviously, electrostatic repulsions will be stronger when SPEEKH• reacts with LAT photogenerated in films containing NaCMC than those made with 2-HEC, which explains the faster decay of the polyketone radical in the latter case.

The introduction of additional polymer components was envisioned to affect the rate of oxygen diffusion into the films thereby altering the SPEEKH• oxidation rates. For instance, utilization of PVA as a copolymer was anticipated to lower the solubility of O_2 in the films, since the oxygen

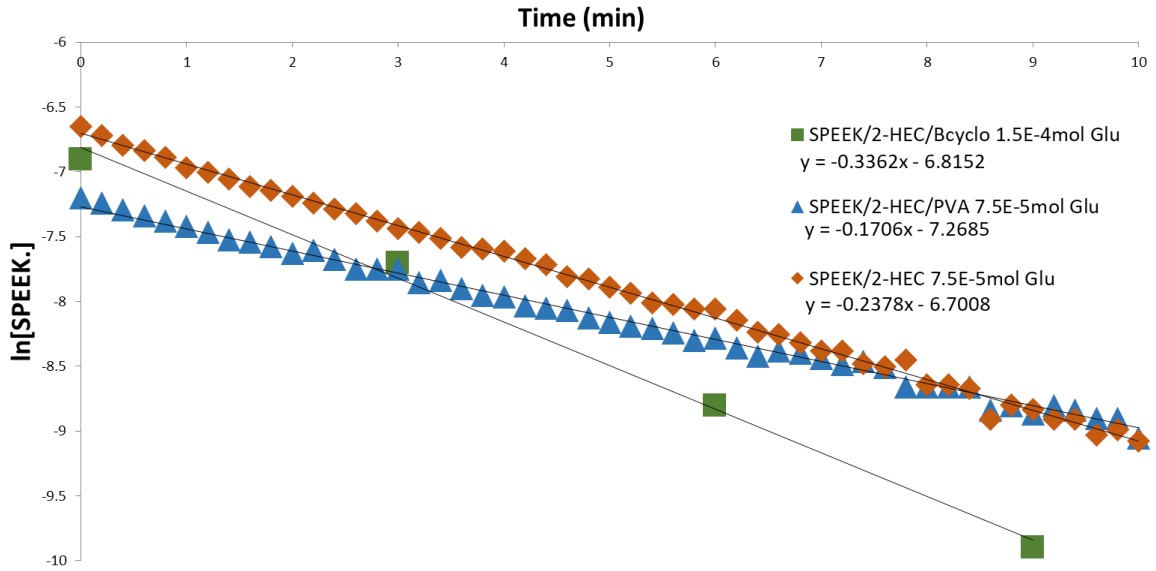

Figure 2.14: Comparison of radical oxidation pseudofirst-order plots for: (♦) 0.050 mm thick SPEEK/2-HEC film, (■) 0.054 mm thick film containing 4.4 x 10^{-4} mol β-cyclodextrin, (▲) 0.061 mm thick film containing 4.4 x 10^{-4} mol PVA.

permeability in the polyol is much lower than that of the cellulosic materials.[13] In contrast, the open (cone-like) structure of the cyclodextrin was expected to facilitate diffusion of oxygen into the films. Representative results are shown in Figure 2.14 for SPEEK/2-HEC films; [Glu] was increased in relation to the moles of additional polymer to maintain an equivalently cross-linked structure of the polymeric system. As expected from the previous results obtained with the

SPEEK/PVA system,[2] introduction of PVA as a co-polymer yielded a rate constant of SPEEKH• oxidation that was about 71 % of the value determined in the absence of the polyol. On the other hand, the rate constant for SPEEKH• oxidation increased by about 42 % when β-cyclodextrin was present in the films. Such faster radical decay was consistent with the anticipated increased oxygen diffusion into the films due to the open ring structure of the cyclodextrin. While 2-HEC films with

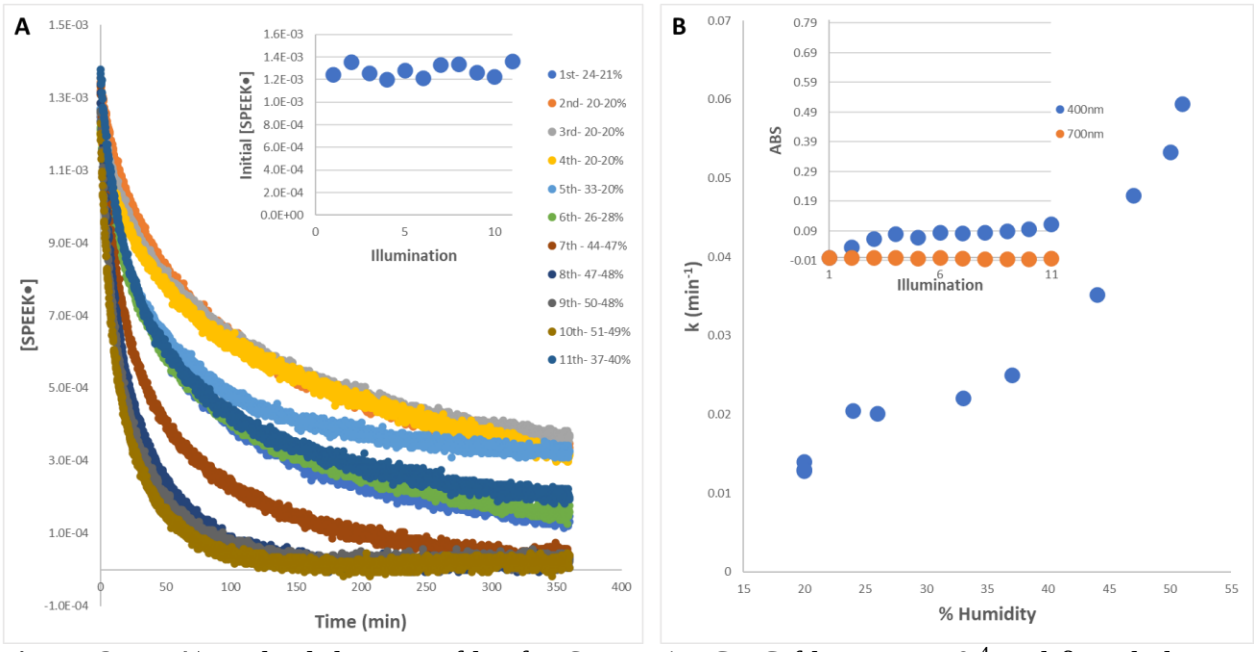

Figure 2.15: A) Radical decay profiles for SPEEK/NaCMC film, 4.4 x 10^{-4} mol β-cyclodextrin crosslinked with Glu, after 11 consecutive illuminations at different R.H. Inset: [SPEEKH•] attained after each illumination. B) Pseudofirst-order rate constants as a function of R.H; inset: absorbance at 400 nm for LAT (●) and at 700 nm (●).

β-cyclodextrin showed increased oxidation, NaCMC films incorporating β-cyclodextrin showed pseudofirst-order rates constants of k = 0.014 min^{-1} at 20% R.H. to k = 0.0595 min^{-1} at 51% R.H. shown in Figure 2.15 which are similar to the values rate constants of NaCMC films without β-cyclodextrin. This was assumed to originate from crosslinking of the carboxylate from NaCMC causing the film to become much stiffer, negating the benefits of incorporating β-cyclodextrin.

SPEEK/NaCMC films with or without β-cyclodextrin exhibited similar LAT absorptions, implying that electrostatic repulsion effects remained unchanged when uncharged materials were introduced in the films. Also, the initial amounts of photogenerated SPEEKH• remained the same in films with or without cyclodextrin over several consecutive illuminations, confirming that the amounts of LAT photogenerated were insufficient to interfere with the SPEEK* formation.

Presented in Figure 2.16 are data from tests on NaCMC/β-cyclo films crosslinked using 2.25 x 10^{-4} mol Tar as crosslinker. The pseudofirst-order rate constants for SPEEKH• decay in such films ranged from k = 0.0124 min^{-1} at 20% R.H. to k = 0.0479 min^{-1} at 49% R.H., which were slightly lower when compared to the values of films crosslinked with 2.25 x 10^{-4} mol Glu. A similar trend was noticed with NaCMC films without β-cyclodextrin. LAT was photogenerated at similar levels compared with all SPEEK/NaCMC crosslinked films. As shown in Figure 2.16A

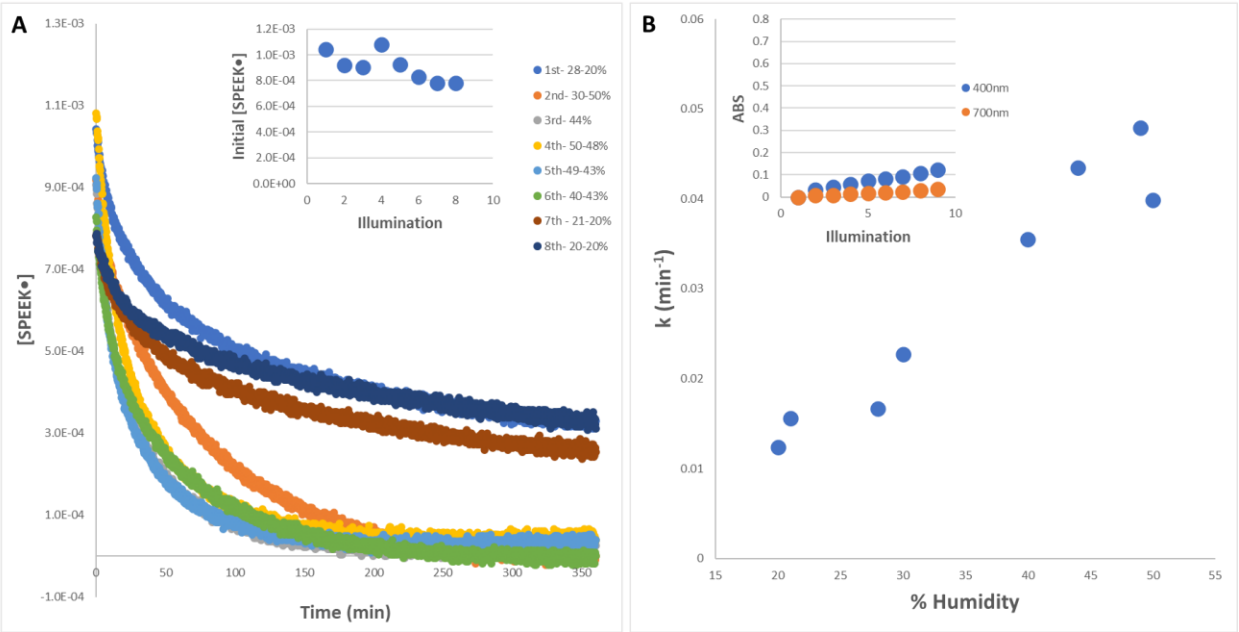

Figure 2.16: A) Radical decay profiles for a SPEEK/NaCMC film with 4.4 x 10^{-4} mol β-cyclodextrin film crosslinked with Tar, after 9 consecutive illuminations at different R.H. Inset:

[SPEEKH•] attained during each illumination. B) Pseudofirst-order rate constant as a function of R.H. Inset: absorbance at 400 nm for LAT (●) and at 700 nm (●).

inset, the generation of initial [SPEEKH•] declined by 25% over 9 consecutive illuminations which was also seen with NaCMC films without β-cyclodextrin. Such kind of interference in the formation of the SPEEK* was not detected with NaCMC/β-cyclo films see inset of Figure 2.15A. The resulting SPEEK/NaCMC films crosslinked with β-cyclodextrin can be used without sacrificing oxidation rates or increasing the amount of SPEEK rinsed out. The rinsing out of SPEEK from SPEEK/cellulose films occurs with all formulations; however, this was prevented by means of a polyurethane (PU) coating. This was achieved via the application of the polyurethane layer to the entire surface area of a dry film following the usual rinsed with H_2O. Testing of the resulting films was conducted after drying them for 24 hours; the resulting data is shown in Figure 2.17.

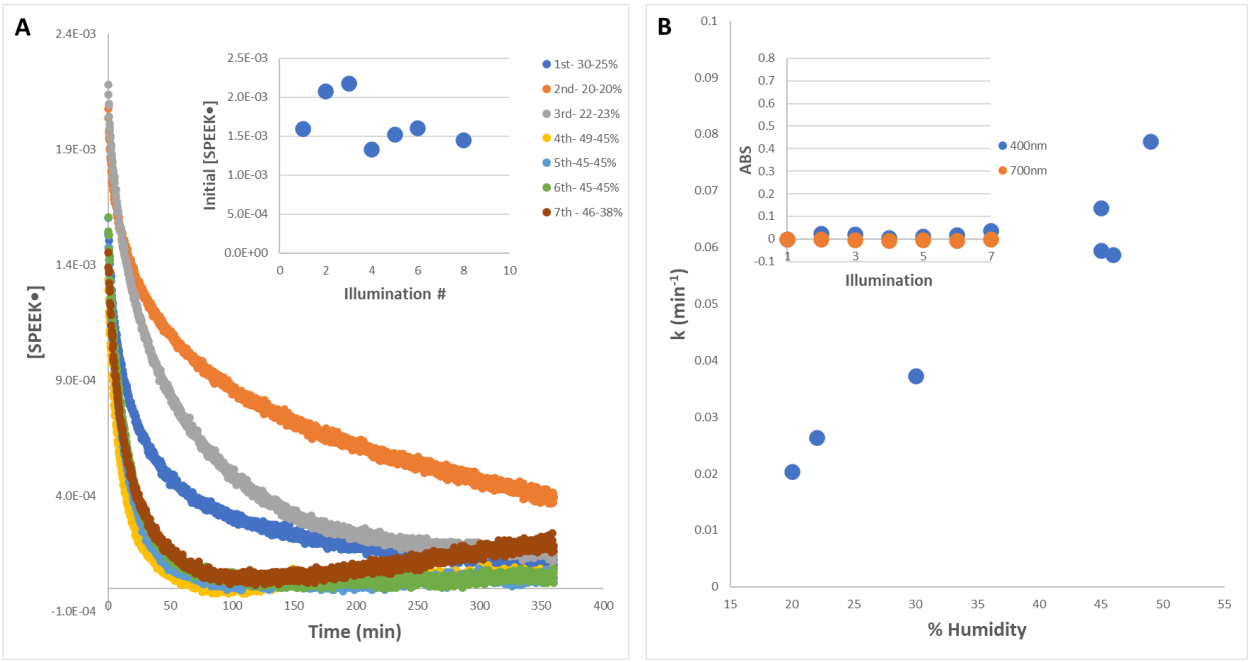

Figure 2.17: A) Radical decay profiles for a SPEEK/NaCMC film with 2.25 x 10^{-4} mol Glu coated with polyurethane, exposed to 7 consecutive illuminations. Inset: [SPEEKH•] attained

during each illumination. B) Pseudofirst-order rate constant as a function of R.H. The inset shows absorbance at 400 nm for LAT (●) and at 700 nm (●).

As illustrated in Figure 2.17A, the rate of SPEEKH• oxidation increased as the ambient humidity increased. The results portrayed in the inset indicate that the initial [SPEEKH•] photogenerated 17A decreased by 10% as the number of photolytic steps increased, which is comparable to most NaCMC films. The pseudofirst-order rate constants for NaCMC films coated with polyurethane ranged from k = 0.0204 min^{-1} at 20% R.H. to k = 0.0787 min^{-1} at 49% R.H, which amounted to a 40% – 20% increase compared with films without the coating. Interestingly, SPEEK/cellulose films without a PU coating exhibited a significant increase in SPEEKH• oxidation rates only at R.H values > ~35%. In contrast, the results shown in Figure 2.17B indicate that the rate constant of radical decay increased linearly vs R.H. This suggests that PU being incorporated into the films reduces the H_20 needed to start expansion by occupying all free space. According to the data of the inset in Figure 2.17B, NaCMC films coated with PU exhibited a 50% reduction in LAT absorption at 400 nm when compared with SPEEK/NaCMC films without coating.

2.4 Conclusion

Investigation into the development of SPEEK/cellulose films oxygen sensors resulted in increased SPEEKH• oxidation compared with previous SPEEK/PVA films. 2-HEC films were found to have high SPEEKH• oxidation rates but also significant LAT formation during every illumination. LAT photogeneration is detrimental for two reasons: the process consumes the ketone function of SPEEK and yields an absorption at wavelengths below 420 nm. Thus, LAT competes with the BP groups from SPEEK for the 350 nm photons, decreasing the amount of SPEEKH• produced with each illumination. This results in 2-HEC films being increasingly less efficient to produce SPEEKH• upon multiple illuminations. The amount of LAT photogenerated

was significantly lower for NaCMC films, which reduced the associated problems in generating SPEEKH•. This is due to the electrostatic effects of both SPEEK and the cellulose macromolecules being negatively charged. NaCMC films were found to have lower SPEEKH• oxidation rates compared with 2-HEC films which was due to the carboxylic group acting as a crosslinker.

SPEEK/cellulose films also showed changes in the rate of radical oxidation due to the influence of ambient humidity. These findings indicate that structural changes of the films induced by the presence of H_2O altered [O_2] within the films. The effect of H_2O on the rate of oxidation was seen to increase above 45% R.H. Experiments also found that non-toxic Tar could be utilized instead of Glu as a crosslinker without negatively affecting the SPEEKH• oxidation rates. The introduction of β-cyclodextrin into SPEEK/Cellulose films resulted in an increase in SPEEKH• oxidation rates; however, NaCMC films showed no increase or decrease in SPEEKH• oxidation. The effect of the carboxylic acid of NaCMC crosslinking restricts structural changes caused by β-cyclodextrin. All SPEEK/cellulose films resulted in small amounts of SPEEK coming out during washing of the HCl catalyst. NaCMC films were tested with a PU coating to prevent SPEEK loss and were found to have increased rates of oxidation compared to NaCMC films. The films also showed a linear response to R.H. which could mean that NaCMC films could be used as a humidity sensor. The findings of the project show the potential to create SPEEK/cellulose films for oxygen sensing but were sensitive to relative humidity.

References

1. Korchev, A. S.; Shulyak, T. S.; Slaten, B. L.; Gale, W. F.; Mills, G. Sulfonated poly(ether ether ketone)/poly(vinyl alcohol) sensitizing system for solution photogeneration of small Ag, Au, and Cu crystallites. *J. Phys. Chem. B,* **2005**, *109*, 7733-7745.
2. Little, B. K.; Lockhart, P.; Slaten, B. L.; Mills, G. Photogeneration of H_2O_2 in SPEEK/PVA aqueous polymer solutions. *J. Phys. Chem. A,* **2013**, *117*, 4148-4157.
3. Lockhart, P.; Little, B. K.; Slaten, B. L.; Mills, G. Photogeneration of H_2O_2 in Water-Swollen SPEEK/PVA Polymer Films. *J. Phys. Chem. A,* **2016**, *120*, 3867–3877.
4. Korchev, A. S.; Konovalova, T.; Cammarata, V.; Kispert, L.; Slaten, B. L.; Mills, G. Radical-induced generation of small silver particles in SPEEK/PVA polymer films and solutions: UV-Vis, EPR, and FT-IR Studies. *Langmuir* **2006**, *22*, 375-384.
5. Mills, A. Oxygen indicators and intelligent inks for packaging food. *Chem. Soc. Rev.* **2005**, *34*, 1003-1011.
6. Yousefi, H.; Su, H.-M.; Imani, S. M.; Alkhaldi, K.; Filipe, C. D. M.; Didar, T. F. Intelligent food packaging: a review of smart sensing technologies for monitoring food quality. *ACS Sens.* **2019**, *4*, 808-821.
7. Gibis, D.; Rieblinger, K. Oxygen scavenging films for food application. *Procedia Food Sci.* **2011**, *1*, 229–234.
8. Ghaani, M.; Cozzolino, C. A.; Castelli, G.; Farris, S. An overview of the intelligent packaging technologies in the food sector. *Trends Food Sci. Technol.* **2016**, *51*, 1-11.
9. Korchev, A.S.; Sartin, M.; Mills, G.; Slaten, B.L.; Gale, W.F. Light induced metal nanoparticle formation (M=Ag,Au,Cu,Pd,Pt) in aqueous solutions and polymer films composed of SPEEK-PVA. *Int. Symp. Clusters Nano-Assem.,* **2003**, *10*, 371-377.

10. Ollis, D.; Mills, A.; Lawrie, K. Kinetics of methylene blue (MB) photocatalyzed reduction and dark regeneration in a colorimetric oxygen sensor. *Appl. Catal. B Environ.* **2016**, *184*, 201-207.
11. Heller, H.G.; Langan, J.R. Photochromic heterocyclic fulgides. Part 3. The use of (E)-α-(2,5-dimethyl-3-furylethylidene) (isopropylidene)succinic anhydride as a simple convenient chemical actinometer. *J. Chem. Soc. Perkin Trans.* 2 **1981**, 341–343.
12. Korchev, A.S.; Bozack, M.J.; Slaten, B. L.; Mills, G. Polymer-initiated photogeneration of silver nanoparticles in SPEEK/PVA films: direct metal photopatterning. *J. Am. Chem. Soc.* **2004**, *126*, 10-11.
13. Ulanski, P.; Bothe, K.; Rosiak, J. M.; von Sonntag, C. OH-Induced Crosslinking and Strand Breaking of Poly(vinyl alcohol) in Aqueous Solution in the Absence and Presence of Oxygen. A Pulse Radiolysis and Product Study. *Macromol. Chem. Phys.* **1994**, *195*, 1443-1461.
14. Wang, X.; Wolfveis, O. S. Optical methods for sensing and imaging oxygen: materials, spectroscopies and applications. *Chem. Soc. Rev.* **2014**, *43*, 3666-3761.

Chapter 3

3.1 Introduction

As demonstrated in Chapter 2, photogeneration of SPEEKH• with thin SPEEK/cellulose films is achievable upon exposure to 350 nm photons. However, the intensity of the radical signal centered at λ_{max} = 565 nm is not strong enough to be easily detected visually, limiting the usefulness of the films as oxygen sensors. Therefore, the present chapter will be devoted to the preparation and properties of films containing a redox indicator able to optimize the visual detection of color changes induced by O_2. Numerous studies have reported the utilization of multicomponent film systems loaded with redox-indicating dyes.[1-5] These systems can function as O_2 indicators by exhibiting color changes through brief illumination with UV light which induces dye reduction. Upon exposure to O_2, the redox indicator is oxidized back to the initial state exhibiting an identifiable change. While such sensors work, they are complex systems, and leakage of the toxic dyes from the films into the food is a recurrent issue.

Past studies have shown that the introduction of the redox dyes thionine (Th) and cresol violet (CV) into SPEEK/PVA films is feasible via film swelling in aqueous solutions of the dyes.[6] These cationic dyes diffuse into the films and electrostatically bind with the SPEEK sulfonic acid groups. As a result, the colorants become fixed inside the solid polymer matrices preventing leakage and the dye-doped SPEEK/PVA films showed fast and reversible redox behavior under swollen conditions. On the other hand, while dye reduction was fast when dry films were illuminated with 350 nm photons, re-oxidation of the reduced dyes under such conditions was slow, taking more than 45 days for the colorants to return to their initial redox states.[6] Incorporation of Th and CV in SPEEK/cellulose films was successfully conducted, but such systems exhibited long dye re-oxidation times as well. A reasonable explanation for such

behavior is related to the structural characteristics of the dyes because the cationic charges of Th and CV are localized on terminal nitrogen atoms. Hence, electrostatic bonding between the dyes and the SO_3^- groups from SPEEK was anticipated to be tight, yielding constricted structures that restrict the oxygen permeability of SPEEK/cellulose films.

Improvements in the ability of SPEEK-based films to serve as O_2 indicators were anticipated using methyl viologen (MV^{2+}) as the redox dye together with the utilization of cellulose polymers as the main structural components and H-atom donors. The lack of terminal nitrogen atoms on MV^{2+} was anticipated to result in higher O_2 permeability and a faster re-oxidation of the methyl viologen radical cation (MV^+) generated from the MV^{2+} reduction by SPEEKH•. Such a reaction appeared thermodynamically feasible given that in water the standard reduction potential of MV^{2+} is -0.45 V,[7] whereas the oxidation potential of SPEEKH• has been estimated to be about 1.3 V.[8] Because the viologen radical is readily oxidized by oxygen, detection of O_2 present in gases using photochemically generated MV^+ has been previously achieved.[9] Furthermore, changes in the redox state of the viologen are easily detected by visual means due to the strong coloration of MV^+.[7] The findings of this chapter demonstrate that SPEEK/cellulose films containing MV^{2+} can function as efficient photoactivated, reversible O_2 indicators.

3.2 Methods and Procedures

The sources of most employed chemicals were identified in the previous chapter, which also described film preparation methods as well as illumination and analytical procedures. Methyl viologen was obtained from Sigma-Aldrich as the dichloride salt. Unless specified, dry SPEEK/cellulose films free of the HCl catalyst were immersed into a 20 mL solution of 1×10^{-4} M MV^{2+} for 24 h in order to incorporate the viologen into the solid polymer matrices. This was followed by drying the films in the absence of light. Square wave voltammetry was used to

determine the concentration of methyl viologen. All electrochemical measurements were performed with CHI potentiostat model CHI660E. All electrochemical measurements were collected using a three-electrode cell system consisting of a platinum counter electrode, a Ag/AgCl reference electrode, and a glassy carbon working electrode. Voltammetry parameters were as follows: the amplitude and the increment were 25 mV and 1 mV. The potential window between −0.3 V and −0.75 V and frequency at 15 Hz. All solutions were prepared with 0.5 M KCl. All experiments were run at least in triplicate; kinetic results exhibited deviations of about 20%, which is typical of heterogeneous film systems.[6] Relative humidity was measured using the JEDEW hygrometer/thermometers model ROUND. Temperature determinations used a VWR 7x7 hot/stir 120V and a HH11B omega digital thermometer with a type K thermocouple.

3.3 Results and Discussion

Exposure of SPEEK/cellulose films containing MV^{2+} to 350 nm photons resulted in a blue color due to the generation of MV^{+};[7] a typical absorption spectrum is presented in Figure 3.1. The spectrum determined after 3 min illumination is free of the characteristic signal of SPEEKH• at 565 nm because the polyketone radical reduced MV^{2+}. The concentration of MV^{2+} in the films was determined to be 1×10^{-2} M within NaCMC films and 1.2×10^{-3} M within 2-HEC films using SWV by looking at the loss of current as MV^{2+} was absorbed. An earlier study showed that, at low viologen concentrations, reduction of MV^{2+} in cellophane and PVA films yielded MV^{+}.[10] However, the radical dimer $(MV^{+})_2$ and a MV^{+}-MV^{2+} complex formed at higher viologen concentrations. The spectrum depicted in Figure 3.1 is identical to the one of monomeric MV^{+} probably because binding of the cationic dye to the polyketone, or to NaCMC, prevented formation of more complex radical species. This is a reasonable explanation as the concentration of the polyketone is 1 M and NaCMC is 2.12 M in the films.

The data of Figure 3.1 implies that the establishment of a steady state [MV^{+}] was feasible within 3 min of photolysis in the presence of air. Obviously, reduction of MV^{2+} was faster than several dark reactions such as the O_2-induced SPEEKH•/MV^{+} oxidation and the radical-radical decay processes of SPEEKH• leading to LAT. As in the case of the polyketone radical presented before, MV^{+} generated inside polymer films was sensitive to the presence of O_2. A similar behavior was also reported when MV^{2+} was reduced in cellophane and PVA films.[10] The kinetics

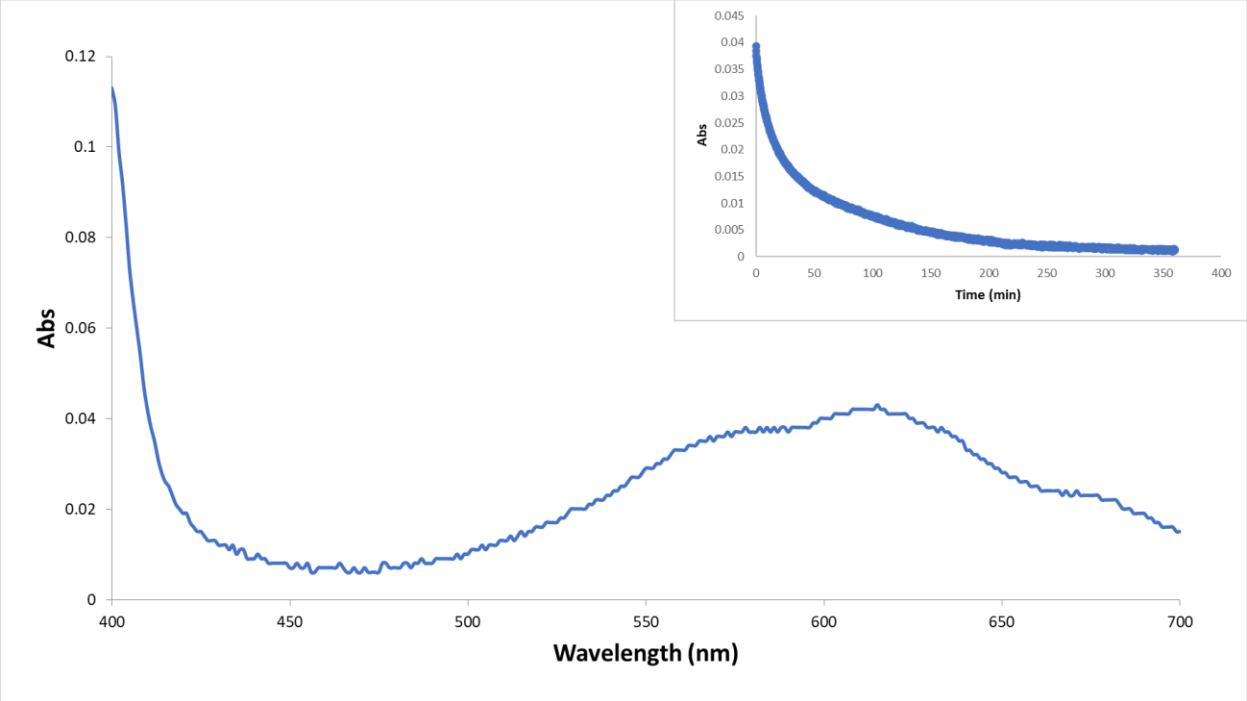

Figure 3.1: Absorption spectrum of MV^{+} generated via a 3 min illumination of a SPEEK/NaCMC film crosslinked with 2.25 x 10^{-4} mol Glu exposed to a 0.1 mM MV^{2+} solution for 24 h prior to photolysis. Inset: decay of the kinetic data at 606 nm resulting from the oxidation of MV^{+} by O_2.

of MV^{+} oxidation by O_2 in SPEEK/cellulose films were monitored spectrophotometrically by following the decay at 606 nm over time, an example is presented in the inset of Figure 3.1. Fits to the data were attempted using first and second-order rate laws after evaluation of [MV^{+}] from

the absorbance values. The calculations based on the Lambert-Beer law used an extinction coefficient (ε) for the radical signal at 606 nm of 1.37 x 10^5 M^{-1} cm^{-1},[7] together with a path length equal to the thickness of a particular film. As in the case of SPEEKH•, the best results were obtained when the MV^+ decay was fitted according to a pseudofirst-order rate law.

SPEEK/NaCMC films containing MV^{2+} were also tested to assess if there was any significant decay of MV^+ in the absence of air. Illustrated in Figure 3.2 is the evolution of [MV^+]

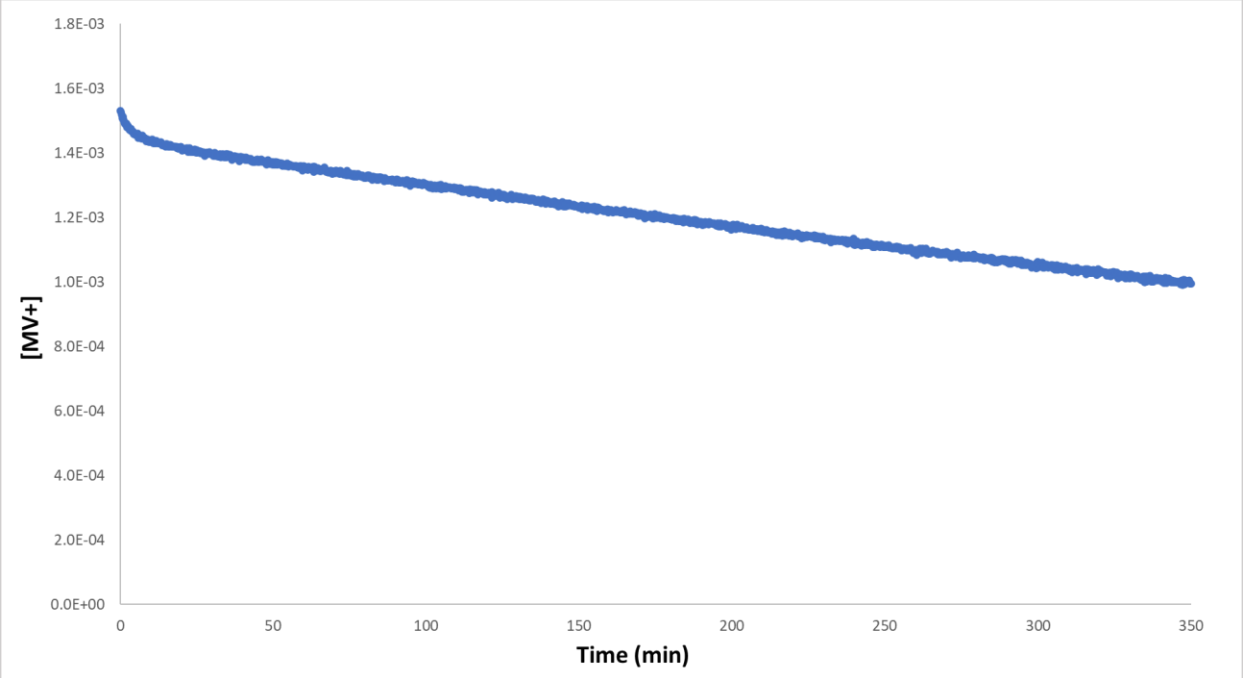

Figure 3.2: Kinetics of the MV^+ oxidation in a SPEEK/NaCMC film crosslinked with Glu under N_2.

as a function of time for a NaCMC film first degassed with nitrogen for several hours and then photolyzed under N_2. During the first 10 min a small consumption of MV^+ took place that followed no simple rate law. At longer times the MV^+ decay was sluggish following a linear function of time with k_{decay} = 1.28 x 10^{-6} M/min^{-1} which was slower than for SPEEK• in the absence of air, see Chapter 2. Comparison of the results shown in Figure 3.2 with the data presented in the inset of Figure 3.1 clearly indicates that oxidation of MV^+ in the presence of air

was significantly faster than the slow decay of the viologen radical that took place in the absence of O_2. Similar to SPEEK•, the MV^+ decay in the absence of O_2 probably originated from a reaction between some photogenerated LAT species and the viologen radical.

The effects induced by repeated photolysis of NaCMC films with Glu containing MV^{2+} are presented in Figure 3.3. The curves shown in Figure 3.3A indicate that MV^+ decayed within a similar timespan as the SPEEK• decay. Also, the MV^+ decay was faster when R.H. increased in agreement with the SPEEK• oxidation by O_2. The inset of Figure 3.3A indicates that SPEEK/NaCMC films with Glu generated 9 x 10^{-4} M MV^+ compared to 1 x 10^{-3} M SPEEKH•, implying a 10% decrease in radical formation when the viologen was present. A reason for the decrease in photogenerated MV^+ will be presented later. The results of the inset of Figure 3.3A also reveal that the initial [MV^+] remained unchanged over 7 consecutive illuminations, meaning that no significant interference due to the LAT absorption at 350 nm occurred. Such conclusion is supported by the data of the inset of Figure 3.3B indicating that incorporation of MV^{2+} in the films inhibited formation of LAT. The complete prevention of LAT formation implies that the radical-radical reactions generating this species was unable to compete with the MV^{2+} reduction by SPEEKH•.

The results illustrated in Figure 3.3B show that SPEEK/NaCMC films with Glu exhibited pseudofirst-order rate constants ranging from k = 0.0272 min^{-1} at 20% R.H. to k = 0.1097 min^{-1} at 49% R.H. Compared to the values for SPEEKH• discussed in Chapter 2, the decay of MV^+ was 80% faster when the humidity was low but only 30% faster at high R.H. These findings suggest that the internal structure of the films expanded due to incorporation of MV^{2+} analogous to the effect induced by H_2O discussed in Chapter 2. SPEEK/NaCMC films with MV^{2+} showed an increase in rate constants above ~30% R.H. similar to those without the viologen. This

implies that a minimum [H_2O] is needed to induce expansion of the film even in the presence of the viologen.

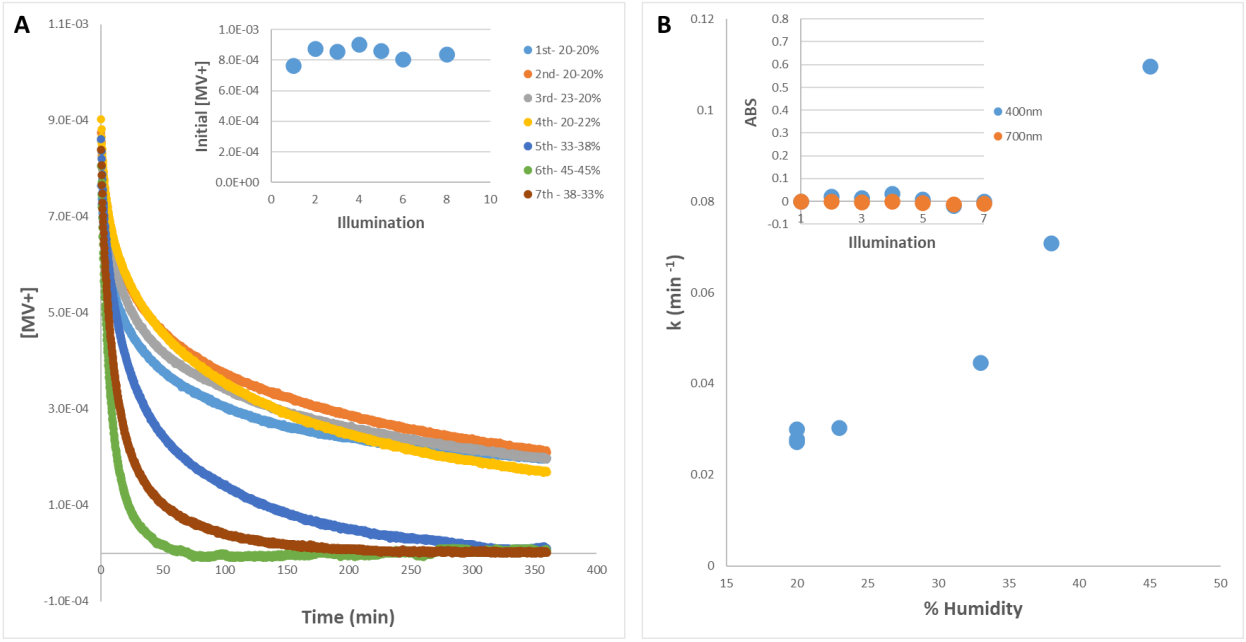

Figure 3.3: A) MV^+ decay profiles for a SPEEK/NaCMC film made with 2.25 x 10^{-4} mol Glu exposed to consecutive irradiations; inset shows the maximum [MV^+] attained during each illumination. B) Pseudofirst-order rate constant as a function of R.H. for a SPEEK/NaCMC film made with 2.25 x 10^{-4} mol Glu. Compared in the inset are the LAT absorbance at 400 nm (●) and at 700 nm (●).

According to the photogeneration mechanism of SPEEKH• proposed in Chapter 2, the initially formed singlet excited state of SPEEK evolves into a triplet excited state that then yields the polyketone radical via H-atom abstraction. Such a pathway is analogous to the sequence of events that forms α-hydroxy radicals of BP,[11] and was adopted since benzophenone is the model for the photochemical behavior of SPEEK. Conversion of the BP singlet to triplet excited state is fast and efficient, leading to phosphorescence as the dominant form of emission. Interestingly, the BP phosphorescence is quenched fast (k_q = 2.6 x 10^9 M^{-1} s^{-1}) by MV^{2+} in solution.[12] An

analogous quenching (via energy transfer) of the SPEEK triplet excited state by the viologen was anticipated to decrease the efficiency of SPEEKH• formation. As mentioned previously, the available evidence suggests that in SPEEK/cellulose films, MV^{2+} is electrostatically bonded to the sulfonic group of the polyketone. This, in turn, should facilitate static quenching of the SPEEK excited states by the bonded MV^{2+}. Presented in Figure 3.4 are emission spectra of SPEEK/NaCMC films with and without MV^{2+}; only broad signals were detected. In contrast, the phosphorescence spectrum of BP in solution exhibits 3 sharp signals with the central and strongest at about 450 nm.[13]

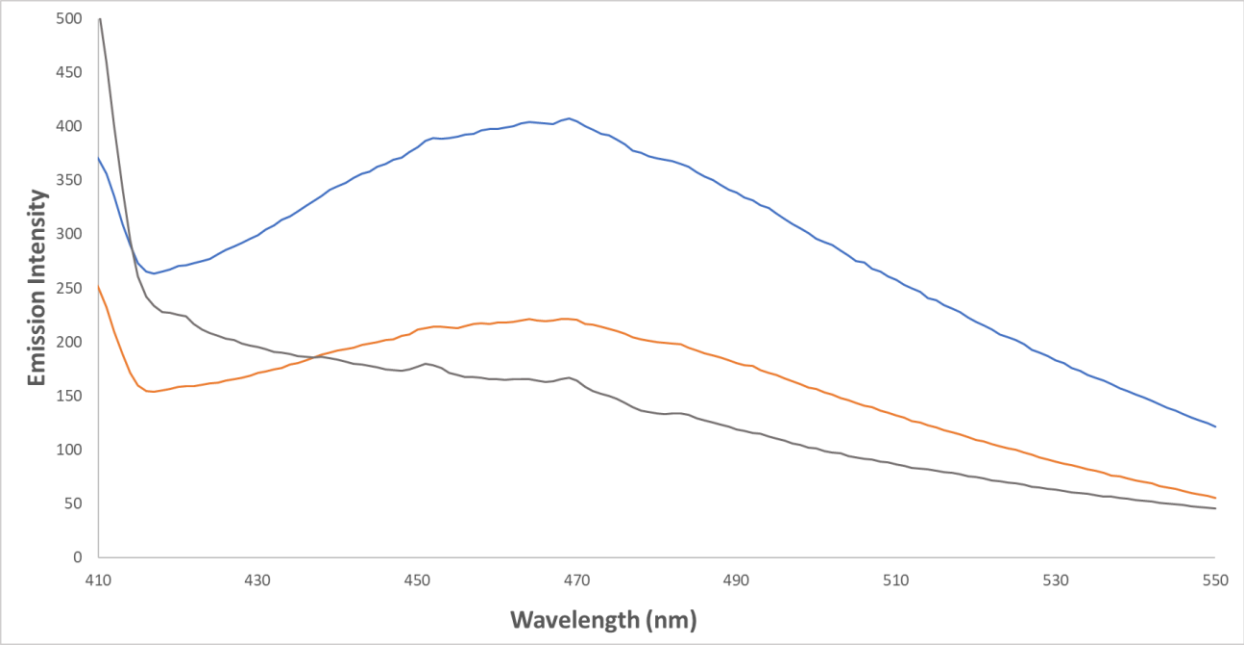

Figure 3.4: Emission spectra for SPEEK/NaCMC films with 2.25 x 10^{-4} mol Glu (●), and after a 24 h in solutions containing 1 x 10^{-4} M (●) and 4 x 10^{-4} M MV^{2+} (●); λ(excitation) = 364 nm.

However, the spectrum of the macromolecular analogue poly(p-vinylbenzophenone), pVBP, is characterized by two broad signals with the strongest at about 440 nm. The blue curve shown in Figure 3.4 corresponds to the spectrum of a SPEEK/NaCMC film without MV^{2+} consisting of a broad signal centered at about 468 nm. In view of the similarities of the spectra obtained with the

SPEEK/NaCMC film free of viologen and that of pVBP, the blue curve presented in Figure 3.4 is assigned to the phosphorescence spectrum of SPEEK. Also shown in Figure 3.4 are spectra obtained after exposing films to solutions with 0.1 and 0.4 mM MV^{2+}. Clearly the intensity of the emission decreased with increasing viologen concentration. These observations are clear evidence that part of the SPEEK* is quenched by the viologen, decreasing the initial [MV^{+}] photogenerated in NaCMC films containing MV^{2+}.

Presented in Figure 3.5 are the results from repeated photolysis of SPEEK/NaCMC films crosslinked with 2.25 x 10^{-4} mol Tar. The curves shown in Figure 3.5A indicate that MV^{+} decayed within a similar timespan as that of films crosslinked with Glu and also exhibited an analogous effect of humidity. Such films photogenerated 8.9 x 10^{-4} M MV^{+} compared to 1.2 x 10^{-3} M SPEEKH• obtained in the absence of MV^{2+}, which amounts to a 26% decrease in radical concentration. This efficiency decrease can be attributed to the quenching effect of MV^{2+} on SPEEK*. As shown in the inset of Figure 3.5A, the initial [MV^{+}] remained unchanged over 7 consecutive illuminations as was found for films crosslinked with Glu, see inset of Figure 3.3A. In contrast, the photogeneration of SPEEKH• exhibited a 15% decrease in the [radical] over 10 illuminations. The LAT absorption at 400 nm is presented in the inset of Figure 3.5B indicating a significant decrease (39%) in the formation of this species as compared to films without viologen.

Depicted in Figure 3.5B are the values of the pseudofirst-order rate constants for MV^{+} oxidation by O_2 in SPEEK/NaCMC films with Tar as a function of R.H. The rate constants ranged from k = 0.0354 min^{-1} at 37% R.H. to k = 0.0958 min^{-1} at 50% R.H. Compared with SPEEKH• oxidation rates, see Chapter 2, the decay of MV^{+} was 40% faster mol Tar.

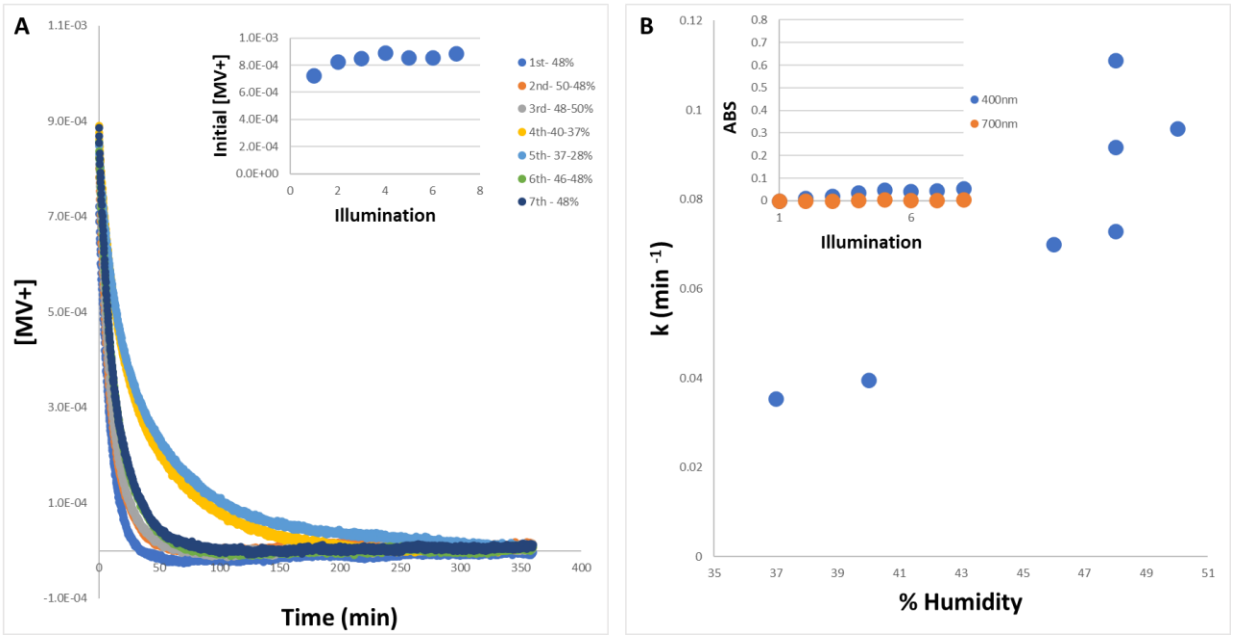

Figure 3.5: A) MV^+ decay profiles for a SPEEK/NaCMC film with 2.25 x 10^{-4} mol Tar exposed to consecutive irradiations; inset shows the maximum [MV^+] attained during each illumination. B) Pseudofirst-order rate constants as a function of R.H. for a SPEEK/NaCMC film with 2.25 x 10^{-4} Compared in the inset are the LAT absorbance at 400 nm (●) and at 700 nm (●).

when the humidity was low but only 20% faster at high R.H. An analogous increase in rate constants was illustrated in Figure 3.3B for NaCMC films crosslinked with Glu. These findings support the idea that the internal structure of the film expanded due to incorporation of MV^{2+}, facilitated O_2 incorporation analogous to the effect induced by H_2O discussed in Chapter 2. Comparison of the MV^+ oxidation rates of films with the two crosslinking agents shows that the viologen radical decayed faster when Glu acted as the crosslinker. A similar behavior was reported in Chapter 2 for films without MV^{2+}, which was rationalized in terms of a difference in molecular size of the crosslinkers and the additional hydrogen bonding from OH groups attached to Tar.

SPEEK/2-HEC films containing MV^{2+} were then tested to determine if presence of the viologen affected the LAT generation. Presented in Figure 3.6 are the profiles of MV^{+} oxidation by O_2 resulting from repeated photolysis of 2-HEC films with MV^{2+} utilizing Glu and Tar as crosslinkers. The curves shown in Figures 3.6A and 3.6B indicate that MV^{+} decayed within a similar timespan for films made with either cross-linker, which also coincided with the behavior noted for the SPEEK• decay. Also, in agreement with the SPEEK• oxidation by O_2, the MV^{+} decay turned faster when R.H. increased. The insets of both figures show the initial $[MV^{+}]$ attained after each consecutive irradiation.

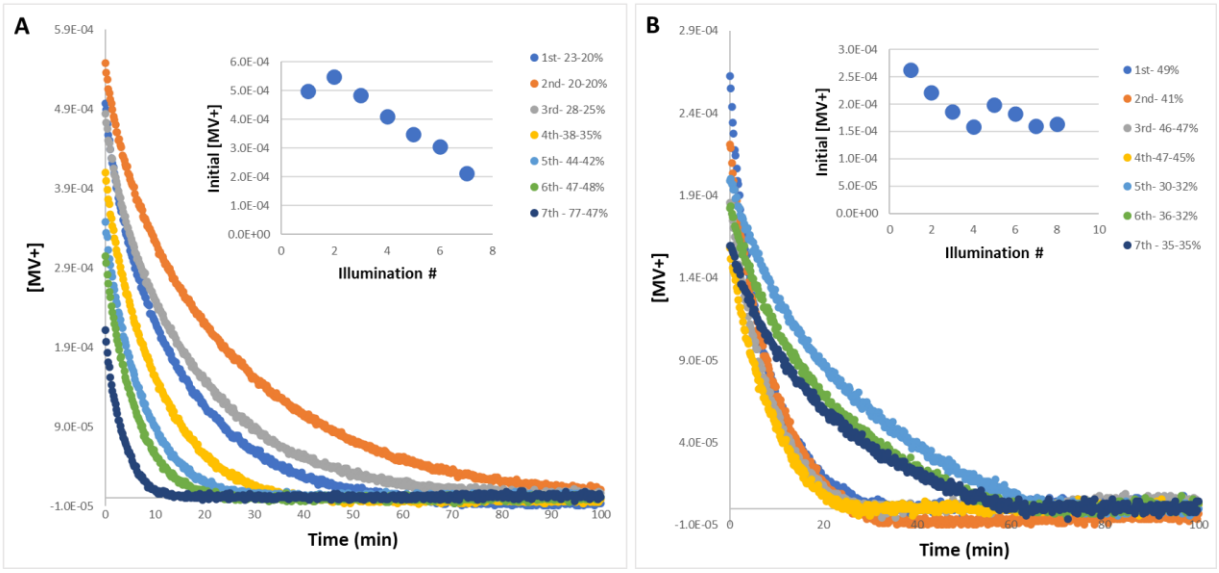

Figure 3.6: Comparison of radical decay profiles for consecutive illuminations of SPEEK/2-HEC films made with A) 1.5 x 10^{-4} mol Glu and B) 1.5 x 10^{-4} mol Tar. Both insets show the steady state $[MV^{+}]$ attained after each illumination.

A comparison of the data collected during the first illuminations of 2-HEC films containing Glu indicated that the initial $[MV^{+}]$ was 33% lower than the initial [SPEEKH•] obtained for films without viologen, see Chapter 2. Given that the polyketone radical forms MV^{+} via reduction of

the viologen, these findings mean that the efficiency of SPEEKH• photogeneration decreased in films containing MV^{2+}.

A comparison of the data collected during the first illuminations of 2-HEC films containing Tar indicated that the initial [MV^{+}] was 50% lower when compared with films with Glu. However, as discussed in Chapter 2, 2-HEC films without viologen showed only a 4% decrease in [SPEEKH•]. Thus, the effect made evident in Figure 3.6 is presumed to be due to the shorter molecular length of tartaric acid facilitating quenching of MV^{2+} of the SPEEK*. Repeated photolysis of 2-HEC films resulted in the initial [MV^{+}] decreasing by 58% after the 7^{th} illumination for Glu, and by 38% when Tar was the cross-linker. Incorporation of MV^{2+} reduced the effects of LAT on repeated photolysis of 2-HEC films since they still generated significant amounts of MV^{+} by the 7^{th} illumination compared to the efficiency of SPEEKH• formation in films free of MV^{2+}.

Shown in Figure 3.7A are the rate constants of MV^{+} oxidation for 2-HEC films with MV^{2+}, which exhibit a dependence on the ambient R.H. similar to that of SPEEKH• discussed in Chapter 2. The oxidation rate constants for 2-HEC films with Glu ranged from k = 0.046 min^{-1} at 20% R.H. to k = 0.17 min^{-1} at 49% R.H. Comparing these values with those for SPEEKH• (Chapter 2) reveals that the rate constants were ~35% lower throughout the humidity range. The decrease in oxidation rate is caused by MV^{2+} through electrostatic binding between SPEEK molecules constricting the polymer matrix. Previous work has shown that using Th or CV in SPEEK/cellulose films also resulted in much slower SPEEKH• oxidation times.[6] However, the charge localization of MV^{2+} being on the nitrogen atoms within the aromatic ring results in a weaker electrostatic binding and therefore less effect on oxygen permeability and structure constriction. Incorporation of MV^{2+} decreased the rate of oxidation; however, an increase in the

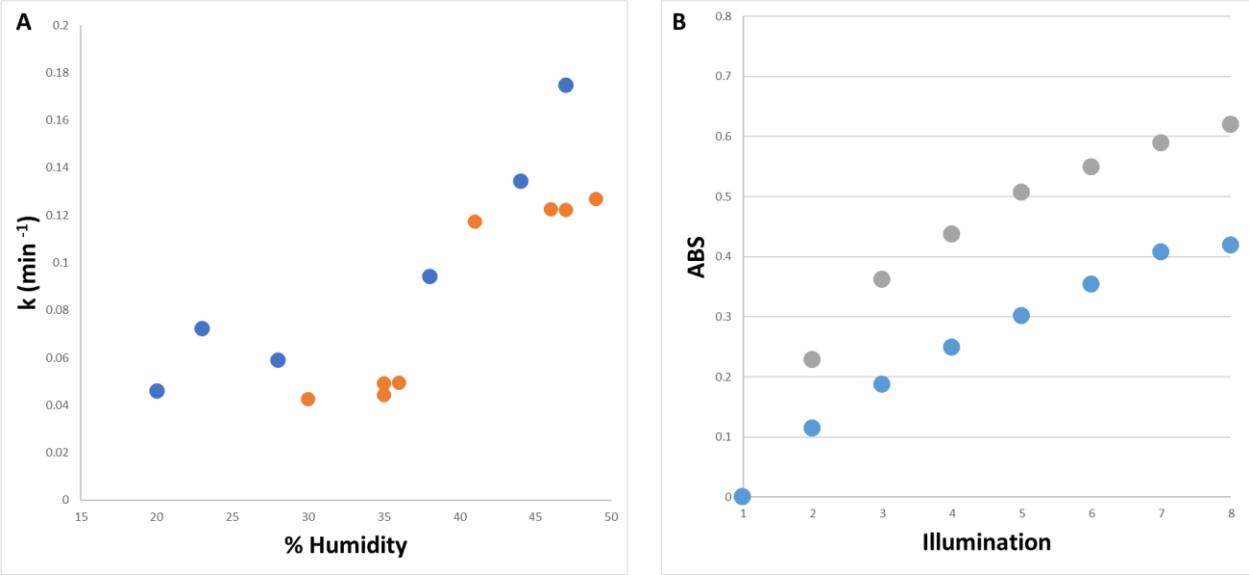

Figure 3.7: A) Pseudofirst-order rate constants for MV^+ oxidation versus R.H. for SPEEK/2-HEC films crosslinked with Glu (●) and Tar (●). B) LAT absorbance at 400 nm over multiple illuminations of a 2-HEC film crosslinked with Glu unexposed (●) or exposed to a 1 x 10^{-4} M MV^{2+} solution (●).

speed of this process was still noted above ~35% R.H. caused by the higher [H_2O] in the films discussed in Chapter 2.

According to the data displayed in Figure 3.7A the oxidation rates for 2-HEC films with Tar ranged from k = 0.0425 min^{-1} at 30% R.H. to k = 0.1224 min^{-1} at 47% R.H. Compared to the MV^+ oxidation rates of Glu-crosslinked films this represents a ~30% decrease in reaction speed. A similar decrease in the oxidation rate was also noted for SPEEKH• in CMC films crosslinked with Tar. This stems from the smaller molecular length of tartaric acid creating a tighter structure and reducing the permeability of oxygen in the polymer structure. Despite the change in crosslinker, an increase in the rate of oxidation at ~35% R.H. still took place showing that the enhanced O_2 diffusion into the films facilitated by increases in [H_2O] also occurred when MV^{2+} was present.

Repetitive photolysis of SPEEK/2-HEC films with MV^{2+} rendered them increasingly yellow due to a rise in absorbance at $\lambda \leq 450$ nm. An analogous coloration took place in SPEEK/PVA films yielding an absorption with $\lambda_{max} = 420$ nm.[14] In the case of SPEEK/cellulose films formation of LAT manifested itself by a strengthening in absorbance at $\lambda \leq 450$ nm that became more intense with decreasing wavelength without exhibiting a maximum .[14] Hence, the results of Figure 3.7B indicate that the LAT absorbance at 350 nm was strong enough to impede SPEEK from absorbing the incident photons, which stopped the photogeneration of SPEEKH•. Obviously, LAT formation in SPEEK/2-HEC films was significantly faster than in SPEEK/PVA solid matrices given that the latter turned yellow only after long light exposures.[14] These findings suggest that SPEEK interacts with 2-HEC more strongly than with PVA (probably via hydrogen bonding), thereby enhancing LAT formation through radical-radical reactions.

The data of Figure 3.7B demonstrates that incorporation of MV^{2+} into SPEEK/2-HEC films with Glu yielded a 30% reduction in LAT over 8 consecutive illuminations. Such an inhibiting effect of MV^{2+} on LAT formation resulted in the higher initial $[MV^{+}]$ illustrated in the inset of Figure 3.6A. Scavenging of SPEEKH• by MV^{2+} prevented reactions between the polyketone radicals that produced LAT. Figure 3.7A depicts the effect of LAT on the oxidation rate of MV^{+} in SPEEK/2-HEC films with Tar. Consecutive illuminations with rising humidity increased somewhat the rate of oxidation only at R.H. values higher than 35%. A similar trend was also observed with the oxidation of SPEEKH• in SPEEK/2-HEC films with Glu, where the oxidation rates decreased upon consecutive illumination at 50% R.H., as shown in Figure 3.7A. A possible explanation is that as more LAT is produced, the internal structure of the films is less able to expand.

3.4 Conclusion

Incorporating MV^{2+} in SPEEK/cellulose films improved the rates of radical oxidation, enabling easy detection of O_2 by visual means, in contrast to previous data using Th and CV as redox indicators. An explanation is that the cationic charges of MV^{2+} being localized mainly on nitrogen atoms positioned within the aromatic ring structure result in steric hindrance from the terminal methyl group (situated outside the aromatic rings), yielding a less rigid electrostatic bond.[7] This resulted in a higher O_2 permeability and a faster re-oxidation of the MV^{+} generated from the MV^{2+} reduction by SPEEKH•. The beneficial effect of MV^{2+} counterbalanced the lower efficiency of radical photogeneration that originated from quenching of SPEEK* by the viologen.

Incorporation of MV^{2+} into SPEEK/NaCMC films resulted in electrostatic binding to the sulfonate of SPEEK polyketone and the carboxylate groups of the cellulose. The rates of MV^{+} oxidation compared with SPEEKH• showed an increase in oxidation rates with Glu films having a more significant increase. This is presumed due to the internal crosslinking of the carboxylic acid group creating a stricter structure. So, the electrostatic binding of MV^{2+} behaves similarly to water expanding the structure. There was also minor quenching of SPEEK* in NaCMC films which affected the maximum MV^{+} concentration.

MV^{2+} was also incorporated into SPEEK/2-HEC films however sulfonate groups of SPEEK were the only sites for electrostatic binding of the viologen. Hence, quenching of SPEEK* was more pronounced in 2-HEC films resulting in a significant decrease in the MV^{+} concentration. Although quenching of SPEEK* took place, the fast scavenging of SPEEKH• by MV^{2+} hindered the reaction between polyketone radicals that form LAT. As an example, inhibition of LAT generation in 2-HEC films with MV^{2+} was significant enough to yield steady-

state radical concentrations over more consecutive illuminations compared to 2-HEC films without viologen.

In contrast to NaCMC films, the oxidation rate of MV^+ decreased for 2-HEC films, presumably because electrostatic binding of the viologen to SPEEK stiffened the polymer matrix, thereby inhibiting oxygen diffusion. The findings of the project show the ability to increase the optical detectability of SPEEK/cellulose films for oxygen sensing. Continued study in the incorporation of alternative redox dyes and polymeric matrixes could provide invaluable knowledge of the effects of electronic interactions on radical reactions.

References

[1] Mills, A. Oxygen indicators and intelligent inks for packaging food. *Chem. Soc. Rev.* **2005**, *34*, 1003-1011.

[2] Lee, S.; Sheridan, M.; Mills, A. Novel UV-activated colorimetric oxygen indicator. *Chem. Mater.* **2005**, *17*, 2744-2751.

[3] Wang, X.; Wolfveis, O. S. Optical methods for sensing and imaging oxygen: materials, spectroscopies and applications. *Chem. Soc. Rev.* **2014**, *43*, 3666-3761.

[4] Mills, A.; Hazafy, D.; Lawrie, K. Novel photocatalyst-based colourimetric indicators for oxygen. *Catal. Today* **2011**, *161*, 59-63.

[5] Gibis, D.; Rieblinger, K. Oxygen scavenging films for food application. *Procedia Food Sci.* **2011**, *1*, 229–234.

[6] Dissanayaka, R. H. Reversible and irreversible light-induced reactions initiated by SPEEK/PVA polymer systems. Ph.D. Thesis, Auburn University, May 2021.

[7] Watanabe, T.; Honda, K. Measurement of the extinction coefficient of the methyl viologen cation radical and the efficiency of its formation by semiconductor photocatalysis. *J. Phys. Chem.* **1982**, *86*, 2617-1619.

[8] Korchev, A. S.; Shulyak, T. S.; Slaten, B. L.; Gale, W. F.; Mills, G. Sulfonated Poly(Ether Ether Ketone)/Poly(Vinyl Alcohol) Sensitizing System for Solution Photogeneration of Small Ag, Au, and Cu Crystallites. *J. Phys. Chem. B* **2005**, *109*, 7733−7745.

[9] Sweetser, P. B. Colorimetric Determination of Trace Levels of Oxygen in Gases with the Photochemically Generated Methyl Viologen Radical-Cation. *Anal Chem.* **1967**, *39*, 979-982.

[10] Wolszczak, M.; Stradowski, C. Methylviologen cation radical, its dimer and complex in various media. *Radiat. Phys. Chem*. **1989**, *33*, 355-359.

[11] Gilbert, A.; Baggott, J. Essentials of molecular photochemistry, CRC *Press: Boca Raton*, **1991**; 287-353.

[12] Das, P. K. Electron Transfer Reactions from Aromatic Carbonyl Triplets to Paraquat Dication. *Tetrahedron Lett.* **1981**, *22*, 1307-1310.

[13] Knoesel, R.; Weill, G. Room Temperature Phosphorescence of Poly(p-vinylbenzophenone) in Solution. *Polym. Photochem.* **1986**, *7*, 119-127.

[14] Lockhart, P.; Little, B. K.; Slaten, B. L.; Mills, G. Photogeneration of H_2O_2 in Water-Swollen SPEEK/PVA Polymer Films. *J. Phys. Chem. A* **2016**, *120*, 3867–3877.

[15] Lien, L.; Fellows, C. M.; Copeland, L.; Hawkett, B. S.; Gilbert, R, G. Water-binding and oxygen permeability in poly(vinyl alcohol) films. *Aust. J. Chem.* **2002**, *55*, 507-512.

Chapter 4

4.1 Introduction

As demonstrated in the previous chapters, SPEEK/cellulose films act as oxygen sensors where the oxidation kinetics is affected by effects of the polymeric matrix and environmental conditions. The electrostatic inhibition of radical reactions and the dependence of MV^+ oxidation kinetics on R.H. are effects characteristic of such films that deserve further investigation. Previous work on SPEEK/PVA systems showed that mechanistic information gathered from solution studies facilitated understanding of the photoreactions taking place in swollen films.[1-4] This is reasonable given that photo processes taking place in the fluid medium are less hindered by complications frequently found in solid matrices. Illuminated degassed SPEEK/PVA solutions generated SPEEKH• that experienced radical-radical decay processes lasting over 30 min, which is atypical for small radicals in water.[1] This phenomenon is not unusual for radicals from bulky polyelectrolytes, which experience diffusional restrictions that are exacerbated by significant interchain electrostatic repulsions.[5] In contrast, the decay of SPEEKH• in films of SPEEK/PVA took 10 times longer because motion of radicals is severely hindered in solid matrices.

Furthermore, investigations on the photoreduction of halomethanes in SPEEK/PVA solutions provided key mechanistic information that aided understanding of the kinetic features governing the dehalogenation of $CHCl_3$ in swollen polymer films.[6-8] Also, findings obtained from solution photolytic experiments enabled to rationalize kinetic features of earlier work on O_2 indicators based on SPEEK/PVA films containing Th and CV dyes.[9] Hence, solution studies were expected to provide insight about some unexpected observations, such as the slow zero-order decay of SPEEKH• and MV^+ in polymer films where air was rigorously excluded. Experiments were, therefore, conducted with SPEEK/cellulose solutions and swollen films, thought to

constitute simpler analogous of the dry polymer matrices with the purpose of gaining further mechanistic knowledge.

4.2 Methods and Procedures

The sources of most employed chemicals were identified in the previous chapter, which also described film preparation methods as well as illumination and analytical procedures. Sodium formate (HCO_2Na) was purchased from Sigma Aldrich. SPEEK/cellulose solutions were of 7.5 x 10^{-4} M cellulose and 3.8 x 10^{-2} M SPEEK without incorporating the crosslinker. Solutions for methyl viologen experiments contained 0.3 M sodium formate and 1 x 10^{-4} M MV^{2+} unless otherwise declared. All SPEEK/cellulose swollen films and solutions were Ar sparged and then photolyzed using the setup shown in Figure 4.1. The films were 2.5 cm by 1.25 cm to prevent curling

Figure 4.1: Setup for solution and swollen films utilizing glass test tubes sealed with rubber septa placed in a Shimadzu UV/Vis holder.

and maintain the thickness of a single film during UV/Vis measurements. All illuminations and optical measurements were conducted with Milton Roy #33-17-80 optical test tubes with a

pathlength of 1 cm and a cutoff at $\lambda \leq 300$ nm) without removal of the test tube to reduce error. Irradiation of cellulose polymer solutions and films was conducted inside a Rayonet RPR-100 circular illuminator equipped with 16 RPR-3500A lamps for 5 min producing 10 μM/s photons of 350 nm. Photogenerated radicals were detected optically using a Shimadzu UV-2501 PC UV-VIS spectrophotometer. Tests were run at least in triplicate; the resulting kinetic results exhibited deviations of about 20%. FTIR measurements employed a Thermo Scientific iS50 ATR instrument. EPR measurements were conducted using a Bruker EMX EPR spectrometer.

4.3 Results and Discussion

Exposure of Ar sparged SPEEK/cellulose solutions to 350 nm photons for 5 min failed to generate detectable SPEEKH•, indicating that the radicals derived from the Solvay precursor decay fast via combination/disproportionation reactions. The same outcome resulted after addition of 0.3 M HCO_2^- and 1 x 10^{-4} M MV^{2+}, although formate ions are efficient H-atom donors that facilitate radical reactions as was shown during the reduction of chloromethanes.[6-8] The lack of MV^{2+} reduction is unsurprising given that the viologen is able to quench SPEEK* (as was shown in the previous chapter). Only upon illumination times > 30 min was the MV^+ signal observed meaning the free movement of radicals in cellulose solutions facilitates radical-radical reactions. Swollen films were next studied to understand these processes and limit radical-radical reactions. The study of Ar sparged swollen SPEEK/cellulose films focused on MV^{2+} reduction as the SPEEKH• signal was never observed. Illumination of SPEEK/2-HEC films swollen in solutions with 1 x 10^{-4} M MV^{2+} generated a low amount of MV^+; however, the absorbance at $\lambda >$ 400 nm increased significantly due to LAT formation. Irradiation of swollen SPEEK/NaCMC films crosslinked with 2.25 x 10^{-4} mol Glu yielded analogous results except that no LAT was formed. Different findings occurred when SPEEK/NaCMC films were photolyzed in solutions of

0.3 M HCO_2^- and 1 x 10^{-4} M MV^{2+}. As shown in Figure 4.2, the resulting absorption spectra corresponds to that of MV^+; an image of the illuminated film is included in the inset demonstrating that all the viologen radical cation formed was bound to the film and not in the solution. Such an outcome implies that the reaction generated MV^+ electrostatically bound to

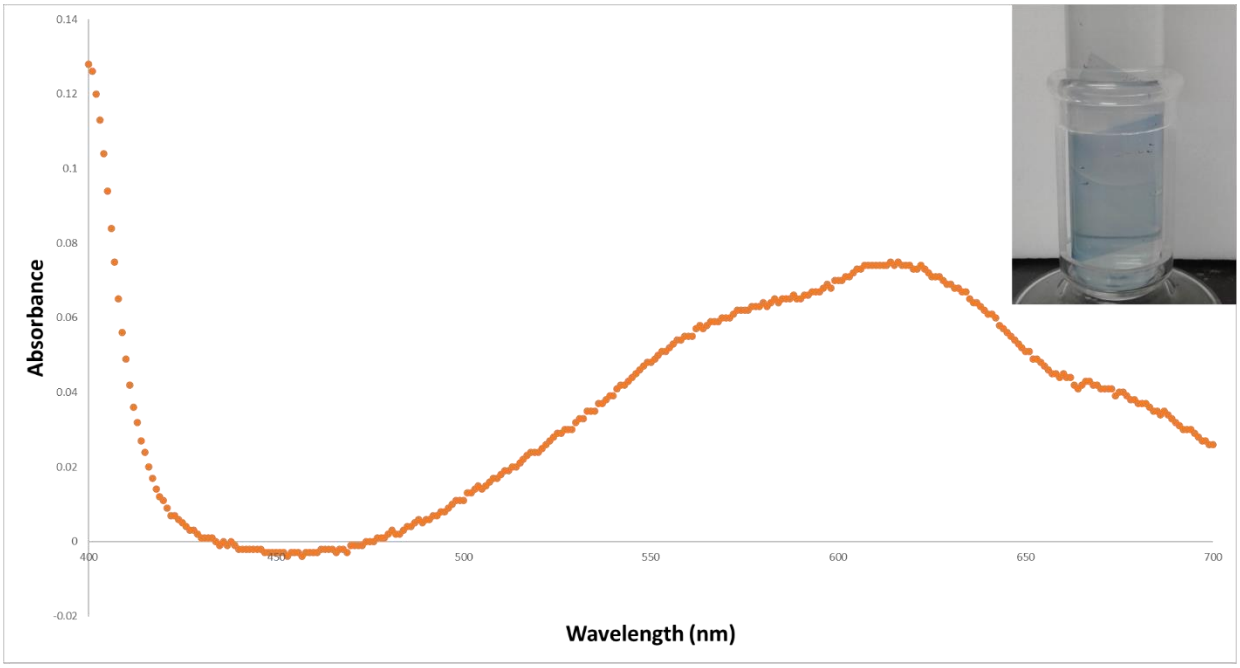

Figure 4.2: Absorption spectrum of MV^+ generated via a 5 min illumination of a SPEEK/NaCMC film crosslinked with 1.5 x 10^{-4} mol Glu swollen in an Argon sparged solution containing 0.3 M HCO_2^- and 1.0 x 10^{-4} M MV^{2+}. Inset shows an image of the film after irradiation.

NaCMC and SPEEK. In formate solutions H-atom abstraction from HCO_2^- by SPEEK* yields $\bullet CO_2^-$,[7] and reduction of MV^{2+} in swollen SPEEK/cellulose films can be understood in terms of the mechanism described in Chapter 2 with the addition of the reactions shown in Scheme 2.1. Unlike the bound radicals of SPEEK and cellulose, $\bullet CO_2$- is free to diffuse through the swollen film facilitating reduction of MV^{2+}. Surprisingly, monitoring the MV^+ signal revealed a fast oxidation of the radical cation in the absence of air. Decay curves of MV^+ in a swollen

(1) $^{3}\{R'RC=O\}_z^{*} + HCO_2^- \rightarrow \{R'RC\bullet OH\}_z + \bullet CO_2^-$

(2) $\{R'RC\cdot OH\}_z/\bullet CO_2^- + MV^{2+} \rightarrow \{R'RC=O\}_z/CO_2 + H^+ + MV^+$

Scheme 4.1: Mechanism for the formation of MV^+ utilizing SPEEK and HCO_2^-. SPEEK is denoted as $\{R'RC=O\}_z$ and $\{R'RC\bullet OH\}_z$ represents SPEEKH•.

SPEEK/NaCMC film are presented in Figure 4.3, showing that this oxidation process took place in the same timescale as that of non-swollen films containing air, see Chapter 3.

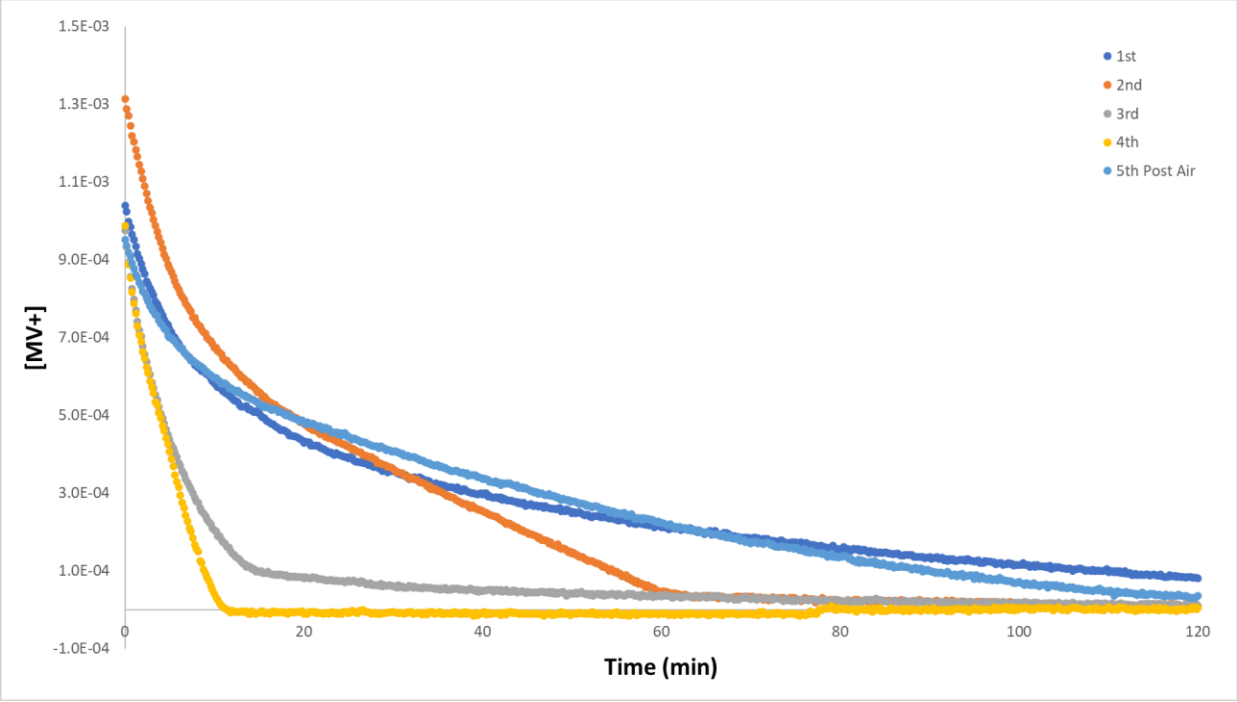

Figure 4.3: MV^+ decay profiles for a SPEEK/NaCMC film with 2.25 x 10^{-4} mol Glu swollen in an air-free solution of 0.3M HCO_2^- and 1 x 10^{-4} M MV after exposure to consecutive illuminations. 5th illumination (●) conducted after exposure to air for 24 h and Ar bubbling.

In fact, this oxidation of MV^+ was substantially faster than the decay of the radical in air-free non-swollen films. Such observations imply that an unknown oxidizing agent (X) was formed during the photoreduction of MV^{2+} induced by the swollen films.

In addition, a continuous increase in decay rate took place with each subsequent illumination. For instance, the 1st illumination yielded a decay with a half-life of ~16 min, for the second irradiation $t_{1/2} \approx 11.2$ min, and $t_{1/2} \approx 4.6$ min for the third exposure to light. A reasonable explanation is that each subsequent illumination generated excess oxidizing product, inducing an increase in the rate of decay. The initial $[MV^+]$ of each illumination was equivalent except for the second irradiation which lasted 6 min, yielding a 25% increase in $[MV^+]$. By the 4th photolytic exposure, the rate of decay was a linear function of time with a $t_{1/2} \approx 4.4$ min. After the 4th illumination, the solution containing the swollen film was exposed to air for 24 h and then Ar bubbled. The subsequent 5th illumination exhibited a rate of MV^+ decay similar to the 1st illumination shown in Figure 4.3. This unusual finding implies that the oxidizing product X was removed upon reaction with O_2.

The decay data was analyzed in terms of first and second-order rate laws, the corresponding plots are depicted in Figure 4.4. As shown in Figure 4.4A, the kinetic results of the MV^+ decay that occurred after the 1st and 2nd illuminations, as well as the data gathered after the 5th irradiation, yielded good fits when plotted according to a second-order rate law. Such findings seem to imply that the decay process involved a reaction of two compounds with roughly equal concentrations, that is, $[MV^+] \approx [X]$. After the 3rd illumination, the kinetic data of the MV^+ oxidation was best fitted using a first-order rate law as illustrated in Figure 4.4B implying that $[X] > [MV^+]$. Following the 4th irradiation the rate of MV^+ oxidation was a linear function of time (see Figure 4.3), meaning that $[X] >> [MV^+]$.

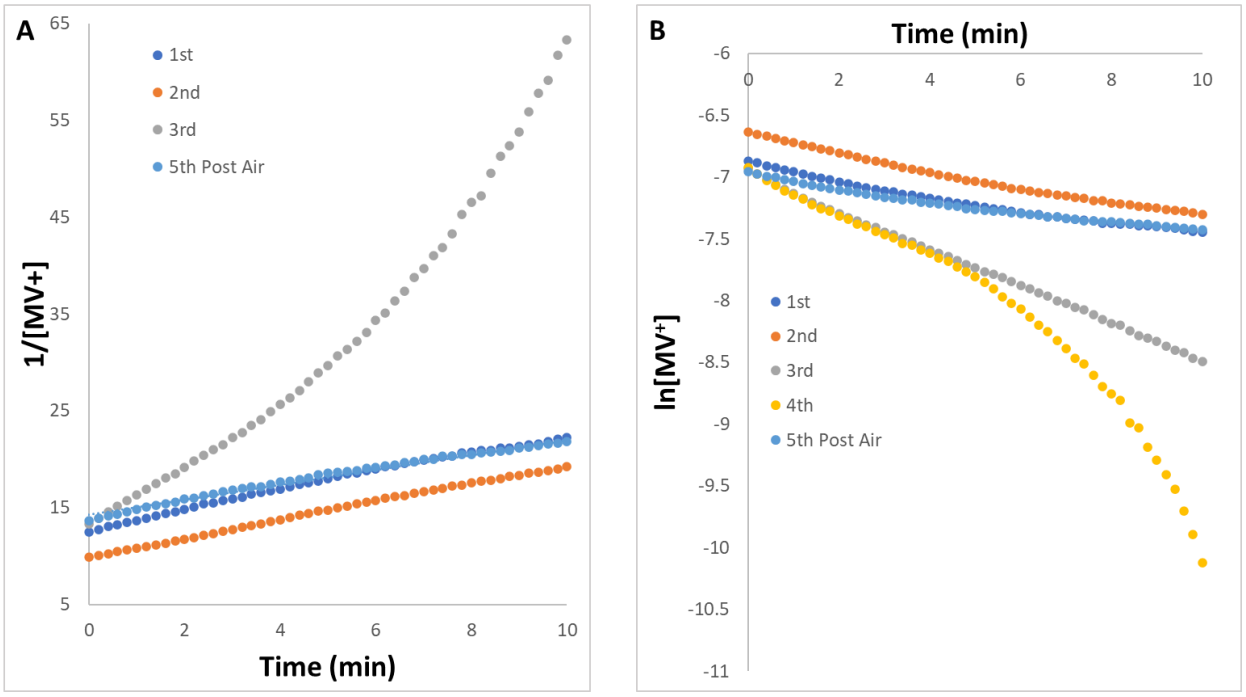

Figure 4.4: A) Second-order plots of the MV^+ decay in a SPEEK/NaCMC film with 2.25 x 10^{-4} mol Glu swollen in an air-free solution of 0.3M HCO_2^- and 1 x 10^{-4} M MV. B) First-order plots of the data.

These observations support the idea that the side product X was formed in excess of [MV^+]. The decay of MV^+ was not a result of a reduction of the viologen radical to MV^0 because the characteristic signal of such product with λ_{max} = 395 nm was not detected.[10,11] Perhaps the most intriguing finding of the experiments involving multiple illuminations was the reversibility of the entire process after air was admitted into the system.

Subsequent tests were conducted to ascertain if the use of the cellulose as the H-atom donor was a determining factor in the formation of X. For that purpose PVA was utilized instead of the cellulose polymers as the photoreactions of SPEEK/PVA mixtures have been studied extensively.[1-4,6-9] In agreement with earlier reports, illumination of air-free solutions containing PVA and the polyketone prepared using the PEEK precursor from Solvay failed to photogenerate long-lasting SPEEK radicals.[7] Coinciding with observations made using air-free solutions of

SPEEK and NaCMC, only low amounts of MV^{+} were generated upon exposure to 350 nm photons for long times. In contrast, Figure 4.5A shows that MV^{+} formed efficiently during irradiation of a SPEEK/PVA film crosslinked with 7.5 x 10^{-5} mol Glu and swollen under Ar in a solution containing 0.3 M HCO_2^- and 1 x 10^{-4} M MV^{2+}. Curiously, the photogenerated MV^{+} was present in solution as well as attached to the film, probably because in this system only the sulfonic groups of SPEEK were available to bind the viologen electrostatically.

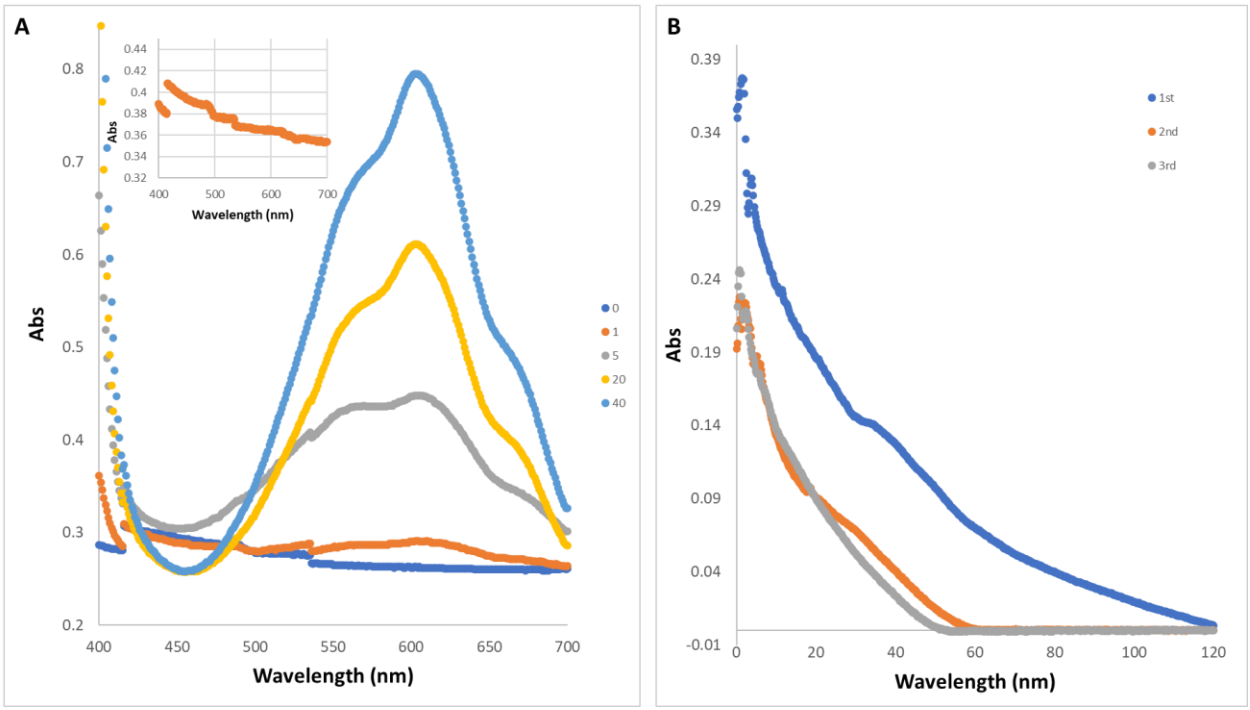

Figure 4.5: A) Spectra of SPEEK/PVA film crosslinked with 7.5 x 10^{-5} mol Glu swollen in an air-free solution of 0.3 M HCO_2^- and 1 x 10^{-4} M MV^{2+} at different illumination times. Inset shows a spectrum of a SPEEK/PVA film swollen in a solution of 1 x 10^{-4} M MV^{2+} illuminated for 40 (●) min. B) MV^{+} decay in a SPEEK/PVA film crosslinked with Glu swollen in an air-free solution of 0.3M HCO_2^- and 1 x 10^{-4} M MV^{2+} after 3 consecutive illuminations for 5 min.

In agreement with observations made with SPEEK/NaCMC swollen films, the data presented in the inset of Figure 4.5A demonstrate that SPEEK/PVA films illuminated in an Ar sparged solution without HCO_2^- yielded no viologen reduction even after illumination times > 40 min. Presented in Figure 4.5B are the MV^+ decay curves, the fluctuations noticed in the kinetic data probably originated from diffusion of the viologen radical in and out of the films. As reported earlier for swollen SPEEK/NaCMC films, an increase in MV^+ oxidation rate took place with rising number of consecutive illuminations. The half-life after the 1st irradiation was $t_{1/2} \approx 19.4$ min, $t_{1/2} \approx 13$ min after the second illumination, and $t_{1/2}$ amounted to ≈ 13 min for the third photolytic step. These findings mean that X was formed regardless which macromolecular H-atom donor (cellulose or PVA) was employed.

Several efforts were made to gain further insight about the nature of X, including experiments to ascertain if a radical species was involved in the MV^+ oxidation. For that purpose, EPR spectra were acquired after illumination of swollen films under the conditions described in the caption to Figure 4.2. The sample was prepared inside a glass EPR tube that was photolyzed at room temperature in the absence of air and then frozen with liquid N_2. Only the EPR signal from MV^+ was detected which decayed upon warming the sample to room temperature. Only a very weak Cu^{2+} signal remained after the decay of MV^+. Tests using atomic absorption spectroscopy confirmed that approximately 1.1×10^{-7} mol of Cu^{2+} were present as an impurity in 0.1g of SPEEK, which explains the source of the copper signal. These findings provided evidence that the decay of MV^+ was not induced by a radical species.

Next, attempts were made to scavenge X using ascorbate anions (AA) since these species are known to be efficient reducing agents.[12] For this purpose, a swollen SPEEK/NaCMC film was

exposed to light in an air-free solution containing 1.32 x 10^{-2} M of the sodium salt of ascorbic acid

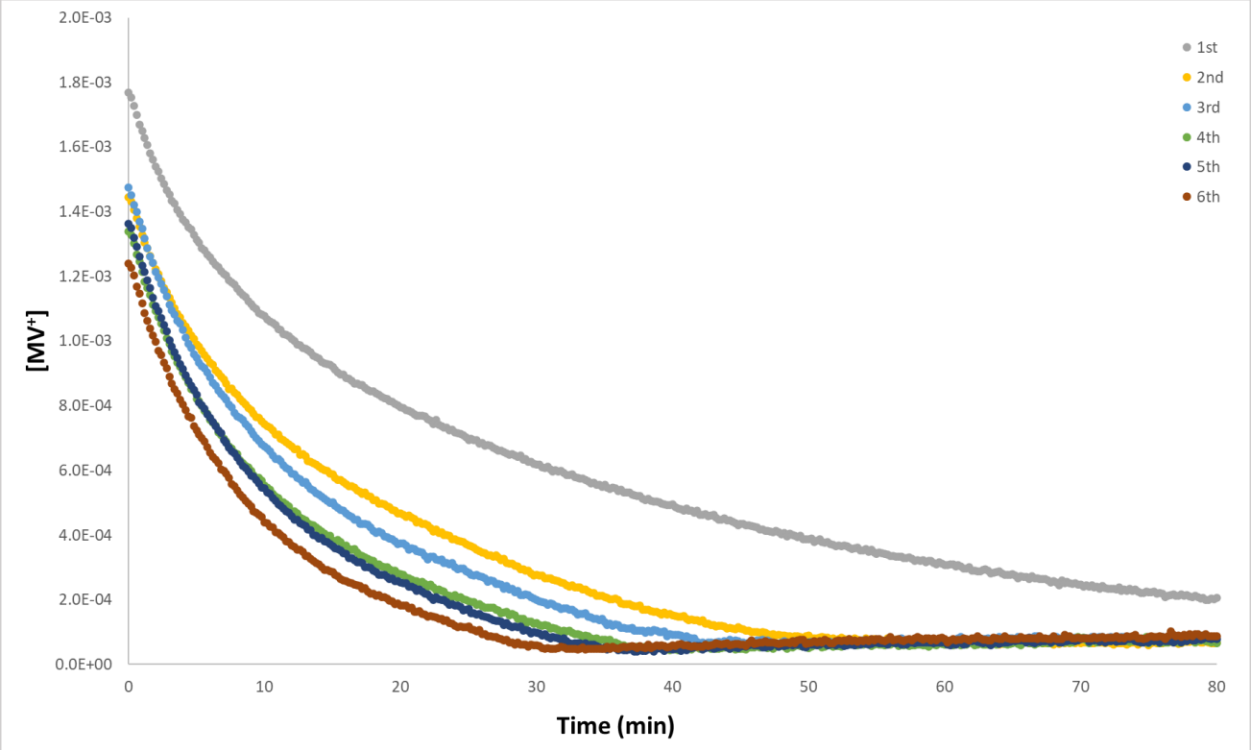

Figure 4.6: Plot of kinetic decay profiles of SPEEK/NaCMC film with 2.25 x 10^{-4} mol Glu swollen in a solution of 1.32 x 10^{-2} M ascorbic acid, 0.3M HCO_2^-, and 1 x 10^{-4} M MV exposed to consecutive illuminations.

together with HCO_2^- and MV^{2+}. Illustrated in Figure 4.6 are the MV^+ decay profiles for the several consecutive illuminations. Again, the rate of MV^+ decay increased with each subsequent illumination with a half-life of ~16.2 min after the 1st illumination with $t_{1/2}$ continuously decreasing to ≈ 6.6 min after the 6th illumination step. Overall, the rates of MV^+ decay were lower than in the absence of AA and increased in a less pronounced fashion with rising number of illumination steps. These observations mean that X was only partially eliminated when AA was present in the swelling solution. However, AA are known to scavenge radicals including α-hydroxy carbon-centered radicals (such as SPEEKH•).[13,14] A reasonable explanation for the data

of Figure 4.6 is that AA scavenged the precursor of X decreasing the production of the oxidizer. Interestingly, as shown in Figure 4.6, each photolytic step generated a higher [MV^+] in the presence of AA, which is consistent with the notion that the ascorbate ions interfered with the formation of X.

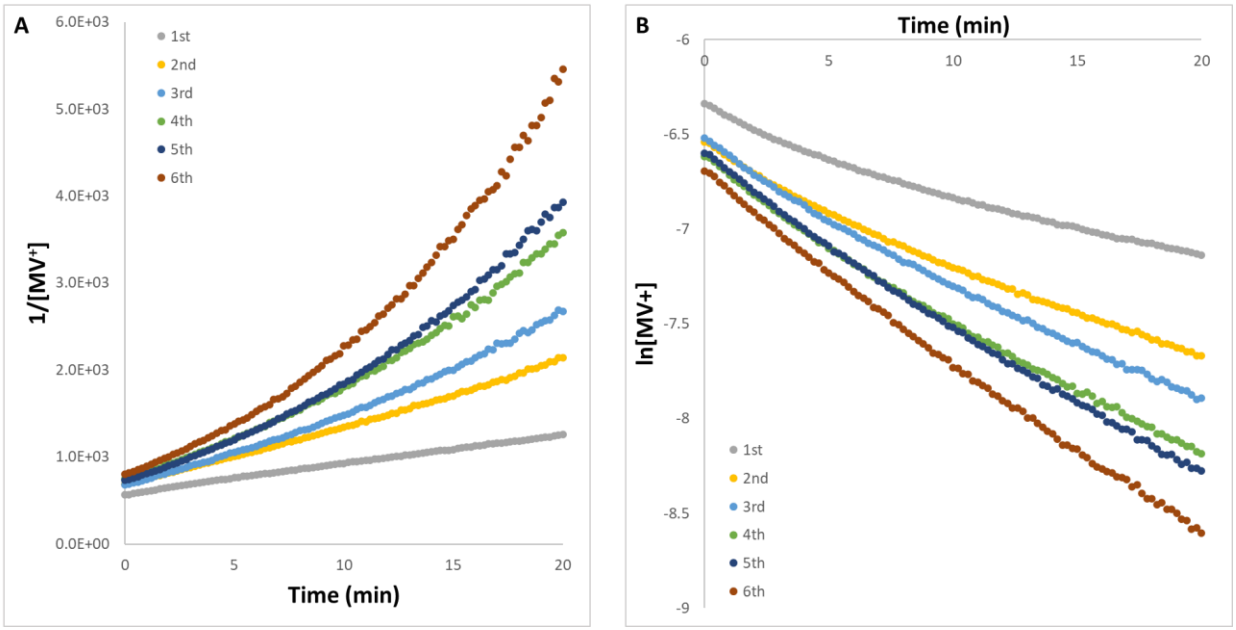

Figure 4.7: A) Second-order plots of data from the radical decay in a SPEEK/NaCMC film with 2.25 x 10^{-4} mol Glu swelled in a solution of 1.32 x 10^{-2} M ascorbic acid, 1 x 10^{-4} M MV^{2+} and 0.3M HCO_2^-. B) First-order plots of the data shown in Figure 4.6.

Presented in Figure 4.7 are plots of the data from Figure 4.6 according to first and second-order rate laws. According to Figure 4.7A, a reasonable fit to a second-order rate law was obtained with the kinetic results of the MV^+ oxidation after the first illumination, suggesting that the transformation involved two reactants of similar concentrations. However, the data acquired during the subsequent four irradiations increasingly deviated from the trend expected for a second-order reaction. In fact, the data for the MV^+ oxidation following the 6^{th} illumination

agreed best with a first-order rate law. These observations suggest that AA act as scavengers for the precursor of X thereby hindering the formation of this oxidizer.

Additional infrared spectroscopy (IR) measurements were conducted on the SPEEK/NaCMC film to provide more insight into the reactions that occur upon illumination. Representative spectra are shown in Figure 4.8 for an unirradiated film as well as for films irradiated in air-free formate

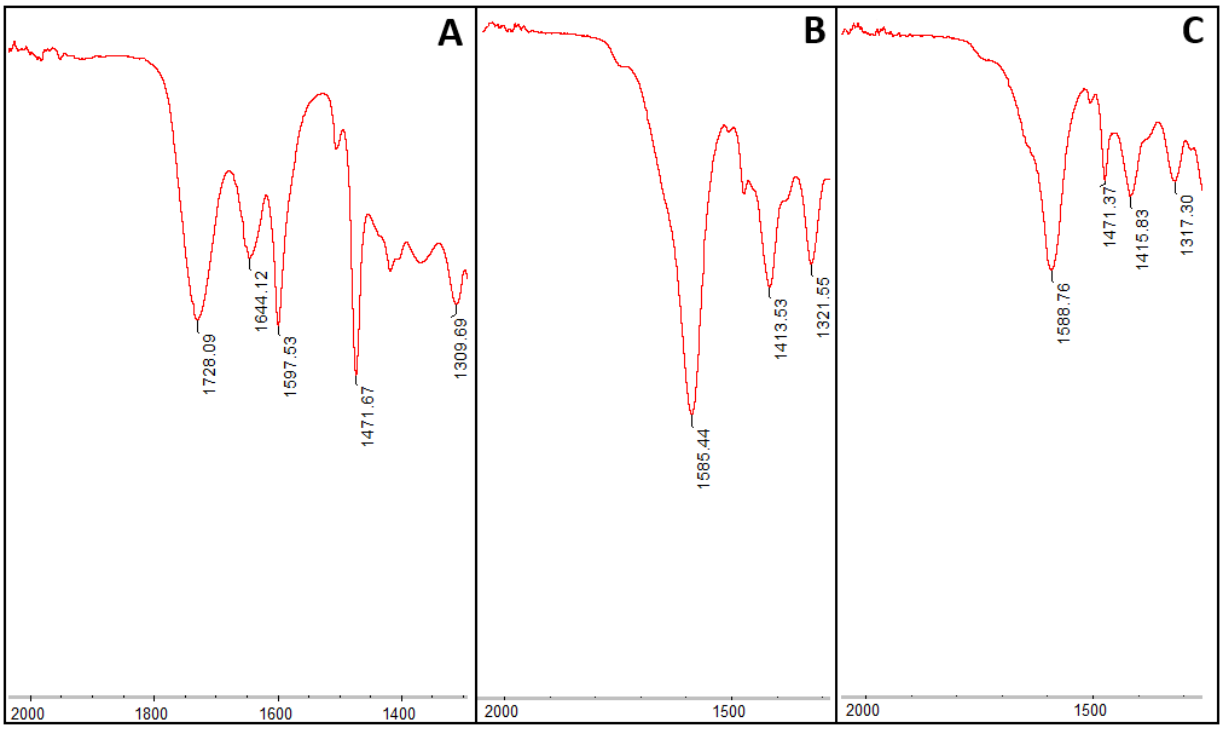

Figure 4.8: IR spectra of SPEEK/NaCMC films A) before illumination, B) after illumination in 0.3 M HCO_2^- solution and C) illuminated in a solution containing 0.3M HCO_2^- and 1 x 10^{-4} M MV^{2+}.

solutions with and without MV^{2+} that were exposed to air after illumination. Significant changes were found for the IR signals of the ester linkages at 1730 cm^{-1} and carboxylic acid at 1588 cm^{-1} from NaCMC, as well as the SPEEK ketone C=O stretch at 1651 – 1644 cm^{-1}, benzophenone C=C stretch at 1595 – 1588 cm^{-1}, and sulfonated benzene C=C stretch at 1502 – 1471 cm^{-1}.

Figure 4.8A displays the IR spectrum of a film before illuminated. This spectrum is compared with those of films photolyzed without O_2 followed by exposure to air after irradiation. Presented in Figure 4.8B is the spectral data obtained from a film immersed in a 0.3 M HCO_2^- solution, whereas Figure 4.8C shows the spectrum swollen in a solution containing 0.3 M HCO_2^- and 1 x 10^{-4} M MV^{2+}. In both samples irradiated in solution the ester linkage signal at 1730 cm^{-1} was found to decrease in intensity upon illumination while the signal at 1588 cm^{-1} became more intense. Such changes are consistent with the scission of the ester linkage and simultaneous emergence of a carboxylate function. While changes to the ketone C=O stretch at 1651–1644 cm^{-1} cannot be determined due to signal overlap with those of carboxylic acid and benzophenone C=C stretch 1595–1588 cm^{-1}, the presence of a shoulder on the C=O stretch at 1651–1644 cm^{-1} confirms the presence of a ketone functionality. The signal of the sulfonated benzene C=C stretch at 1502–1471 cm^{-1} however shows a significant intensity decrease in both films. This means that a product was formed in which the SPEEK benzene ring to which the SO_3^- group is bonded experienced a complete loss of aromaticity.

4.4 Conclusion:

Experiments with SPEEK/NaCMC solutions and swollen films were conducted in efforts to gain further insight into the mechanism of the SPEEK/cellulose system because earlier studies showed that useful mechanistic information was accessible from tests in the fluid medium. However, such expectation was not realized in the case of aqueous solutions because of a combination of quenching of SPEEK* by MV^{2+} together with fast reactions of generated radicals. Instead, photolysis of SPEEK/NaCMC films swollen in formate solutions free of air that contained MV^{2+} yielded several unexpected findings. For instance, viologen photoreduction occurred exclusively in the presence of HCO_2^- ions and all the MV^+ produced remained bonded

to the swollen film. Other examples included the post-irradiation MV^+ decay in the absence of air which was accelerated by conducting consecutive illuminations. These findings indicated the formation of byproduct X able to oxidize MV^+ back to the parent viologen. Interestingly, formation of such oxidizer provided an explanation for the slow decay of MV^+ after photolysis of SPEEK/cellulose films in the absence of air that was discussed in Chapter 3. Furthermore, while X was completely consumed in the presence of air this species acted as an oxidizer toward MV^+. Perhaps the most surprising outcome of the experiments with swollen SPEEK/NaCMC films was their ability to function as photoadaptive systems over multiple exposures to light. In fact, exposure of the systems to air restored their ability to function in a reversible fashion. Illuminations of SPEEK/PVA films confirmed that the presence of SPEEK was necessary for generating the side product X. Another significant finding was that [X] increased as a result of consecutive irradiations. Although efforts to elucidate completely the nature of X were not successful, experiments conducted in the presence of AA and also by means of EPR determinations revealed that the oxidizer is not a radical species. IR data indicated formation of a product that suffered a significant loss of aromaticity of the SPEEK sulfonated benzene ring.

References:

[1] Korchev, A. S.; Shulyak, T. S.; Slaten, B. L.; Gale, W. F.; Mills, G. Sulfonated poly(ether ether ketone)/poly(vinyl alcohol) sensitizing system for solution photogeneration of small Ag, Au, and Cu crystallites. *J. Phys. Chem. B,* **2005**, *109*, 7733-7745.

[2] Korchev, A. S.; Konovalova, T.; Cammarata, V.; Kispert, L.; Slaten, B. L.; Mills, G. Radical-induced generation of small silver particles in SPEEK/PVA polymer films and solutions: UV-Vis, EPR, and FT-IR Studies. *Langmuir* **2006**, *22*, 375-384.

[3] Little, B. K.; Lockhart, P.; Slaten, B. L.; Mills, G. Photogeneration of H_2O_2 in SPEEK/PVA aqueous polymer solutions. *J. Phys. Chem. A,* **2013**, *117*, 4148-4157.

[4] Lockhart, P.; Little, B. K.; Slaten, B. L.; Mills, G. Photogeneration of H_2O_2 in Water-Swollen SPEEK/PVA Polymer Films. *J. Phys. Chem. A*, **2016**, *120*, 3867–3877.

[5] Ulanski, P.; Bothe, E.; Hildenbrand, K.; Rosiak, J.M.; von Sonntag, C. Hydroxyl-Radical-Induced Reactions of Poly(Acrylic Acid); a Pulse Radiolysis, EPR and Product Study. Part I. Deoxygenated Aqueous Solutions. J. Chem. Soc. Perkin Trans. 2 1996, 13–22.

[6] Black, J. R.; Islam, M.S.; Carmichael, H.L.; Slaten, B.L.; Little, B. K.; Mills, G. Radical chain reduction of CCl_4 initiated by illumination of SPEEK solutions. *J. Phys. Chem. A* **2017**, *121*, 3918-3928.

[7] Islam, M. S.; Duin, E. C.; Slaten, B. L.; Mills, G. Photoreduction of $CHCl_3$ in Aqueous SPEEK/HCO_2^- Solutions Involving Free Radicals. *J. Phys. Chem. A* **2018**, *122*, 7118-7130.

[8] Dissanayaka,R. H.; Islam, M. S.; Mills, G. Chain Photoreduction of $CHCl_3$ Photocatalyzed by SPEEK/PVA Films Swollen in Air-saturated HCOsNa Solutions. *Materials* **2023**, *16*, 6629.

[9] Dissanayaka, R. H. Reversible and irreversible light-induced reactions initiated by SPEEK/PVA polymer systems. Ph.D. Thesis, Auburn University, May 2021.

[10] Watanabe, T.; Honda, K. Measurement of the extinction coefficient of the methyl viologen cation radical and the efficiency of its formation by semiconductor photocatalysis. *J. Phys. Chem.* **1982**, *86*, 2617-1619.

[11] Wolszczak, M.; Stradowski, C. Methylviologen cation radical, its dimer and complex in various media. *Radiat. Phys. Chem.* **1989**, *33*, 355-359.

[12] Du, J.; Cullen, J. J.; Buettner, G. R. Chemistry, Biology and Treatment of Cancer. *Biochem. Biophys. Acta* **2012**, *1826*, 443-457.

[13] Brinkevich, S.; Shadyro, O. The effects of ascorbic acid on homolytic processes involving α-hydroxyl-containing carbon-centered radicals. *Bioorg. Med. Chem. Lett.* **2008,** *18*, 6448-6450.

[14] Tu Y.; Njus, D.; Schlegel, H. B. A theoretical study of ascorbic acid oxidation and HOO•/O2•⁻ radical scavenging. *Org. Biomol. Chem.* **2017**, 15, 4417–4431

Appendix 1

The Influence of Various Grease Compositions and Silver Nanoparticle Additives on Electrically Induced Rolling-element Bearing Damage

S. Bond[1], R. L. Jackson[2], and G. Mills[1],
[1]Department of Chemistry and Biochemistry
[2]Department of Mechanical Engineering
Auburn University

A1.0 Abstract

Leakage currents accelerate surface degradation of metal contacts via small scale arcing across lubricating films, but recent observations suggest that metallic nanoparticle additives in lubricants may be useful to improve contact performance. These findings prompted a study dealing that examined electrically induced surface pitting of steel contacts in the presence of several lubricating greases including some containing nanometer-sized colloidal Ag particles. Reciprocating rolling sphere-on-disk experiments were conducted under electro-tribological loads employing polyurea greases derived from mineral and synthetic base oils with and without additives. Friction forces and electrical resistance were monitored continuously during the tests; surface changes were characterized by means of optical spectroscopy, stylus profilometry and scanning electron microscopy (SEM) including compositional analysis using energy dispersive spectroscopy (EDS). The observations demonstrate that surface pitting induced by arcing occurs mainly at the points were the rolling motion changes direction and that eroded metal is deposited along the wear grove. Micron-sized pits are formed which contain carbon and oxygen indicating that arcing causes decomposition of the hydrocarbon lubricants. All the findings indicate a significant inhibition of pitting induced by the Ag nanoparticles; some greases containing other additives exhibit a similar, although less pronounced, effect.

Keywords: Electric Motor Bearings, Wheel Bearings, Electric Vehicles, Arcing, Electrically Induced Bearing Damage, Pitting, Leakage Current, Stray Current, Fluting, Frosting, Shaft Voltage

A1.1 Introduction

Electric vehicles continue to grow in usage which also brings into focus their tribological performance and reliability [1]. In electric vehicles there is growing concern about the performance and reliability of mechanical components such as rolling element bearings and gears [2, 3]. This is due to not only increased temperature and speed expectations, but also because of potential damaging electric currents flowing across the surfaces [4-6]. These electrically induced bearing failures have also been widely observed in wind turbine bearings [7]. Stray electric currents and charges can build in several ways in a vehicle, and can occur in electric vehicles when the inverter converts power from the batteries to the electric motor. Accumulation of a large charge can induce arcing across the lubricating film of a bearing or gear. Arcing yields a plasma that melts and vaporizes the metal surfaces, causing what is termed as electrical discharge machining (EDM) or by others as electrically induced bearing damage (EIBD). As a consequence, small surficial pits form that can lead to noise, surface fatigue and eventual failure of an operating bearing [8].

In addition to rolling element bearings, electrical arcing damage can also occur in hydrodynamic sliding bearings[9]. In 2011, Sunahara et al. [10] performed an interesting experiment on a transparent EHL test rig so that the arcing events could be viewed while the film thickness was measured. They coated a non-conductive transparent disk with a layer of

conductive chromium to achieve this. However, their observations could differ from results obtained when contacts occur between a steel bearing raceway and steel rolling elements. Several researchers have also found that electrically conductive greases could prevent electrical pitting in bearings [6, 11, 12]. Other recent work suggested that metallic nanoparticles could enhance the performance of lubricated electrical contacts [13, 14]. Subsequently, reviews of the lubricants required for EV suggested the use of nanoparticles to improve the electrical, thermal and tribological properties of the lubricants[15]. Morris et al. [16] recently laid the foundation for a theoretical approach to the problem by predicting the electrostatic charge in an EHL film that can lead to EIBD. Recently numerical models have also been developed to include the non-conductive lubricating film development between rough surfaces in relative motion due to hydrodynamic lift [17, 18].

Bolted electrical contacts may also use conductive greases to improve performance [19, 20]. The continuous supply of power for electrically powered mass transit vehicles, such as trains and buses, is critically dependent on sliding electrical contacts and pantographs [20-22]. Due to the vibratory nature of aircraft, lubricants are often used to reduce fretting and corrosion of electrical contacts [23, 24]. Slip ring brushes in wind turbines, hydro-generators, and vehicles could also benefit from using conductive lubricants [25]. Utilization of these systems is widespread and growing, and therefore the need for improved lubricants that are electrically compatible is increasing in importance [26].

Most recently, Farfan-Carbara et al. [27] studied the influence of electrification on sliding contacts. Their work found that the application of electricity caused significant wear damage, but slightly reduced the friction. In addition, they found that formulated fluids for gears and automatic transmissions performed better than mineral base oil without additives. According to

these investigators [27], the increased damage noticed with mineral base oil resulted from the higher dielectric strength exhibited by this lubricant. Since the dielectric strength is inversely related to conductivity, the observations suggest that lubricants exhibiting higher conductivities could reduce the surface damage derived from electrical discharges.

Grease is also desirable in many applications given that this material is able to reduce the possibility of lubricant leakage [28]. Sanchez Garrido et al. [29] recently investigated the effects of temperature and roughness on grease performance under the conditions experienced by the bearings of electric motors. That work also considered synthetic and mineral base oils thickened by lithium and polyurea, with lithium greases having the best overall performance. However, the extensive use of lithium for battery production has rendered supplies of this element less abundant, which is expected to increase the use of other types of grease thickeners.

Although the main focus of this work is to study nanoparticle laden greases for bearings of automotive rolling elements, the results could also be applied to other important cases such as electrical connectors. This has become increasingly important for electric vehicles where charging ports and many other connectors in the drive system must perform reliably. A seminal review on lubrication in electrical connectors was provided in 1978 by Campbell [30], who noted that additives to the lubricating fluid are often added to enhance performance. For friction and wear, common additive materials are fatty acids, sulfur compounds, solid lubricants, and zinc-dialkyl-dithiophosphate (ZDDP) [31]. Solid materials such as molybdenum disulfide, PTFE, and graphite can sometimes be used in lubricants to reduce friction and wear. However, in many cases these solid lubricants and additives will often induce the formation of a non-conductive film between the surfaces [13, 32, 33].

Nanoparticles and lubricants laden with them (i.e. nano-lubricants) have received a great deal of attention due to their unique properties from a wide variety of materials and applications [34, 35]. Nano-lubricants are colloids, or fluids with nano-scale particles suspended in them (See Fig. A1.1), which have already been shown to have desirable friction and wear performance qualities [34-36]. Some nanoparticles have proven to reduce the coefficient of friction by 20-30% [37] and even up to 50% for WS_2 and other nanoparticles [38, 39]. Ag nanoparticles have shown to reduce friction by 25-40% [40-43] and even when added to already fully-formulated lubricants[44]. The preparation of stable dispersions of particles in hydrocarbons has proven to be a difficult task as well [45] because only a few particle stabilizers that dissolve in hydrocarbons are known to be effective at hindering precipitation. Without a stabilizer the particles will also most likely precipitate. While nano-lubricants have shown promising results, quantitative agreement of the available data is missing. This is unsurprising since nano-lubricants are usually prepared via exposing nm-sized particles to some dispersing force, such as mechanical agitation or ultrasound waves. However, the resulting dispersions undergo particle aggregation and precipitation once the dispersing force is no longer applied. Particle precipitation results in time-dependent properties not easily reproduced that are of questionable scientific or practical value. Therefore, the use of a semi-solid, such as grease, is also advantageous in that greases can improve significantly the stability of particle suspensions.

Concentrated silver (Ag) colloids (1.3 wt%) were achieved in hydrocarbons containing oleoyl sarcosine (OS) via fast thermolytic reduction of Ag ions at 180 °C [46]. OS served as a surfactant to suspend and stabilize the particles within the hydrocarbons. These spherical colloidal particles with an average diameter of 6 nm were free of precipitation for over 2 years, or after subjecting them to several heating and cooling cycles. An analogous procedure yielded

Ag colloids in liquid polyethylene glycol as a solvent consisting of particles with diameter of 7 nm that possess very good lubrication properties[41]. The lubricating properties of this nano-lubricant were studied using the pin on disk method, at different lubrication regimes and across the Stribeck curve. These Ag nanoparticles additives were shown to decrease friction in both the boundary and elasto-hydrodynamic lubrication regimes[47]. For the previously studied Ag particles the most dominant friction control mechanism was probably the reduction of contact area [48], because energy dispersive X-ray spectroscopy (EDS) measurements demonstrated that no Ag were deposited on the surface.

However, for electrical contacts, the most appealing property of a nano-lubricant (as compared with conventional lubricants) may be an enhanced electrical conductivity. This of course would only be true for a lubricant containing conductive particles. This study therefore focuses on the use of Ag nanoparticles. Even though the contact area is diminished by the particles, the contact resistance is not drastically increased by the presence of the conductive particles. In contrast, many other friction reducing additives such as ZDDP [13] will coat nearly all of the contacts with a non-conductive film [13, 32, 33]. Although the conductivity of a contact lubricated by a fluid containing conductive nanoparticles is not as high as that of pure metallic conductors, in vibrating and sliding electrical contacts the former may show advantageous properties. In these situations, lubricant films or oxide debris can form and the conductive particles might help to bridge across the surfaces or even pierce the non-conductive layer. This suggests that nano-lubricants could be very useful for fretting corrosion and electrical pitting applications, such as for electrical connectors, bearings and brushes used in automotive and other applications.

More recently, the effect of a lubricant containing different concentrations of Ag particles on electrical contacts was compared with that of a conventional lubricant containing a commercial paraffinic oil [14, 49]. In these tests, the contacts were slid over a range of speeds to capture the behavior for different regimes of lubrication. The change in ECR determined from measurements performed before and after each test was lower for the nanoparticle-laden lubricant than that of a conventional proprietary lubricant. However, the wear of the samples when employing nanoparticle lubricants was slightly higher than after using the commercial paraffinic oil. Note that no other additives were present in these nanoparticle lubricants. Therefore, a reasonable assumption is that an optimal ratio of nanoparticle lubricant with existing additives could yield a superior performance. However, no external electric load was applied in that previous study, and the contacts were sliding instead of rolling as in the current test.

A1.2 Objectives

The current study experimentally investigates the use of lubricating greases consisting of Ag nanoparticles suspended in an alkane and blended into typical electric motor bearing grease formulations. Ag nanoparticles are chosen as one of the additives to be investigated, because they have been previously found to display superior tribological and electrical performances. The effect of different greases with and without Ag nanoparticle additives on the electrical pitting phenomena are evaluated using a rolling element test that features a voltage difference applied across the surfaces. The surficial pitting will be investigated by means of techniques such as profilometry, scanning electron microscope (SEM) and energy dispersive X-ray spectroscopy (EDS).

A1.3 Methodology

The nanoparticle-laden greases were synthesized by mixing an Ag colloid made in dodecane with professionally prefabricated grease. All the greases considered here are of NLGI 2 consistency and thickened with polyurea. The greases were all based on commercial products provided by Shell [50, 51]. Mineral base grease, synthetic base grease, formulated mineral base grease and formulated synthetic grease were tested with and without Ag nanoparticles. Note that the synthetic base oil used is poly-alpha-olefin (PAO). Since the Ag nanoparticles were originally suspended in dodecane, grease samples modified only with dodecane were also tested. This procedure yielded twelve different greases to be tested that are now listed in Table 1. The blending was conducted using a small-scale mixer/temperature controller and will be described in detail in the following paragraphs. Only small amounts of grease are required for friction and wear testing.

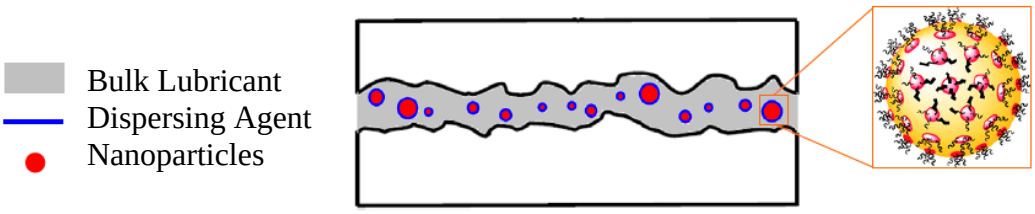

Figure A1.1: Schematic of nanoparticle suspension mechanism in a bulk lubricant (base oil).

Table 1: List of considered grease samples

Grease Sample Description	Abbreviated Label
Mineral Base Grease	min
Mineral Base Grease with Dodecane	Do min
Mineral Base Grease with 0.19 wt% Ag Nanoparticles	NP min
Mineral Fully-formulated Base Grease	FF min
Mineral Fully-formulated Base Grease with Dodecane	Do FF min
Mineral Fully-formulated Base Grease with 0.19 wt% Ag Nanoparticles	NP FF min
Synthetic PAO Base Grease	syn
Synthetic PAO Base Grease with Dodecane	Do syn
Synthetic PAO Base Grease with 0.19 wt% Ag Nanoparticles	NP syn
Synthetic PAO Fully-formulated Base Grease	FF syn
Synthetic PAO Fully-formulated Base Grease with Dodecane	Do FF syn
Synthetic PAO Fully-formulated Base Grease with 0.19 wt% Ag	NP FF syn

Nanoparticles	

The nanoparticle additives to be tested are Ag colloids (or sols) synthesized in dodecane ($C_{12}H_{26}$) or eicosane ($C_{20}H_{42}$) according to a procedure developed previously[46]. This method involves the thermal reduction of Ag neodecanoate in either hydrocarbon solvent at 180 °C. Also present in the colloids was oleoyl sarcosine (OS), consisting of a C_{17} olefinic chain terminated with a carboxylate group able to stabilize Ag particles against precipitation via ionic interaction with the particle surface. The synthesis was performed using an oil bath placed on a hot plate equipped with a thermometer/thermocouple combination to control the temperature. Dodecane containing 0.1 M OS was stirred at 180 rpm with a magnetic stirring bar and heated to 150°C. After this temperature was reached, enough Ag neodecanoate was quickly added to reach the desired Ag concentration. After complete dissolution of the Ag salt, the temperature was ramped to 180°C and held constant for 11 minutes.

Concentrated colloids with a metal mass fraction of up to 1.3 % were achieved in $C_{12}H_{26}$ (dodecane). The colloids contained spherical Ag crystallites with an average diameter of 6 nm; in the dodecane system the particles have remained free of precipitation for over 2 years at room temperature. An image of the resulting Ag/dodecane colloid is shown in in the Supplemental Information as Fig. A. Hydrocarbons are miscible with other alkanes at high temperatures, which enables mixing the colloids with base greases under such conditions. Colloids were examined in terms of particle composition via elementary analysis, XRD, TEM, UV-Vis spectroscopy; the long-term stability toward precipitation of the sols was also characterized.

Additive packages for lubricating greases are typically mixed into a thickened grease at the end of the processing. As mentioned at the beginning of the section, a similar process was used to incorporate the nanoparticles into existing 'clean' greases without other additives. Greases without additives (only thickeners and base oil) were used as control samples during the tests. The wear properties of such sample were compared relative to those of 'clean' greases with only nanoparticles, a fully formulated grease, and a fully-formulated grease with nanoparticles. Greases containing nanoparticles were prepared by mixing 10 g of grease with 2 mL of the previously described colloid solution. The mixing procedure employed pulses generated by a motorized mixer consisting of 15-20 s bursts while applying pressure on the grease between bursts for compaction. All greases were mixed for a minimum of 1 min, and care was taken to homogenize the grease during this process until a uniform product was obtained. A typical image of polyurea greases with and without Ag nanoparticle additives in shown in the Supplemental Information file as Fig. B. The resulting Ag nanoparticle laden greases contains approximately 0.19 wt% of Ag. This concentration was chosen since previous work showed success with it in reducing friction and wear, but without a significant electrical load [14].

3.1 *Experimental Testing.*

Reciprocating rolling sphere-on-disk (i.e. ball-on-disk) friction tests were performed using a CETR-UMT3 Tribotester (see Fig. A1.4). An electrical circuit was also secured across the contact as shown in Figure A1.5. This circuit allowed for the electrical contact resistance to be measured during the test using an Agilent 34410A multimeter. In this initial study the authors used the simplest setup of a reciprocating motion to avoid complexities. Few other, if any, existing studies use reciprocating motion, so this work also provides a unique perspective. The

reciprocating motion captures the start-stop motion that will occur in a real vehicles that other tests do not capture. The reciprocating test was also selected so that the electrical lead contacts were fixed as sliding contacts would introduce noise during the test. A power supply was also connected to the samples in parallel and the voltage through the circuit was set to 31 V. This could be considered a 4-wire resistance test measurement as is common in electrical contact literature. Utilization of a heating element provided an additional load on the circuit. This results in approximately 0.5 Amps, or based on the Hertz contact area under 50 N of load, a current flux of 11.1 MAmp/m^2. This value is similar to that used by the Southwest Research Institute in cylindrical contact tests [52]. However, the applied electric current and voltage are expected to vary significantly due to changes in the electrical properties across the contact (when the oil film grows or decreases and during arcing).

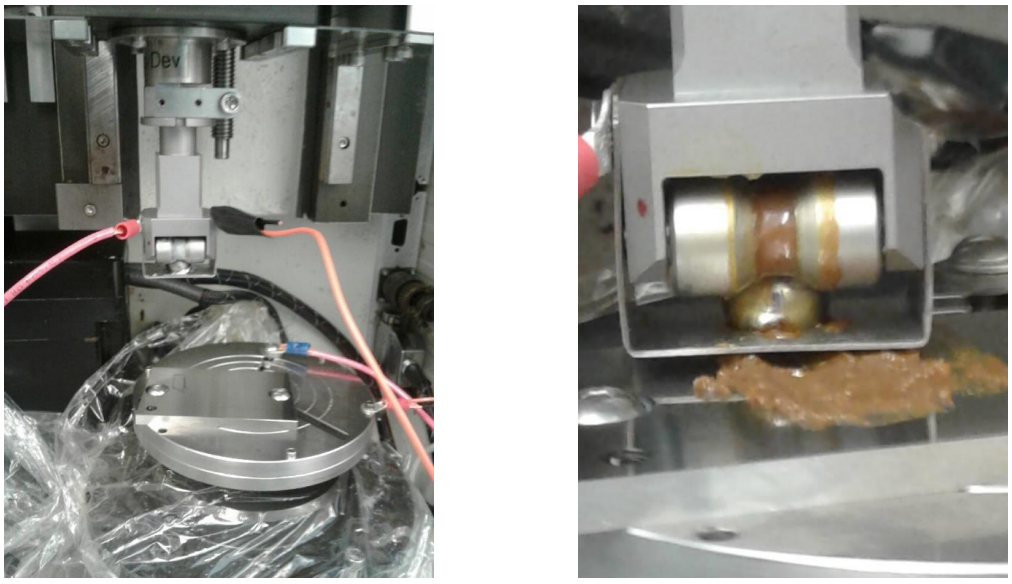

(a) (b)

Figure A1.4: Photographs of the test setup and fixture before and during testing (when the grease is applied).

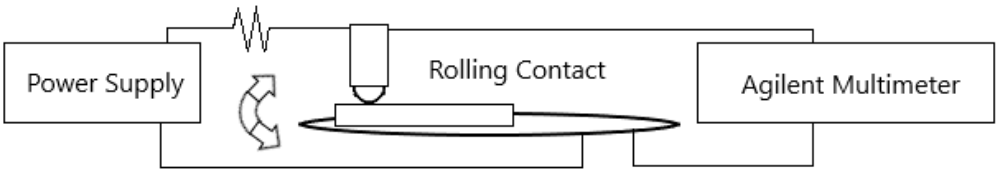

(a)

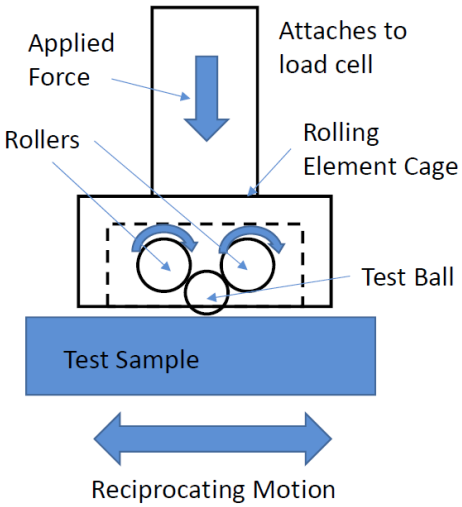

(b)

Figure A1.5: Schematic of electrical test setup (a) and rolling ball fixture (b).

The load of 50 N is chosen to achieve a Hertz pressure similar to that expected in electric vehicle applications (1.72 GPa). The flat samples were finely ground 52100 steel and loaded against a 3/8" 52100 steel ball. A special roller fixture was used to facilitate rolling of the test balls against the flat steel specimen (see Fig. A1.4b, A1.5b). Greases were applied to all rolling contact surfaces and tests lasted for 1.5 hrs. The tests were run at an average reciprocating speed of 0.005 m/s with a sliding distance of 1 cm. While possible damage of the roller fixture was of concern, no significant problems were encountered during testing.

Using elasto-hydrodynamic theory [53] the current test is expected to operate with a full-film thickness of approximately 30 nm, although it may fluctuate due to the reciprocating motion.

Nonetheless, the film thickness will resist compression to a degree (i.e. the squeeze film effect) since the motion does not pause for a substantial amount of time. The nanoparticles are shown to still be influential on friction in the thin film elasto-hydrodynamic regime [47], and may influence the film thickness.

The testing procedure evaluated four grease types (mineral base, mineral formulated, synthetic base, and synthetic formulated) with and without Ag nanoparticles or dodecane (used to deliver the nanoparticles). Again a list of these considered samples are in Table 1. All these greases complied with the ISO 100 viscosity specifications and used a polyurea grease thickener to achieve a consistency of NLGI 2 (penetration from 265 to 295). No EP (extreme pressure) additives are present in any of the greases. The finished greases are lubricating materials currently manufactured for industrial use and contain additives that protect them from oxidation and corrosion. The base grease was obtained by removing samples from the manufacturing process before the introduction of additives.

Each experiment was replicated three times, always using a fresh surface and new ball, which resulted in 36 separate tests. A limited selection of tests was also run with no electrical load

(without any applied voltage or current). Such tests resulted in no measurable wear and confirmed that the damage was dominantly produced by the applied electrical load (see Fig. A1.6).

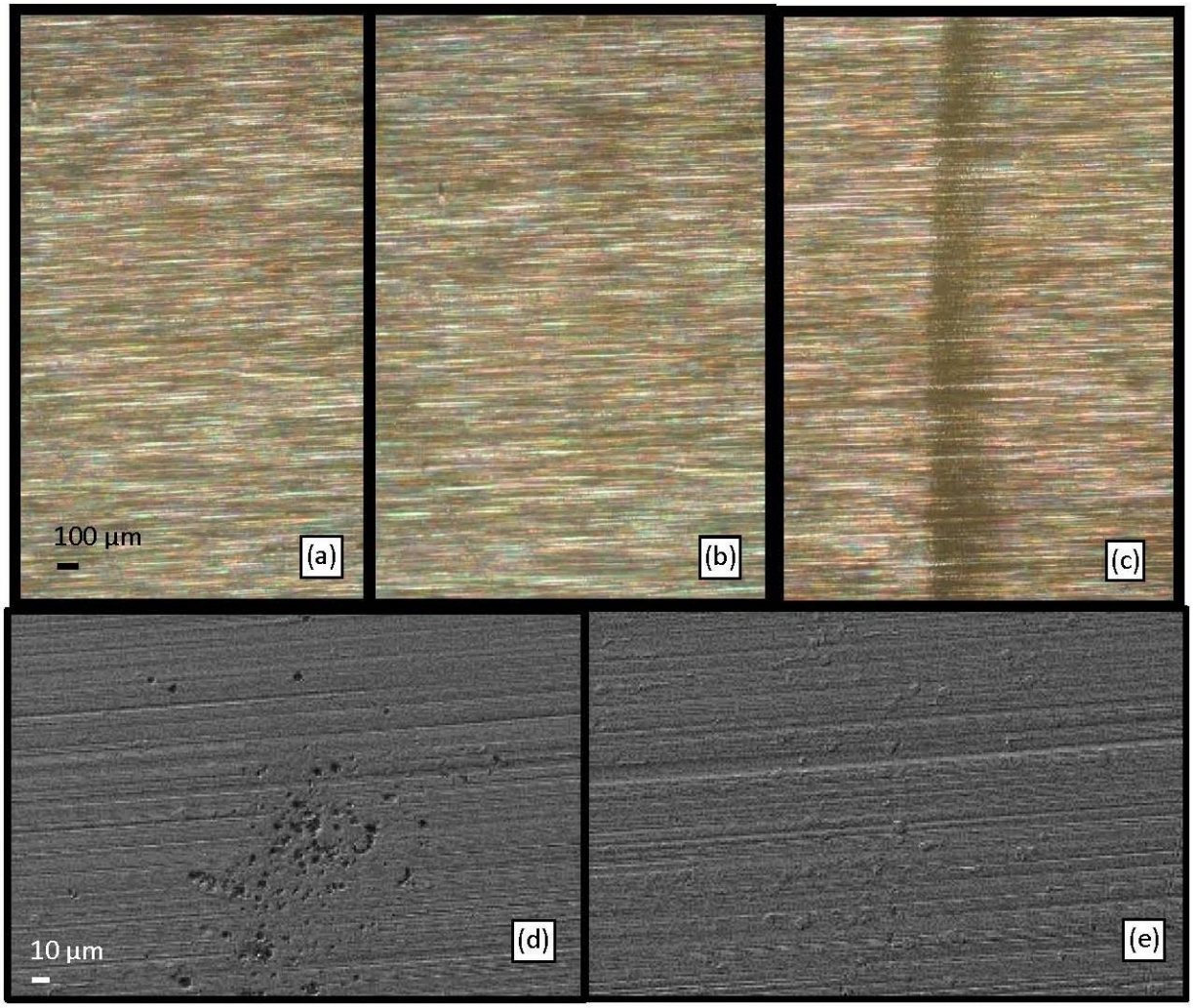

Figure A1.6: Optical microscopy images of surfaces: (a) before a run, (b) after an experiment without electric current and (c) worn in the presence of an electric load. Also included are SEM images of (d) a surface after an electric test showing arc pitting, and (e) redeposition of ablated metal on the steel.

A1.4 Results and Discussion

After testing was completed, the samples were characterized using optical microscopy, stylus profilometry, SEM and EDS. Presented in Figure A1.6 are optical microscopy images of

surfaces: a) before an experiment, b) a test without any electrical load and c) in the presence of an electrical current. The tests were performed with surfaces covered with mineral oil polyurea grease, which was removed prior to imaging. As shown by the images, a clear wear track was noticed only in the experiment performed under an electrical load. This wear track was confined to the region between the starting point of the run and the end point where the direction of rolling was reversed. The wear track became visible because of differences in light reflection between the area containing pitting, deposited metal and the pristine steel surface. Elevated carbon on the wear track may have also played a role. Additional SEM images revealed that metal pitting took place mainly in the locations where rolling started and then changed direction, image d) in Figure A1.6 is a representative example. Evidence that the wear track originated from deposition of metal ablated from the start and end regions of the run is shown in image e). A thorough analysis of the SEM results will be presented later. Note that the test setup also enabled recording of the lateral or friction force. However, since the contacts are rolling there was no measurable difference in the lateral forces between different greases.

Shown in Figure A1.7 are SEM results acquired from an experiment in the presence of an electrical load using mineral grease with dodecane but without Ag particles. The top left image demonstrates that substantial pitting occurred on the surface of the substrate. Also included in Fig. A1.7 are EDS maps showing the distribution of Cr, Mn, Fe, C and O within the same area. Analysis of the EDS maps indicated that the distribution of Cr, Mn and Fe remained unchanged; C and O signals were detected only in samples that experienced arcing. No Ag was observed on the surfaces. Figure A1.8 resulted from an overlay of the distribution maps (excluding the Cr data) and demonstrated that O and C were present mostly within the pits. These observations suggest that arcing produced the pitting and chemically degraded the grease in these locations.

Grease samples were also collected after the tests and examined using Fourier Transform Infrared Spectroscopy (FTIR) to check for this degradation. However, no measureable differences were observed. This is probably due to the micrometer-scale contact patch containing a small amount of grease that is too diluted in the grease sample.

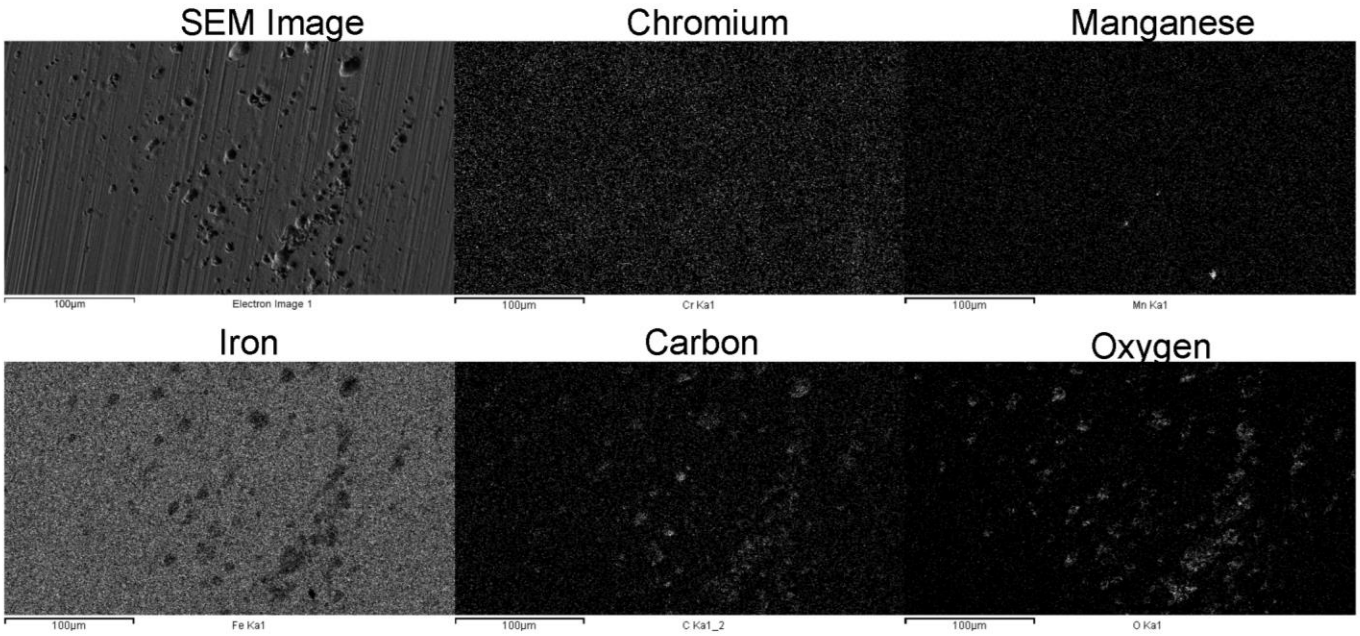

Figure A1.7: SEM and EDS images of a worn surface region. Mineral grease containing dodecane but without Ag particles served as the lubricant. The scale bar included on the bottom left of each image corresponds to 100 μm.

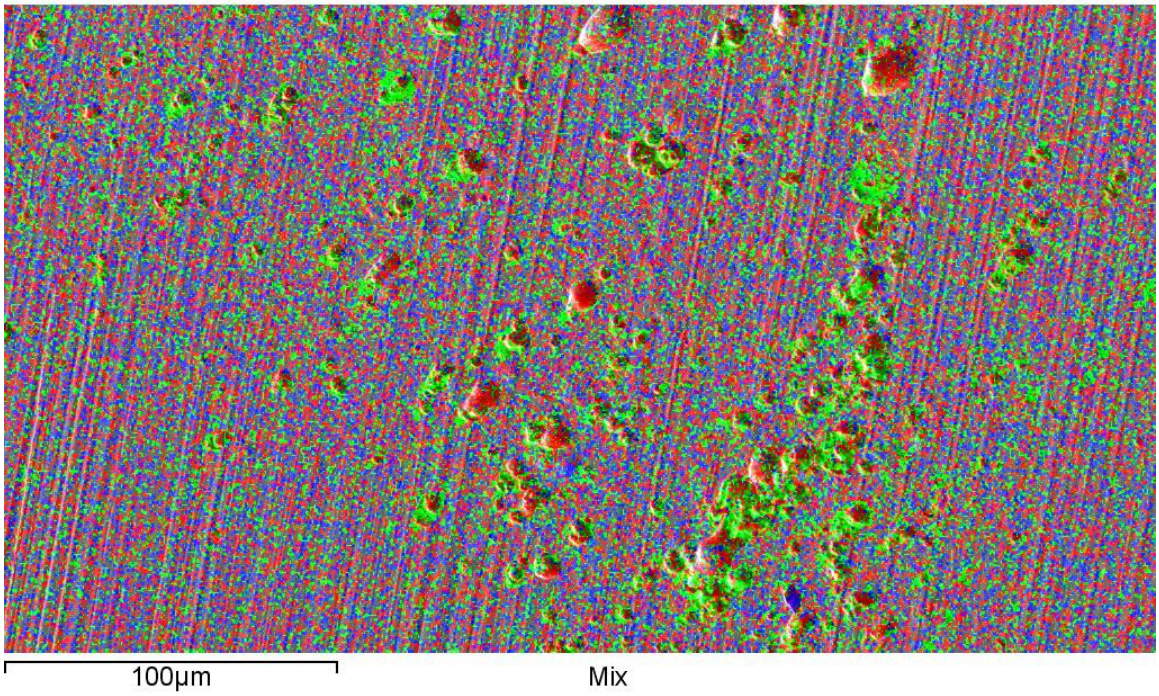

Figure A1.8: An overlay image of the EDS maps for C – Red, O – Green, Fe – Blue, and Mn - Orange. The Cr map was excluded to improve the clarity of presentation.

Analysis of the wear tracks shown in SEM images (see Figs. 9-12) revealed that not only are there quantitative differences in the number of pits detected in tests with different greases, but that a larger number of pits were present at the starting and end points of the wear tracks. The track is the area over which the ball rolls and at the end point the direction of rolling is reversed after a short pause. Several reasons could account for such behavior. At the track end the film thickness should be at a minimum as the surfaces momentarily lose EHL and come closer together. In addition, if the arcing is the result of a build of charge at the asperities on the surfaces, perhaps the charge has more time to grow as the surface motion slows and pauses. As is

also evident from Figs. 9-12, pitting obtained with greases containing nanoparticles (Ag dodecane colloid), and sometimes with just dodecane, is less extensive than the damage noticed with the plain grease. In addition, the fully formulated greases appear to inhibit pitting more efficiently than the clean greases without additives. The goal of the next part is to extract a more quantitative analysis of the SEM observations.

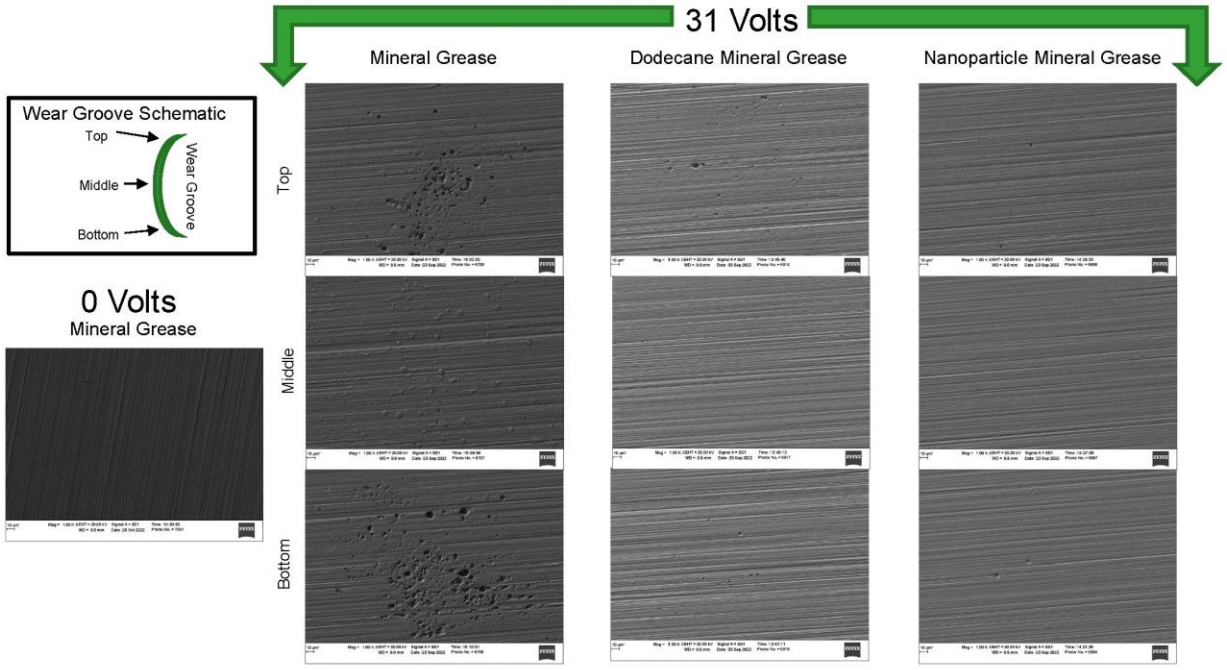

Figure A1.9: SEM image of electrically pitted substrates, experiments conducted with mineral grease samples. Left top scheme labelled “Wear Groove Schematic”: representation of a wear grove on the steel substrate, the top and bottom labels indicate the points at which the ball motion is reversed, middle label marks area of highest metal deposition.

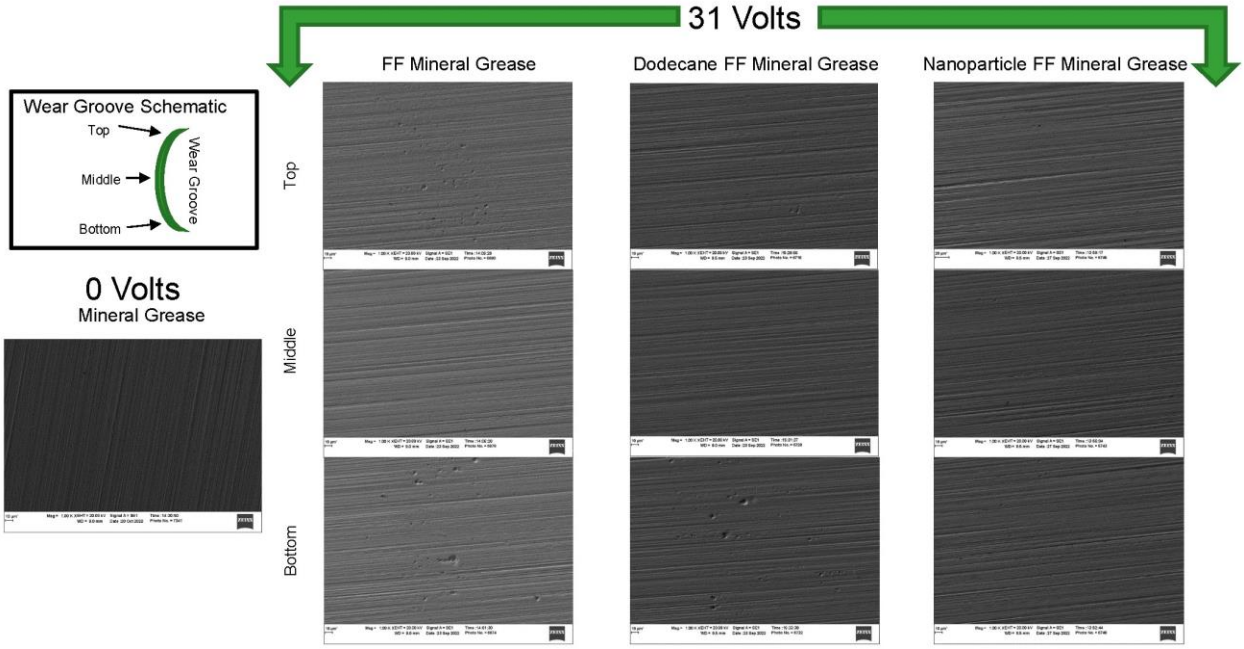

Figure A1.10: SEM image of electrically pitted substrates, experiments conducted with fully-formulated mineral grease samples. Left top scheme: see caption to Fig. A1.9.

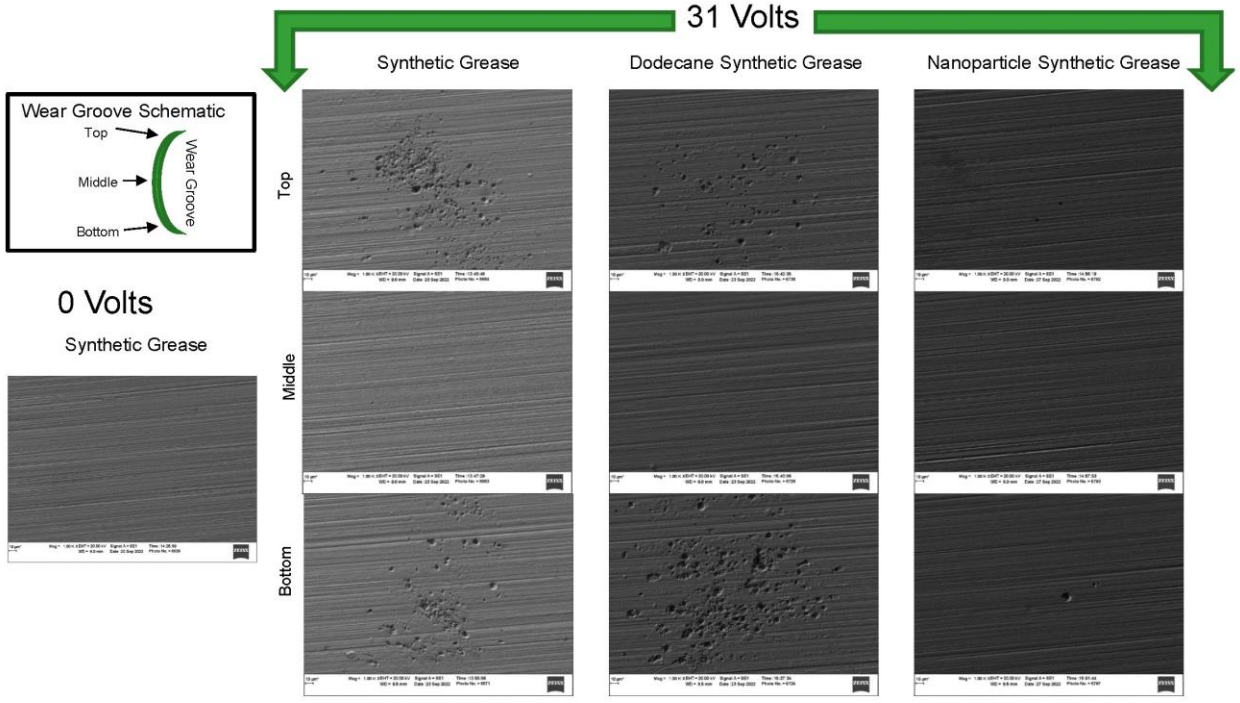

Figure A1.11: Image analysis of SEM of electrically pitted substrates, experiments conducted with synthetic grease samples. Left top scheme: see caption to Fig. A1.9.

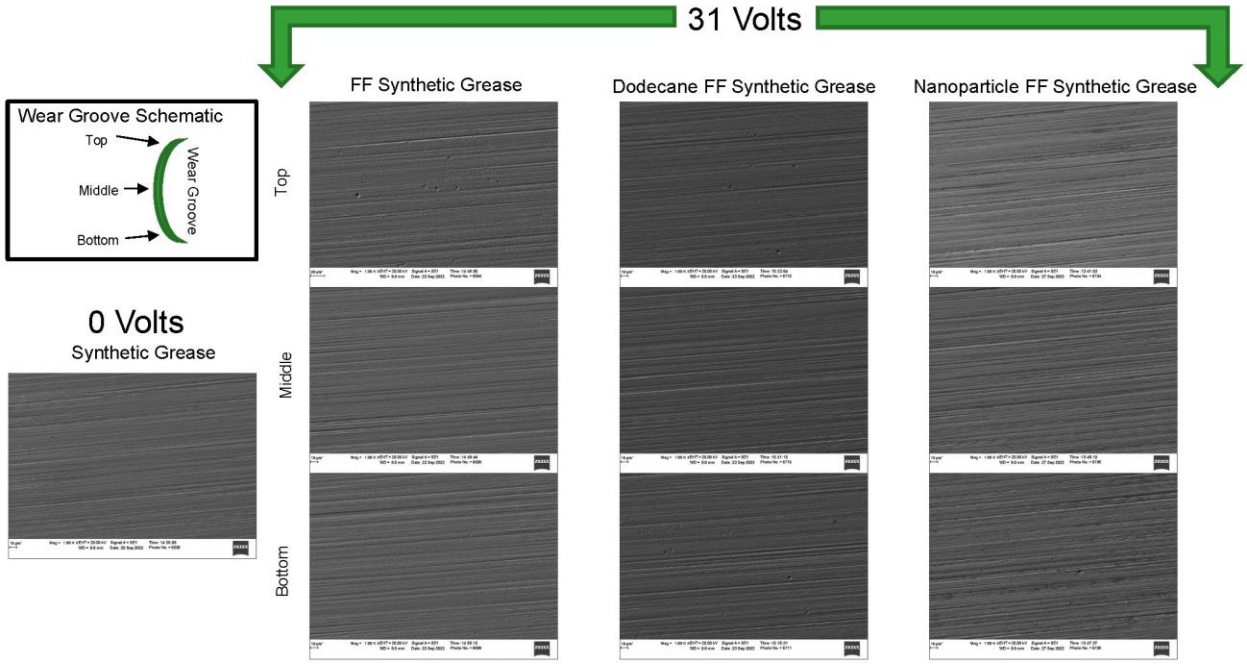

Figure A1.12: SEM image of electrically pitted substrates, experiments conducted with fully-formulated (FF) synthetic grease samples. Left top scheme: see caption to Fig. A1.19.

Quantitative information about the damage resulting from surface pitting was obtained via analysis of the SEM images using the software Image J. The procedure consisted of first identifying the eroded places followed by summation of the surface area of those eroded places. Figure A1.13 depicts a graphical representation of the image analysis for an experiment that employed a mineral grease sample, the eroded areas are identified by green borders. In all tests, the images obtained at both ends of the wear tracks were analyzed using the same scale and methodology. Such analysis yielded a percentage of surface damage for each of the different greases at the end of the resulting wear groove. Since only the ends of the wear grooves are considered, this procedure does not represent the percentage of surface damage across an entire wear track.

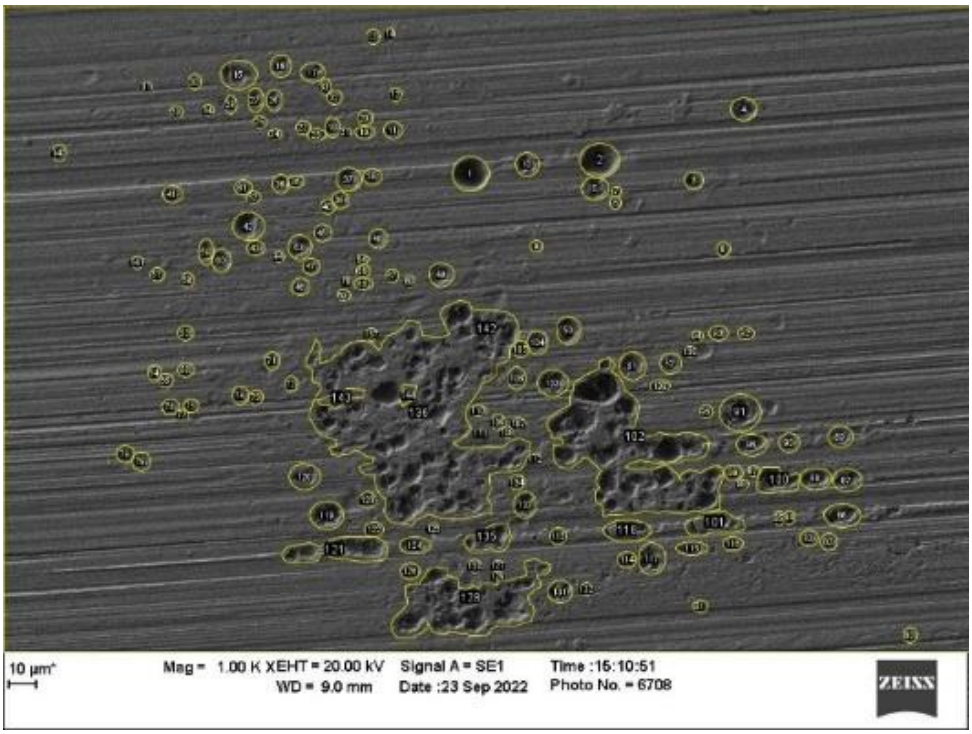

Figure A1.13: Image analysis representation of a flat substrate tested with mineral grease as a lubricant.

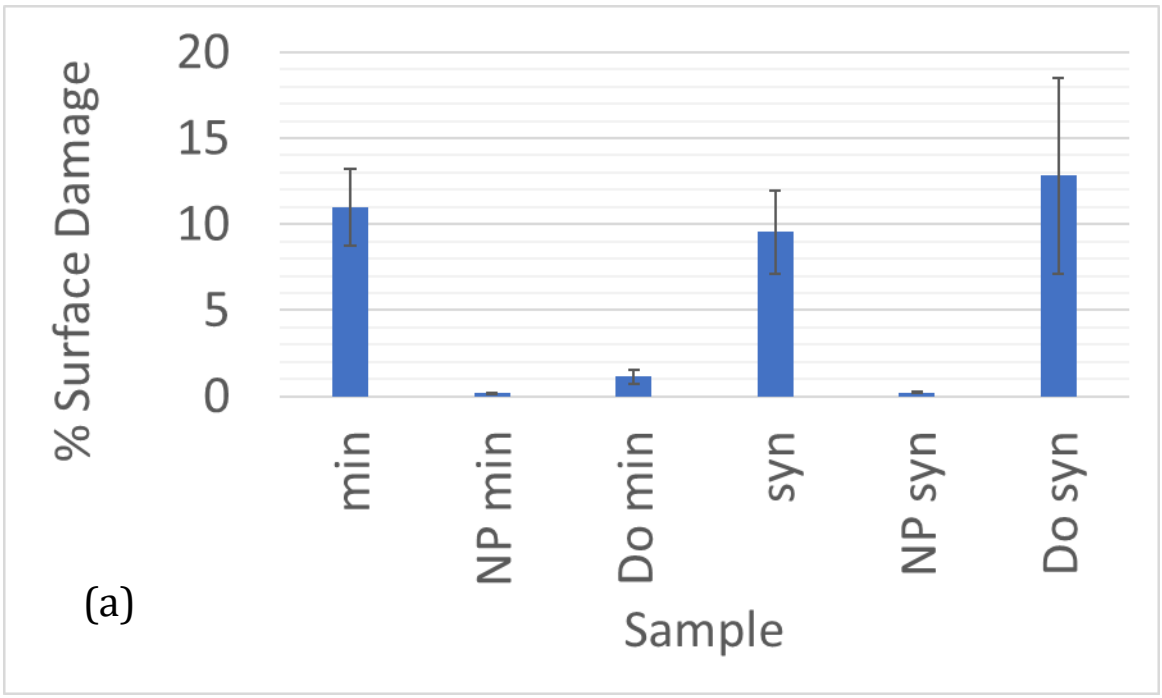

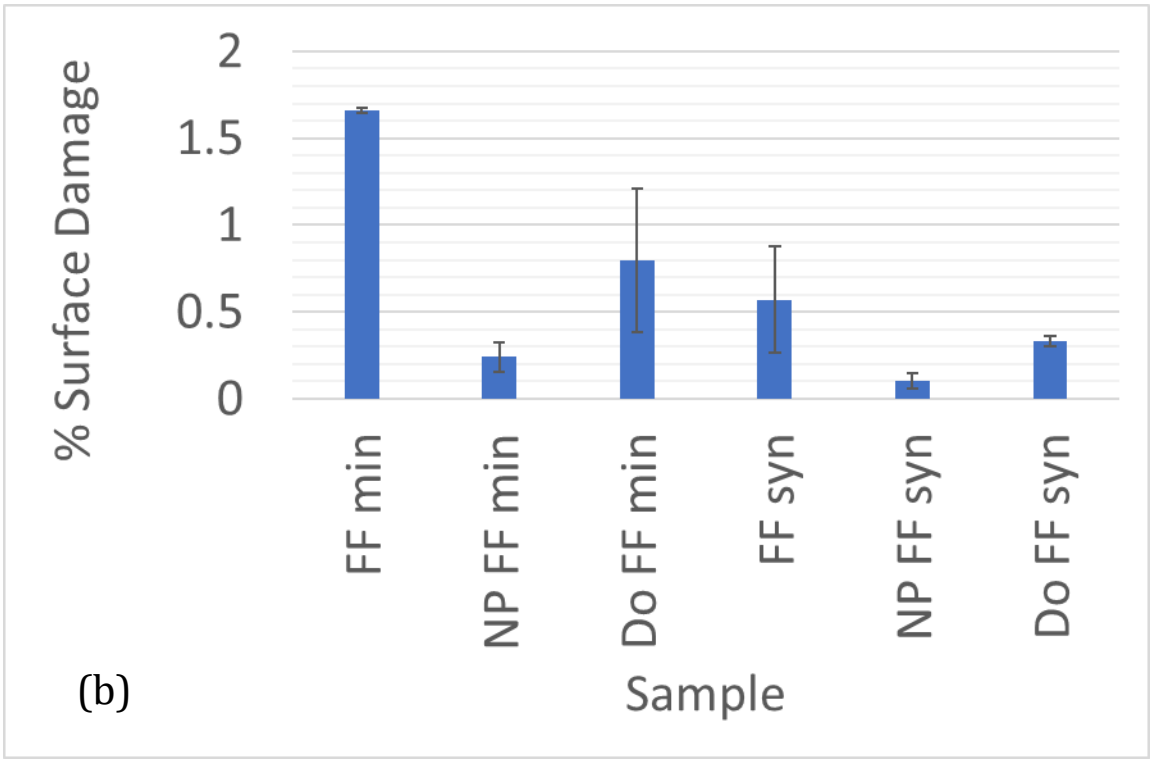

Figure A1.14: Percentage of surface damage for flat substrates in tests with different samples when different greases. Panel (a) depicts the results for the base greases, presented in panel (b)

are the data for the fully formulated greases. Note the following abbreviations: min = mineral, syn = synthetic, NP = nanoparticles, Do = dodecane, and FF = fully formulated.

Plotted in Figure A1.14 are the results obtained by analysis of the images illustrating the damage of the substrates derived from electrical pitting of the surface. First, the image analysis clearly indicated that the highest surface damage induced by electrical pitting took place in experiments that employed unmodified or clean synthetic and mineral greases (Fig. A1.14(a)). Tests run with synthetic grease mixed with dodecane also yielded a larger percentage of surface damage. It is clear from Figure A1.14(a) that the addition of the silver nanoparticles solution to the base greases drastically reduced the surface damage on the samples. Figure A1.14(b) depicts the results for the fully formulated greases that included antioxidants and anti-corrosion additives. Although the additives in the fully formulated oils do appear to reduce the surface damage, the nanoparticles further reduce it beyond the conventional additive formulation alone. Experiments with the four greases containing Ag nanoparticles (dodecane colloid) yielded the lowest percentages of surface damage, supporting earlier conclusions. Furthermore, most experiments with dodecane and fully formulated greases yielded less surface damage as compared to tests with unmodified greases, but in differing degrees.

Next, a stylus profilometer with a 2 μm tip was used to measure all the wear grooves. As illustrated in Figure A1.15, circular shaped pits analogous to those shown in Figures A1.6d) and A1.7a) were detected by means of profilometry. However, the damage was not usually present as a defined or continuous wear groove, so wear rate, wear groove width or wear volume were not evaluated. The trends are not as pronounced as the SEM image analysis results. This is due to the damage on the track not only being represented by pitting, but also by raised peaks of

redeposited debris (recall the discussion about Fig. A1.6d and A1.6e). The profilometry does provide some quantitative dimensions to the pits. They appear to be on the order of 200 nm deep and a few micrometers across.

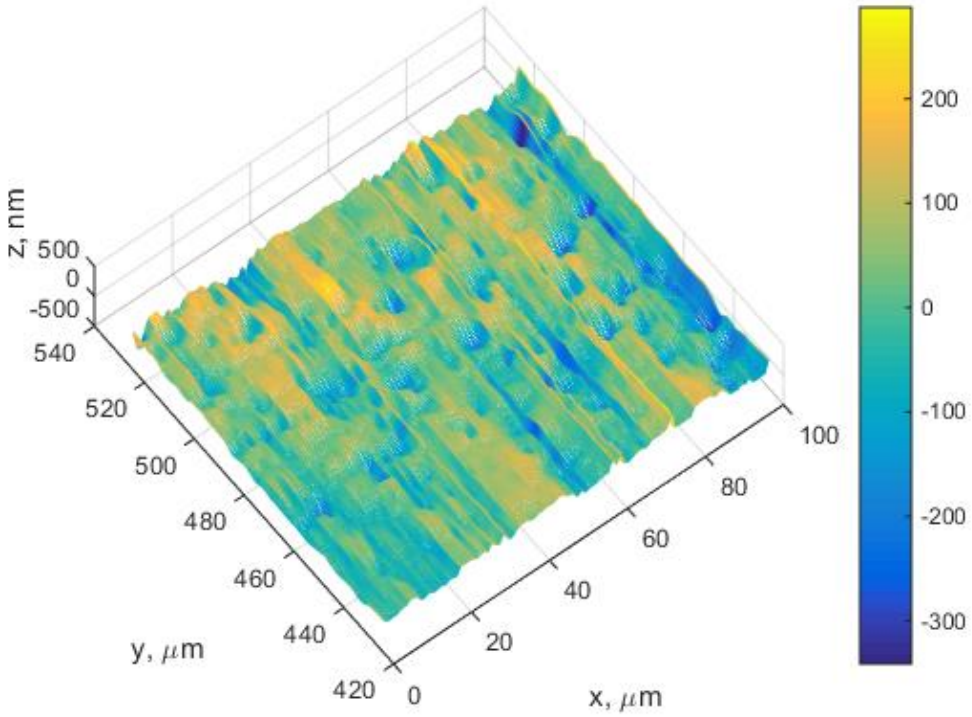

Figure A1.15: Profilometer data obtained in an experiment conducted under electrical load on surfaces lubricated using a mineral grease.

Measurements of the electrical resistance across the contact during testing were conducted as well. Even though the electrical contacts of the leads were made static due to the reciprocating nature of the experiments, significant fluctuations in the data derived from tests were still observed. Note that each point in the plot represents the average resistance measured at 50 Hz during 1 second. Large fluctuations were observed probably because the circuit includes several other moving contacts, such as the roller fixture. The roughness of the surfaces and

changes in local grease film thickness could have also contributed to the large dispersion of the resistance data. Finally, arcing or EDM events themselves may constitute another possible factor contributing to the observed resistance fluctuations. Obviously, the resistance increases drastically at the initiation of motion between the surfaces. This is probably due to the formation of a film between the surfaces containing less conductive grease as predicted by theoretically models [17].

The measured electrical contact resistance over the duration of each test was averaged for each type of grease and is presented in Fig. A1.16. As mentioned previously, this observable was defined as ECR, although such quantity also includes other contributions from the wire, lead contacts, etc. Nonetheless, a comparison of these averages show that the nanoparticles yielded an overall lower ECR as compared to the other greases. Fully formulated greases and also those modified with dodecane also showed a decrease in ECR, but consistency was lacking across all samples. A lower ECR value may suggest a mechanism in which greases containing Ag nanoparticles reduce the surface pitting damage. In theory the particles may provide a shorter path for the electrical current to cross the relatively non-conductive lubricant thereby inhibiting arc formation. Decreasing the path distance could also reduce the size of the arc.

The initiation of arcing across the film can be approximately predicted by the dielectric strength. The dielectric breakdown strength of mineral oil is approximately 10-15 MV/m [54]. If the voltage across a film exceeds this, the electrons may overcome the insulation of the film by breaking it down into a plasma, which disassociates the electrons and facilitates conduction. Usually this requires high voltage and results in high temperatures, causing damage to the surfaces. The thickness of the film multiplied the dielectric strength predicts this voltage, also known as the dielectric voltage. Therefore, a smaller film requires less voltage to arc across.

Following established elasto-hydrodynamic lubrication theory [55] the film thickness in the current experiments is approximately 30 nm. Note that this thickness will vary based on the roughness and the reciprocating motion. Then the dielectric voltage is on the order of single volts.

Now consider if conductive silver nanoparticles are dispersed within the film. In the current work the particle density, n, is $9.1 \cdot 10^{21}$ particles/m^3. The Wigner-Sietz radius [56] is an approximation of the average distance between the center of the particles:

$$r = \sqrt[3]{\frac{3}{4\pi n}} \tag{1}$$

Eq. 1 predicts an average distance between the silver nanoparticles of 29.7 nm. Considering that the nanoparticles are 6nm in diameter, the distance between the surfaces of the particles is approximately 23.7nm, which is over four times less than the film thickness. The authors propose that this might allow the electrical current to conduct the across the films at lower voltages which may result in less damaging arcs. In addition, the nanoparticles might agglomerate and pass between the surfaces providing even shorter distances for the electrons to cross.

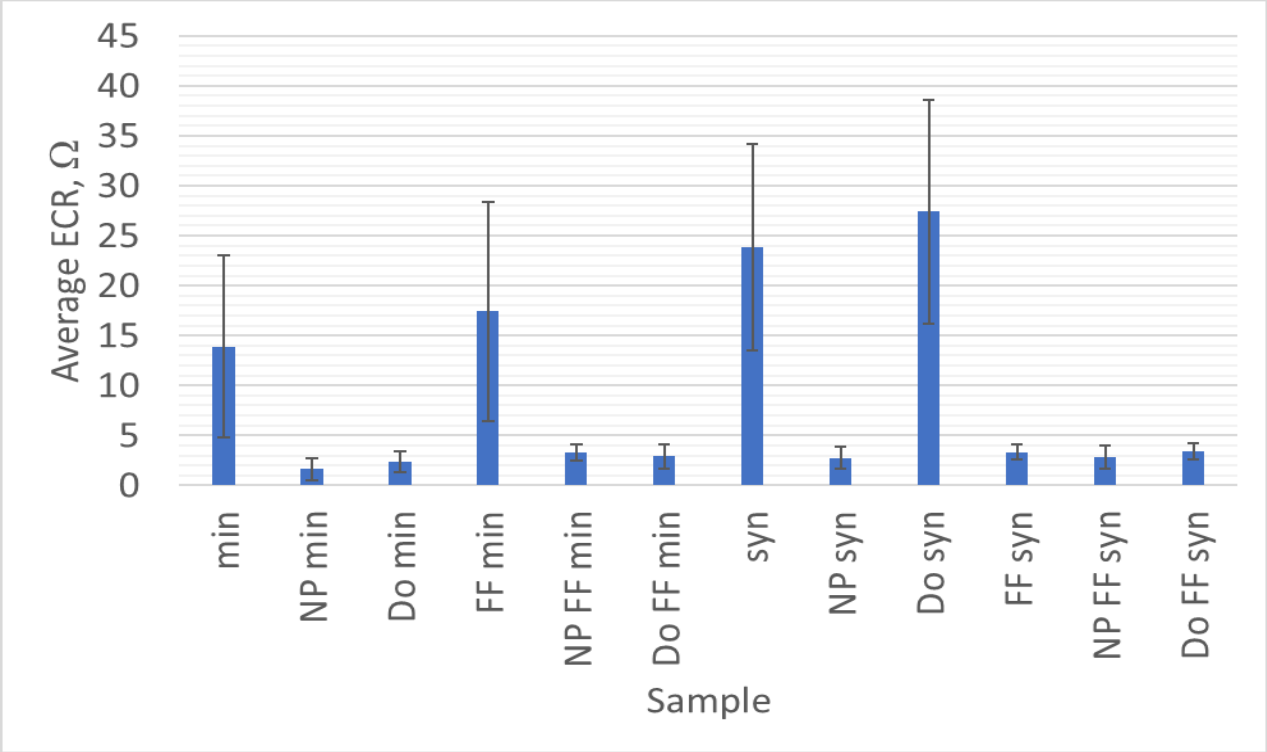

Figure A1.16: Averaged electrical contact resistance (ECR) obtained from the three tests conducted for each grease sample.

A1.5 Conclusions

This work first demonstrated the erosive effect induced by the flow of an electrical current across a greased rolling contact. Electrical current increased the wear on the contacts measurably as compared to the erosion noted in conventional rolling, that is, without current. The damage came in the form of pits believed to be the result of micro-scale arcs occurring between the surfaces and across the film of lubrication. SEM/EDS findings showed that surface erosion was concentrated at the points of the wear track where sliding of the steel ball reversed direction. In addition, some of the eroded metal was deposited in the mid-region of the wear track, away from the turning points. This observation suggests that the greases transported the

eroded metal to the places where deposition occurred. Furthermore, the formed surface pits contained carbon and oxygen implying that chemical decomposition of the greases took place due to micro-scale arcing.

Greases with Ag nanoparticles decrease the surface pitting damage as compared to all other lubricants tested. This conclusion is supported by the SEM image analysis. Fully-formulated greases as well as greases with dodecane also showed an improvement. While no drastic changes in the average electrical contact resistance were noticed, the ECR values appear to decrease for greases with nanoparticles. Note that in previous tests the Ag nano-lubricant yielded lower friction coefficients and less wear as compared to many conventional lubricants [14, 44].

One possible mechanism involves a change in the electrical conductivity of the grease, but some additives could also alter the rheology and facilitate changes in the film thickness between the surfaces. However, previous studies showed that the addition of similar concentrations of nanoparticles to oils induced relatively little change in viscosity [37, 41]. This work also proposes that the particles decrease the distances between conductive surfaces thereby lowering the voltage needed to cross the film, and thereby decreasing the damage of the arcs. The mechanisms by which greases containing Ag nanoparticles reduce the pitting induced by arcing remain unconfirmed, but further studies are planned to elucidate this phenomenon. This is also true for the benefits sometimes observed for dodecane and fully formulated greases.

Acknowledgements

The authors thank NLGI for funding this project via the Academic Outreach-Research Grant, Shell for providing grease samples, the Timken Company for providing flat samples of 52100

steel and Bruker Nano Surfaces for providing the rolling element test fixtures. We also appreciate the guidance of Dwayne (Greg) Morris of Shell throughout the project, and the help of Mike Miller during SEM determinations. Thanks to Hamed Ghaednia for his creation of Figure A1.1 and other discussions about nanoparticle lubrication over the years.

Data Availability

Data sets generated during the current study are available from the corresponding author upon reasonable request. Some of the data (Fig. 16) is created from images that are included in the paper, but more details can be provided.

Conflict of interest

The authors declare no conflict of interest.

References

1. Holmberg, K.; Erdemir, A. The impact of tribology on energy use and CO2 emission globally and in combustion engine and electric cars. *Tribol Int*, **2019**, *135*, 389-396.
2. Farfan-Cabrera, L.I. Tribology of electric vehicles: A review of critical components, current state and future improvement trends. *Tribol Int*, **2019**, *138*, 473-486.
3. Shah, R., et al. Recent trends in batteries and lubricants for electric vehicles. *Advances in Mechanical Engineering*, **2021**, *13*, 16878140211021730.
4. Kudelina, K., et al. Bearing fault analysis of bldc motor for electric scooter application. *Designs*, **2020**. *4*, 42.
5. Prasad, S.; Krishnanunni, S. Review on Analysis of Failures Modes in the Electric Vehicles due to Electric Bearings. *Int Res J Eng Technol*, **2020**, *7*(12), 1722-1725.
6. He, F.; Xie, G.; J. Luo, J. Electrical bearing failures in electric vehicles. *Friction*, **2020**. *8*(1), 4-28.
7. Liu, Z.; Zhang, L. A review of failure modes, condition monitoring and fault diagnosis methods for large-scale wind turbine bearings. *Measurement*, **2020**, *149*, 107002.
8. Raadnui, S.; Kleesuwan, S. Electrical pitting wear debris analysis of grease-lubricated rolling element bearings. *Wear*, **2011**, *271*(9-10), 1707-1718.
9. Chatterton, S.; Pennacchi, P.; Vania, A. Electrical pitting of tilting-pad thrust bearings: Modelling and experimental evidence. *Tribol Int*, **2016**, *103*, 475-486.
10. Sunahara, K.; et al. Preliminary measurements of electrical micropitting in grease-lubricated point contacts. *Tribol Trans*, **2011**, *54*(5), 730-735.
11. Suzumura, J. Prevention of electrical pitting on rolling bearings by electrically conductive grease. *Q Rep of RTRI*, **2016**, *57*(1), 42-47.

12. Chen, Y.; et al. Performance Characteristics of Lubricants in Electric and Hybrid Vehicles: A Review of Current and Future Needs. *Front Mech Eng*, **2020**, *6*, 571464.

13. Jackson, R.L.; et al. An Investigation of Silver Nanoparticle Laden Lubricants for Electrical Contacts. *IEEE Trans Compon*, **2019**, *9*(2), 193-200.

14. Crilly, L.; et al. An Exploration of the Friction, Wear, and Electrical Effects of Nanoparticle Enhanced and Conventional Lubricants. *IEEE Trans Compon*, **2022**, *12*(11), 1757-1770.

15. Shah, R.; Gashi, B.; Rosenkranz, A. Latest developments in designing advanced lubricants and greases for electric vehicles—An overview. *Lubrication Science*, **2022**, *34*(8), 515-526.

16. Morris, S.A.; Leighton, M.; Morris, N.J. Electrical Field Strength in Rough Infinite Line Contact Elastohydrodynamic Conjunctions. *Lubricants*, **2022**, *10*(5), 87.

17. Jackson, R.L.; Angadi, S. Modelling of Lubricated Electrical Contacts. *Lubricants*, **2022**, *10*(3), 32.

18. Jackson, R.L.; Angadi, S. Electrical Contact During a Rolling Vibratory Motion Considering Mixed Lubrication. *ASME J. Tribol.*, **2023**, *145*(8), 082201.

19. Gatherer, J. and R.L. Jackson. *A multi-variable parametric study on the performance of bolted busbar contacts*. in *2015 IEEE 61st Holm Conference on Electrical Contacts (Holm)*. 2015. IEEE.

20. Chudnovsky, B.H., *Lubrication of Electrical and Mechanical Components in Electric Power Equipment*. 2019: CRC Press.

21. Song, Y.; et al. Active control of contact force for high-speed railway pantograph-catenary based on multi-body pantograph model. *Mech Mach Theory*, **2017**, *115*, 35-59.

22. Wu, G.; et al. Electric Contact Material of Pantograph and Catenary, in The Electrical Contact of the Pantograph-Catenary System. *Springer*. **2019**, 195-220.

23. Slade, P.G., *Electrical contacts: principles and applications*. 2017: CRC press.

24. Abbott, W. *Performance of the gold-tin connector interface in a flight environment*. in *Electrical Contacts-1998. Proceedings of the Forty-Fourth IEEE Holm Conference on Electrical Contacts (Cat. No. 98CB36238)*. 1998. IEEE.

25. Fu, Y.; et al. The effect of surface texture and conductive grease filling on the tribological properties and electrical conductivity of carbon brushes. *Tribol Int*, **2021**, *153*, 106637.

26. Larsson, E.; Andersson, A.M.; Rudolphi, Å.K. Grease lubricated fretting of silver coated copper electrical contacts. *Wear*, **2017**, *376*, 634-642.

27. Farfan-Cabrera, L.I.; et al. Electrification effects on dry and lubricated sliding wear of bearing steel interfaces. *Wear*, **2023**, *516-517*, 204592.

28. Hemanth, G.; Suresha, B. *Hybrid and electric vehicle tribology: a review. Surf Topogr Metrol Prop*, **2021**, *9*(4), 043001.

29. Sanchez Garrido, D.; Leventini, S.; Martini, A. Effect of temperature and surface roughness on the tribological behavior of electric motor greases for hybrid bearing materials. Lubricants, **2021**, *9*(6), 59.

30. Campbell, W. The lubrication of electrical contacts. *IEEE Trans Components Hybrids Manuf Technol*, **1978**, *1*(1), 4-16.

31. Rudnick, L.R., *Lubricant additives: chemistry and applications*. 2009: CRC press.

32. Bakunin, V.N.; et al. Tribological behavior and tribofilm composition in lubricated systems containing surface-capped molybdenum sulfide nanoparticles. *Tribol Lett*, **2006**, *22*(3), 289-296.

33. Zhang, M.; et al. Performance and anti-wear mechanism of CaCO3 nanoparticles as a green additive in poly-alpha-olefin. *Tribol Int*, **2009**, *42*(7), 1029-1039.

34. Menezes, P.L., et al., *Tribology for scientists and engineers*. 2013, New York: Springer.

35. Htwe, Y.Z.N., et al., *Review of tribological properties of nanoparticle-based lubricants and their hybrids and composites.* Friction, 2023(https://doi.org/10.1007/s40544-023-0774-2).

36. Singh, A.; Chauhan, P.; Mamatha, T.G. A review on tribological performance of lubricants with nanoparticles additives. *Materials Today: Proceedings*, **2020**, *25*, 586-591.

37. Ghaednia, H.; Jackson, R.L.; Khodadadi, J.M. Experimental analysis of stable CuO nanoparticle enhanced lubricants. *J Exp Nanosci*, **2013**, *10*(1), 1-18.

38. Greenberg, R.; et al. The effect of WS 2 nanoparticles on friction reduction in various lubrication regimes. *Tribol Lett*, **2004**, *17*(2), 179-186.

39. Thampi, A.D.; et al. The effect of nanoparticle additives on the tribological properties of various lubricating oils – Review. *Materials Today: Proceedings*, **2021**, *47*, 4919-4924.

40. Ghaednia, H. and R.L. Jackson. *Experimental Analysis of Silver Nanoparticle-Enhanced Polyethylene Glycol Lubricants*. in *STLE 68th Annual Meeting*. 2013. Detroit, MI.

41. Ghaednia, H.; Hossain, M.S.; Jackson, R.L.; Tribological performance of silver nanoparticle–enhanced polyethylene glycol lubricants. *Tribol Trans*, **2016**. *59*(4), 585-592.

42. Kumara, C.; et al. Organic-Modified Silver Nanoparticles as Lubricant Additives. *ACS Applied Materials & Interfaces*, **2017**, *9*(42), 37227-37237.

43. Chinnachamy, R.; et al. Evaluation of the effect of silver nanoparticles on the tribological and thermophysical properties of bio-lubricants. *Proceedings of the Institution of Mechanical Engineers, Part E: Journal of Process Mechanical Engineering*, **2023**, *237*(2), 410-417.

44. Ghaednia, H., *An analytical and experimental investigation of nanoparticle lubricants*, in *Mechanical Engineering*. 2014, Auburn University: Auburn, AL. p. 150.

45. Azman, N.F.; Samion, S. Dispersion Stability and Lubrication Mechanism of Nanolubricants: A Review. *International Journal of Precision Engineering and Manufacturing-Green Technology*, **2019**, ***6***(2), 393-414.

46. Darvin, J.R.; et al. Concentrated Ag Nanoparticles in Dodecane as Phase Change Materials for Thermal Energy Storage. *ACS Appl Nano Mater*, **2019**, *2*(10), 6187-6196.

47. Ghaednia, H.; et al. *The effect of nanoparticles on thin film elasto-hydrodynamic lubrication.* Appl Phys Lett, **2013**, *103*(26), 263111.

48. Ghaednia, H.; Jackson, R.L. On the Effect of Nanoparticles on the Real Area of Contact, Friction and Wear. *J. of Tribol., Trans. ASME*, **2013**, *135*(4), 041603.

49. Crilly, L., et al. *An Investigation of the Electrical Contact Resistance Change, Lubrication, and Wear Properties of a Nanolubricant*. in *2020 IEEE 66th Holm Conference on Electrical Contacts and Intensive Course (HLM)*. IEEE.

50. *Technical Data Sheet: Shell Gadus S3 T100 2* 2021; Available from: https://shell-livedocs.com/data/published/en-US/345773ce-520f-4d65-9bbf-d73b1ec646d8.pdf

51. *Technical Data Sheet: Shell Gadus S5 T100 2*. 2016.

52. Lee, P.E. and C.J. Sanchez. *Tribotesting for Electric Vehicle Fluids in an Electrified Environment*. in *STLE Annual Meeting & Exhibition*. Orlando, FL.

53. Hamrock, B.J.; Dowson, D. Isothermal elastohydrodynamic lubrication of point contacts: Part 1—Theoretical formulation. *J lubr technol*, **1976**, *98*(2), 223-228.

54. Haynes, W.M., *CRC handbook of chemistry and physics*. 2016: CRC press.

55. Hamrock, B.J., B.J. Schmid, and B.O. Jacobson, *Fundamentals of fluid film lubrication*. Vol. 169. 2004: CRC press.

56. Girifalco, L.A., *Statistical mechanics of solids.* 2003, Oxford: Oxford University Press.